Role of CaMKII-α in the Neurodevelopment of Embryonic Zebrafish

by

Birbickram Roy

A thesis submitted in partial fulfillment of the requirements for the degree of

Doctor of Philosophy

in

Physiology, Cell and Developmental Biology

Department of Biological Sciences
University of Alberta

Abstract

Calcium/calmodulin dependent protein kinase 2 (CaMKII) is a multifunctional serine/threonine kinase that is highly abundant in the central nervous system. It plays important roles in many neuronal functions, including neurite extension and maturation, activity-dependent synaptic plasticity and behavior. Although much focus has been given to elucidate the roles of this enzyme in activity-dependent synaptic plasticity, such as long term potentiation and depression, relatively little attention has been paid to explore the enzyme's role in the synaptic receptor development in embryonic organism. Thus, my overall goal in this thesis is to examine the role CaMKII in the synaptic development of embryonic zebrafish. Zebrafish offers many advantages for developmental studies, rapid development and presence of identifiable Mauthner neurons (M-cells) in the embryos being two of them. Major findings reported in this thesis include (1) two days post fertilization (dpf) zebrafish M-cells predominantly express the alpha transcript of CaMKII genes, (2) knockdown of CaMKII alpha transcript led to increased branching of the ventral dendrite of the M-cells and aberrant locomotor response to touch, (3) development of excitatory synaptic receptor currents, specifically NMDA receptors were affected by knockdown of CaMKII-α transcript, while development of AMPA receptors were unaffected, and (4) knockdown of CaMKII-α transcript also affected the development of inhibitory GABA and glycine receptor currents. These findings contribute to our understanding of the important roles of CaMKII-α in the synaptic and neuronal development of embryonic organisms.

Preface

This thesis is an original work by Birbickram Roy. The study, of which this thesis is a part, has received research ethics approval from the University of Alberta Animal Policy and Welfare Committee. The author has met the Canadian Council on Animal Care (CCAC) mandatory training requirements for animal users on the Care and Use of Animals in Research, Teaching, and Testing.

A portion of the chapter 2 (sections 2.1 and 2.5) of this thesis has been published:

Roy,B., Ali, D.W. (2013). Patch clamp recordings from embryonic zebrafish Mauthner cells. Journal of Visualized Experiments 79, e50551, doi:10.3791/50551.

Birbickram Roy performed the experiments, analyzed data, and wrote the manuscript. Declan W. Ali was the supervisory author and was involved in concept formation, data analysis, and manuscript composition.

A version of the chapters 2, 3, and 4 of this thesis has been published as:

Roy, B., Ferdous, J., and Ali, D.W. (2015). NMDA receptors on zebrafish Mauthner cells require CaMKII-α for normal development. Developmental Neurobiology 75,145-62.

Birbickram Roy permormed the experiments, analyzed data, and wrote the manuscript. Jannatul Ferdous assisted in confocal imaging data acquisition presented in figure 3.8, and analyzed the behavioural data presented in figure 3.10. Declan W. Ali was the supervisory author and was involved in concept formation, data analysis, and manuscript composition.

A version of chapter 5 of this thesis has been published as:

Roy, B. and Ali, D.W. (2014). Multiple types of GABAA responses identified from zebrafish Mauthner cells. Neuroreport 25, 1232-6.

Birbickram Roy permormed the experiments, analyzed data, and wrote the manuscript. Declan W. Ali was the supervisory author and was involved in concept formation, data analysis, and manuscript composition.

Unless otherwise stated, data presented in this thesis are the author's original work.

ACKNOWLEDGEMENTS

I would like to express my sincere gratitude to my supervisor Dr. Declan Ali for his guidance and encouragement over the years of my graduate study. Your support and mentorship has led me to become a critical thinker, a good presenter and a better scientist. It has been a great pleasure working with you. I would also like to thank my supervisory committee members, Ted Allison and Peter Nguyen, for the invaluable insights and advice I received from them.

Thanks to all my present and past fellow lab mates Dr. Kessen Patten, Dr. Chris Coutts, Nicole Sylvain, Daniel Brewster, Marcus Cunningham, Kazi Tanveer Ahmed, Jannatul Ferdous and Rajarshi Mukharjee. Your friendship and company over the years was much appreciated. I would also like to thank the summer students, Zach Mansour, Caitlyn Collins, Taylor Bucyk, Shubham Shan and Savanna Boutin, whose excitement and great company made the lab work more joyful.

Last but certainly not least, I would like to thank my wife and my parents for never losing confidence in me. You have been a boundless source of inspiration and support for me. Thank you!

Table of Contents

List of Tables

List of Figures

List of Abbreviations

AIP	Autocamtide-2-related inhibitory peptide
AMPA	Alpha-amino-3-hydroxy- 5-methyl-4-isoxazole propionic acid
AMPAR	AMPA receptor
APV	D(-)-2-amino-5-phosphonopentanoic acid
BSA	Bovine serum albumin
camk2	CaMKII gene
CaMKII	Calcium/calmodulin dependent protein kinase 2
CNS	Central nervous system
C_t	Threshold cycle
dpf	Day post-fertilization
DRG	Dorsal root ganglia
EPSC	Excitatory postsynaptic current
EPSP	Excitatory postsynaptic potential
GABA	γ- aminobutyric acid
$GABA_AR$	Ionontropic GABAA receptor
GluA	AMPA receptor subunit
GluN	NMDA receptor subunit
GlyR	Glycine receptor
hpf	Hours postfertilization
iGluR	Ionotropic glutamate receptor
KN-62	4-[(2*S*)-2-[(5-isoquinolinylsulfonyl)methylamino]-3-oxo-3-(4-phenyl-1-piperazinyl)propyl] phenyl isoquinolinesulfonic acid ester
KYN	Kynurenic acid
LTD	Long-term depression
LTP	Long-term potentiation
M-cell	Mauthner cell
mEPSC	miniature excitatory postsynaptic current
mEPSP	Miniature excitatory postsynaptic potential
mIPSP	Miniature inhibitory postsynaptic potential
MO	Morpholino oligonucleotide
ms	millisecond
mV	millivolt
MΩ	megaohm
NMDA	N-methyl-D-aspartate
NMDAR	NMDA receptor
pA	picoampere
PBS	Phosphate-buffered solution
PFA	Paraformaldehyde
pS	picosiemens
PSD	Postsynaptic density
PTU	N-phenylthiourea

RT-PCR	Reverse transcription polymerase chain reaction
RT-qPCR	Reverse transcription quantitative real-time polymerase chain reaction
TARP	Transmembrane AMPA receptor regulatory protein
TTX	Tetrodotoxin

Chapter 1: General Introduction

1.1 Introduction

Calcium/calmodulin dependent protein kinase 2 (CaMKII) is a multifunctional serine/threonine kinase that is abundant in the brain and is highly expressed in the synapse (Feng et al., 2011; Hudmon and Schulman, 2002; Kennedy et al., 1983). In mammals, CaMKII is encoded by four distinct genes (α, β, γ or δ) (Hudmon and Schulman, 2002). The holoenzyme is composed of 12 individual subunits of varying stoichiometries (Brocke et al., 1999; Gaertner et al., 2004) and is activated upon binding to calcium/calmodulin, which results in autophosphorylation and persistent kinase activity (Coultrap and Bayer, 2012).

CaMKII has a wide variety of neuronal targets and plays a major role in synaptic plasticity, presynaptic excitability and neuronal development (Hojjati et al., 2007; Liu et al., 2007; Lu and Hawkins, 2006; Pang et al., 2010; Shakiryanova et al., 2007; Shakiryanova et al., 2011). For instance, during hippocampus-dependent learning and memory, CaMKII translocates to the synapse where it binds to the GluN2B subunit and up-regulates NMDA receptor activity (Bayer et al., 2001; Hell, 2014). It regulates the trafficking and gating of AMPA receptors (Hayashi et al., 2000; Kristensen et al., 2011a; Lu et al., 2010; Rongo, 2002) and modulates dendritic spine volume by interacting with cytoskeleton components such as F−actin (Ahmed et al., 2006; O'Leary et al., 2006; Okamoto et al., 2007; Pi et al., 2010). CaMKII activity alters the surface expression of $GABA_A$ receptors (Guetg et al., 2010; Marsden et al., 2010) and enhances the clustering of glycinergic receptors. Furthermore de-regulation of CaMKII leads to changes in

synaptic connectivity, aberrant dendritic branching, impeded dentate gyrus development and substantial behavioral deficits in rodent models (Hagihara et al., 2013; Hardingham et al., 2003; Lo Iacono and Gross, 2008; Pattinson et al., 2006b; Yamasaki et al., 2008). While much attention has been paid to the role of CaMKII in mature organisms, there is comparatively less information on the role of CaMKII at developing and maturing synapses.

Research in the Ali laboratory has focused on the development of synaptic properties associated with zebrafish Mauthner cells (M-cells) (Ali et al., 2000a; Ali et al., 2000b; Brewster and Ali, 2013; Patten and Ali, 2007, 2009). A particularly attractive reason for this focus on the M-cells is that one can return to the same cell from preparation to preparation to study excitatory synaptic development in vivo. Embryonic development is very rapid; the fertilized eggs hatch in two days, and the embryos are transparent, allowing extensive imaging studies to be performed on whole organisms. The genome has been sequenced and the technology is available to either knockdown or knockout proteins of interest (Ekker, 2000; Nasevicius and Ekker, 2000; Patten et al., 2010; Tallafuss et al., 2012). Moreover, one can closely examine escape responses and swimming behaviors. Thus the zebrafish is an excellent organism to investigate the link between synaptic development and locomotor responses.

The overall objective of my research is to understand the role of CaMKII in synaptic development. I am particularly interested to know how CaMKII aids synaptic maturation *in vivo*. Zebrafish express seven different isoforms of CaMKII, therefore, I will focus on

determining which isoforms are expressed in the M-cell, and will then investigate how those isoforms might affect M-cell morphology and synaptic physiology. My work has broad implications because improper synaptic development could lead to a wide range of behavioral and physiological deficits in the developing organisms. Thus, it is important to have a thorough understanding of synaptic development for basic and translational science. My specific research goals are listed below-

Aim 1: To characterize the expression profile of CaMKII isoforms in zebrafish Mauthner cells during hatching.

Aim 2: To determine the role of CaMKII in the development of synaptic currents associated with M-cells.

1.2 Outline of thesis

I present my thesis in 6 chapters. In this first chapter, I give a general introduction to my research and review relevant literature. The second chapter is a detailed description of the methods and materials I have used throughout my research. I present the findings of my research in Chapters three to five. Finally, I present an overview of all research findings, their significance and future direction in chapter six.

1.3 Literature review

1.3.1 Overview

Zebrafish is a suitable model for studying the role of CaMKII in neurodevelopment. In this section, I review embryonic development of zebrafish, with an emphasis on synaptic development onto M-cells, and development of locomotor responses. I summarize the structure and function of synaptic receptors involved in synaptic transmission in M-cells. Finally, I describe structure, function and distribution of CaMKII and how this enzyme influence synaptic transmission.

1.3.2 Overview of the system: Zebrafish M-cells

Zebrafish has been widely used to study vertebrate development since its introduction by George Streisinger in 1981. It is a freshwater fish native to the Ganges river and found in East India, Bangladesh, Nepal and Myanmar. They belong to the Cyprinidae family of teleost fish. Zebrafish offers many advantages for developmental studies, such as high fecundity (females produce hundreds of eggs at bi-weekly intervals), external fertilization, transparent embryos, rapid development, short generation time (3-4 months) and easy maintenance.

Zebrafish embryonic development is divided into eight distinct periods of embryogenesis- the zygote, cleavage, blastula, segmentation, pharyngula, and hatching periods (Kimmel et al., 1995). The newly fertilized eggs are in the zygotic period, which is about 40 minutes long. The cleavage period begins with the first cell division around $^{3}/_{4}$ hours post fertilization (hpf) and continues until 7 cleavage cycles, ending in the 64-

cell stage embryos. The blastula (2 $^{1}/_{4}$-5 $^{1}/_{4}$ hpf) period encompasses development from the eighth zygotic cell cycle, or 128-cell stage, until the beginning of gastrulation. This period is characterized by lengthening and asynchrony of cell cycles, and onset of epiboly, which refers to thinning and spreading of the cell layer due to cell movement over the yolk, producing a blastoderm. During the gastrula period (5 $^{1}/_{4}$-10 hpf), epiboly continues and morphogenetic cell movements of involution, convergence and extension produce the primary germ layers and the embryonic axis. The M-cell is born during this period, around 8-10 hpf (Mendelson, 1986). The segmentation period (10-24 hpf) marks the beginning of primary organogenesis and somitogenesis through which a basic vertebrate body plan emerges. At the pharyngula phase (24-48 hpf) the body straightens up from the curved state, fins develop, and pigment cells differentiate and melanophors begin to form characteristic body stripes. The circulatory system, consisting of a beating heart and a closed set of channels also forms at this stage. The embryos are encased in the chorion and hatch out asynchronously during the hatching period (48-72 hpf). They continue to grow and morphogenesis of many rudimentary organs nears completion by the end of day 3 (72 hpf). During the early larval period, after 72 hpf and onwards, the morphogenesis of the hatched larva is complete and the swim bladder becomes inflated.

The primordial central nervous system of zebrafish begins to develop during gastrulation. By the end of gastrulation the neural plate becomes thick and well defined. Ten distinct folds or neuromeres are formed along the anterior part of the neural plate that will eventually develop into the brain. The posterior cells of the neural plate give rise to the trunk spinal cord. The first two neuromeres form the two forebrain subdivisions, the

diencephalon and telencephalon, while the third neuromere forms the midbrain or mesencephalon. The remaining seven neuromeres represent the hindbrain, which is divided into seven divisions or rhombomeres (r1-r7). Other CNS structures, such as the premordium of hypothalamus, cerebellum, rudimentary structures of the eyes and optic primordia are formed later in the segmentation period.

Morphogenesis of the neural tube closely parallels neuronal differentiation. The first neurons to arise in the nervous system are referred to as primary neurons, which rapidly develop long axons, and form a simple neural network that mediates the early embryonic behaviours such as spontaneous movement of the trunk and tail as well as avoidance response to tactile stimuli (Grunwald et al., 1988; Metcalfe et al., 1990). Different types of identifiable primary neurons, including interneurons of the hindbrain and spinal cord (Kuwada et al., 1990; Mendelson, 1986), motoneurons (Eisen et al., 1986; Myers et al., 1986) and sensory neurons (Metcalfe et al., 1990) have been characterized from very early stages of development. The earliest interneurons to originate in zebrafish are a pair of M-cells, which belong to the reticulospinal neuron (RSN) group and play a key role in the escape response of the organism (Kimmel et al., 1981; Mendelson, 1986; Zottoli, 1978). RSN neurons arise as a single cluster in the midbrain and seven separate clusters in the hindbrain, with each cluster sitting in one neuromere (Lee et al., 1993). The reticulospinal system is comprised of twenty-seven types of RSNs, which are readily identifiable due to their distinct morphology, forming the primary descending system of zebrafish (Eaton and Farley, 1973; Kimmel et al., 1981). The RSNs, together with other descending neurons of the brain stem regulate sensorimotor coordination, and control the

turning and swimming behaviours in zebrafish (Eaton et al., 2001; Gahtan et al., 2002). Arising at about 7.5 hours post fertilization (hpf) during the gastrulation period, M-cells are the first of the RSN neurons to appear in the nervous system, closely followed by their serial homologs MiD2cm and MiD3cm, which appear at 9.5 hpf (Mendelson, 1986). The M-cell has two large crescent shaped dendrites, one projecting laterally (the lateral dendrite) and the other projecting ventrally (the ventral dendrite) (Kimmel et al., 1981). Additional finer dendrites arise from these two prominent dendrites and the cell body.

M-cells receive sensory inputs from the somatosensory, visual, acousto-vestibular and lateral line systems, with each type of afferent projecting to one of the prominent dendrites. The first sensory inputs to the M-cells form around 18 hpf from somatosensory trigeminal ganglion cells, which are also some of the first sensory neurons to arise in the nervous system around 14 hpf (Kimmel et al., 1990; Metcalfe et al., 1990). Peripheral axons from the trigeminal ganglia, located between the eye and the otic vesicle, innervate the skin of the head and rostral part of the yolk sac, while the central axons projects to the hindbrain. M-cells also receive somatosensory input from the Rohon-Beard neurons in the spinal cord that innervate the skin of the trunk and project axons to the hindbrain around 19 hpf (Metcalfe et al., 1990). Transmission of somatosensory stimuli to M-cells is taken over by the neurons of the dorsal root ganglia (DRG) as the Rohon-Beard cells start to die off (Kohashi and Oda, 2008; Lewis and Eisen, 2003). Bipolar neurons of these ganglia begin to differentiate at 36 hpf and appear in the spinal cord by 45 hpf (An et al., 2002; Bernhardt et al., 1990; Reyes et al., 2004). Input from the ears (otoliths) is relayed by the acoustic-vestibular ganglion (VIIIth cranial nerve) to the M-cells beginning at 23

hpf (Kimmel et al., 1990). Input from the lateral line neurons arrive last at around 25 hpf and are believed to modulate M-cell's response to acustico-vestibular input (Chang et al., 1987; Faber and Korn, 1975). The sensory inputs onto M-cells terminate as electrical, chemical or mixed synaptic contacts (Kimmel et al., 1990). Electrical synapses are predominantly found on the ventral dendrites and ventral perikaryon of the M-cell, whereas chemical synapses are found largely on the lateral dendrites and dorsal surface of the cell (Kimmel et al., 1981). Chemical synapses predominate over the electrical and mixed synapses during early development, while gap junctions become identifiable by 3 days post fertilization (Kimmel et al., 1981; Yao et al., 2014). Chemical synapses on M-cells are either excitatory (glutamatergic AMPA and NMDA) or inhibitory (glycinergic and GABAergic) in nature (Ali et al., 2000a; Ali et al., 2000; Ali et al., 2000b; Legendre, 1998; Legendre and Korn, 1994; Triller et al., 1997).

The M-cells relay sensory information to motor centers in the brain and spinal cord. The pair begins to extend axons in the segmentation period (18 h), concurrently with the arrival of axonal growth cones from trigeminal sensory neurons. The axons cross the midline of the brain and descend on the contralateral side to extend the entire length of the spinal cord. The axons send collaterals which synapse onto to the descending spinal interneurons as well as motoneurons that innervate the muscles (Celio et al., 1979; Fetcho, 1992; Fetcho and O'Malley, 1995; Svoboda and Fetcho, 1996). The descending interneurons are electrically coupled to two to four motoneurons (Celio et al., 1979; Gahtan and O'Malley, 2003). Thus, activation of an M-cell results in synchronous

activation of the motoneurons, leading to contraction of the body and tail musculature that drives the escape response of the fish (Fetcho and O'Malley, 1995).

The escape response, an evasive behavior that animals use to flee from the predators, is essential for the survival of the animal (Eaton et al., 1977). The response is a two- stage behavior; the animal makes a C-bend to orient the body away from the stimulus at first and then propel it away from the danger in the direction of the initial turn (Eaton et al., 1988). The M-cells are critically involved in the first stage of the escape response (Eaton et al., 2001; Zottoli, 1977) and are responsible for activation of short-latency C-start (SLC) responses occurring within 5-6 ms of detection of the stimulus (Burgess and Granato, 2007; Kohashi and Oda, 2008; Liu and Fetcho, 1999). Fish where M-cells were ablated lacked SLC and showed long-latency C-start (LLC) responses characterized by an increased latency and turn duration, and decreased angular velocity (Kohashi and Oda, 2008; Liu and Fetcho, 1999). In freely swimming zebrafish, tactile stimuli to the head activates the M-cells and its homologs, producing a large escape response (Foreman and Eaton, 1993). A stimulus to the tail activates only M-cells that produce a rapid but small response. M-cells usually fire only one action potential when activated followed by a temporary inhibition (Nakayama and Oda, 2004; Zottoli, 1977). Inhibition occurs due to activation of inhibitory synaptic inputs onto the M-cells and increased conductance of potassium currents (Brewster and Ali, 2013; Furukawa and Furshpan, 1963; Nakayama and Oda, 2004; Zottoli, 1977). Inhibitory commissural interneurons synapse onto both M-cells and contribute to the feed forward inhibition, whereas inhibitory collateral neurons provide recurrent inhibition to the ipsilateral M-cell.

1.3.3 Synaptic transmission in zebrafish Mauthner cell

The neurons in the central nervous system communicate with each other through specialized anatomical structures called synapses. Presynaptic neurons can pass information to the postsynaptic cell directly through electrical synapses, or via chemical synapses. In the vertebrate brain, chemical synapses are more common than electrical synapses. Electrical synapses allow the direct flow of current from presynaptic neurons to postsynaptic neurons through gap junctions, which provide electrical continuity between cells. Chemical synaptic transmission can be mediated directly by ionotropic neurotransmitter receptors, or indirectly by metabotropic receptors. Ionotropic receptors are ligand-gated ion channels in the postsynaptic membrane that respond to neurotransmitters by allowing ions to flow, thereby mediating chemical synaptic transmission. Metabotropic receptors, which mediate slow, indirect chemical transmission, produce intracellular second messengers in the postsynaptic cell when activated by neurotransmitters released from presynaptic cell. The second messengers then influence ion channels and other intracellular targets that result in excitation or inhibition of the postsynaptic cell.

In the mammalian nervous system three main neurotransmitters mediate the majority of fast synaptic transmission: glutamate, glycine, and γ-aminobutyric acid (GABA). Glutamate is the primary neurotransmitter mediating excitatory synaptic transmission in the mammalian central nervous system. It acts on three types of ionotropic receptors: α-Amino-3-hydroxy-5-methyl-4-isoxazolepropionic acid (AMPA), N-methyl-D-aspartate (NMDA), and kainate (KA) receptors. Ligand binding to these ionotropic glutamate

receptors (iGluRs) leads to opening of the intrinsic cation channels, which allow Na^+, K^+, and sometimes Ca^{2+} to flow down their electrochemical gradients. As a result, excitatory postsynaptic potentials (EPSPs) are generated, which depolarize the postsynaptic membrane potential. These local depolarizations cause the opening of voltage-gated ion channels and lead to the generation of action potentials in the postsynaptic cell, if the depolarization is above threshold. Glycine and GABA are the primary inhibitory transmitters in the adult CNS. They activate ionotropic receptors that are anion channels, allowing Cl^- to flow down its electrochemical gradient. In adult organisms, Cl^- influx into the postsynaptic cell generates inhibitory postsynaptic potentials (IPSPs) causing hyperpolarization of the membrane potential and thus inhibiting action potential production. By contrast, activation of glycine and GABA inotropic receptors during early embryonic development, when intracellular Cl^- concentration is high, causes an efflux of Cl^- and a subsequent membrane depolarization that may induce action potentials to be produced (Ben-Ari, 2002).

In this section, I will briefly discuss fast synaptic transmission through ionotropic receptors. Throughout the thesis, I refer to the mammalian ionotropic receptor subunits and the encoding genes according to the terminology proposed by The International Union of Basic and Clinical Pharmacology (IUPHAR) (Collingridge et al., 2009). The ZFIN Zebrafish Nomenclature Guidelines was followed to refer Zebrafish orthologs of mammalian genes (Zebrafish Nomenclature Committee (ZNC), 1992). Briefly, gene names and symbols are written in lowercase letters and italicized, whereas protein names

and symbols are non-italic with an uppercase first letter. A comprehensive list of the ionotropic receptor subunits that are discussed in the thesis is presented in Table 1.1.

1.3.3.1 AMPA receptors

Subunit Composition and structure

AMPA receptors (AMPARs) are complexes of four subunits (GluA1-4) with varying stoichiometry (Hollmann and Heinemann, 1994). In mammals, four closely related genes, which have approximately 70% sequence identity, encode the subunits. However, zebrafish has eight homologs of the mammalian genes due to genome duplication in teleost fish (Table 1.1). Sequence homology among different subunits suggests that they share a common architecture, with each subunit comprised of four semi-autonomous domains: the extracellular amino-terminal domain, the extracellular ligand-binding domain, the transmembrane domain , and an intracellular carboxyl-terminal domain (Figure 1.2) (Traynelis et al., 2010). The extracellular domain is formed from the first ~450 amino acids and plays important roles in subunit assembly and receptor trafficking (Kumar and Mayer, 2013). Additionally, this domain influences ligand binding, receptor open probability, desensitization, deactivation and contains binding sites for divalent ions, allosteric modulators and extracellular proteins. The ligand binding domain provides the binding pocket for the receptor agonists. It is highly conserved within receptor classes and is formed from two extracellular polypeptide chains referred to as S1 and S2 (Traynelis et al., 2010). A polypeptide section on the amino terminal (N-terminal) of M1 membrane helix forms S1 while the segment between M3 and M4 membrane helices forms S2. Agonist binding leads to a conformational change in ligand binding

domain, which in turn leads to structural rearrangement of M3 membrane helix and channel opening. The transmembrane domain of glutamate receptors is composed of M1, M3, M4 transmembrane helices and the M2 reentrant helix from each of the four subunits, and forms the core ion channel. The carboxyl-terminal domain of glutamate receptors is diverse in amino acid sequence and length. It contains many sites for phosphorylation and binding of intracellular proteins. It influences membrane targeting, stabilization and post-translational modification of the receptors.

All AMPAR subunits undergo alternative splicing in a region N-terminal to the M4 transmembrane helix; producing 'flip' and 'flop' splice variants (Mosbacher et al., 1994; Sommer et al., 1990). The splice variants influence channel desensitization kinetics and sensitivity to various allosteric modulators. The AMPAR subunits can also undergo alternative splicing on carboxyl-terminal domain, giving rise to either 'short' or 'long' isoforms (Gallo et al., 1992). In addition to alternative splicing, AMPARs undergo RNA editing post-transcriptionally at a site that resides at the apex of the reentrant M2 helix converting a glutamine (Q) residue into arginine (R) (Sommer et al., 1991). The vast majority of GluA2 subunits in the CNS are edited at this site. AMPARs with edited GluA2 exhibit low Ca^{2+} permeability and low single channel conductance due to the large size and positive charge on the side chain in the edited form. In addition to the Q/R site, another codon immediately preceding the flip/flop site, the R/G site, may be edited in GluA2, -3, and -4. The RNA editing in AMPAR subunits are carried out by RNA-dependent adenosine deaminase 2. All AMPAR subunits also have glycosylation sites in the S1 region that forms the ligand binding domain. Cell-specific differences in AMPAR

subunit composition and post-translational modifications contribute to the differences in trafficking, ligand affinity, and receptor kinetics.

Trafficking

AMPAR subunits assemble as dimers of dimers in the endoplasmic reticulum (ER). Conformational changes in the subunits which are necessary for normal receptor function also occurs in the ER and influences receptor trafficking to dendritic membrane. Surface AMPARs are incorporated into synapse by lateral diffusion from extrasynaptic sites and stabilized by postsynaptic scaffolding proteins. Under basal condition, mature AMPARs undergo constitutive recycling where synaptic AMPARs are internalized from plasma membrane and trafficked to early endosomes. AMPARs can be inserted back to the plasma membrane from the early endosomes for fast recycling, or through recycling endosomes. AMPARs in late endosomes enter degradation pathway (Anggono and Huganir, 2012). Interactions between AMPARs and their accessory proteins, such as transmembrane AMPA receptor regulatory proteins (TARPs), chornicons (CHINs), and other auxiliary subunits play important roles in AMPAR trafficking.

Distribution

The expression and distribution of AMPAR subunits are developmentally and regionally regulated, which reflects a balance of transcription, translation, receptor assembly, and presentation at the cell surface. AMPAR subunits are widely expressed in the CNS. GluA1, -2, and -3 are highly expressed in the hippocampus, outer layers of cortex, olfactory regions, basal ganglia and amygdala of rat CNS (Hollmann and Heinemann, 1994). In contrast, GluA4 expression is mostly low to moderate throughout the brain. Glial cells also express AMPARs, where they are involved in excitotoxicity (Gallo and Russell, 1995; Yoshioka et al., 1996). AMPARs have also been shown to localize in presynaptic terminals, where they regulate neurotransmitter release (Barnes et al., 1994) and movement of axonal filopodia (Chang and De Camilli, 2001). In embryonic zebrafish, eight AMPAR subunit mRNA express differentially throughout the CNS (Hoppmann et al., 2008). Importantly, all subunits are expressed in hindbrain, hypothalamus, telencephalon and olfactory bulb between 48 and 72 hpf. Expression patterns in earlier developmental periods and in other brain regions are variable.

Physiology and function

Synaptic AMPARs activate upon binding of glutamate, allowing a brief pulse of current with a fast deactivation time course of 1-2 milliseconds. The precise kinetics and amplitude of the currents are determined by the subunit composition and synaptic density of the receptors, along with time course of glutamate release and uptake. Properties of AMPA receptors have been studied extensively in developing zebrafish M-cells previously, where the receptor kinetics becomes faster during development between 33

and 48 hpf (Ali et al., 2000a; Patten and Ali, 2007; Patten et al., 2010). The average amplitude of spontaneous AMPAR mEPSCs in developing zebrafish embryo has a unimodal distribution, with peak amplitude increasing significantly between 33 and 48 hpf, from about 24 pA to about 30 pA along with a fourfold increase of mEPSCs frequency. The deactivation kinetics of AMPARs is best fitted with a single exponential curve, which decreases progressively with development between 33 to 72 hpf. The AMPARs in zebrafish have a fast rise time of about 0.1 ms, which does not change significantly during embryonic development.

AMPA receptors play key roles in the activity-dependent synaptic plasticity phenomena such as long term potentiation (LTP) and long term depression (LTD) which are believed to be the cellular correlate of learning and memory (Nicoll and Roche, 2013). Both forms of synaptic plasticity require trafficking of AMPARs. During LTP AMPARs are inserted into the postsynaptic membrane, resulting in potentiation. During LTD, the rate of synaptic AMPARs internalization outpaces the rate of insertion, leaving reduced number of AMPARs at the synapse. In embryonic zebrafish, AMPARs have been shown to undergo activity-dependent potentiation that relies on the trafficking and insertion of AMPARs into the postsynaptic membrane (Patten and Ali, 2009). AMPAR trafficking is also necessary for the maturation of glutamate synapses, as developmental transition of slow-kinetics AMAPARs to fast-kinetics AMPARs relies on the receptor trafficking (Patten et al., 2010).

1.3.3.2 NMDA receptors

Subunit composition and expression

NMDA receptors (NMDARs), which belong to the ionotropic glutamate receptor family, are transmembrane protein complexes of four large subunits of more than 900 amino acids long (Paoletti et al., 2013). The structure of each subunit is similar to that of other ionotropic glutamate receptors, consisting of four distinct modules (Figure 1.2). There are seven different subunits of NMDARs in mammals, which are grouped into three subfamilies based on sequence homology: GluN1 subunits, four GluN2 subunits (GluN2A, GluN2B, GluN2C and GluN2D), and two GluN3 subunits (GluN3A and GluN3B). The LBD in GluN1 and GluN3 subunits bind to glycine (or D-serine), whereas in GluN2 subunits it binds to glutamate. NMDARs are composed of two copies of the obligatory GluN1 subunits and two copies of GluN2 subunits, or a combination of GluN2 and GluN3 subunits, leading to the formation of di-heteromeric and tri-heteromeric receptors.

The GluN1 subunit, encoded by a single gene, has eight different isoforms resulting from alternative splicing (Paoletti et al., 2013) . It is ubiquitously expressed in the CNS from embryonic stages to adulthood, although isoform-specific differences exist. GluN2 subunits, which are major determinants of NMDARs functional properties, also show differential spatiotemporal expression patterns. In rodents, only GluN2B and GluN2D are expressed at embryonic stages. GluN2A expression begins soon after birth and rises steadily to become the most prevalent isoform throughout the CNS in the adult, while at the same time GluN2D expression is reduced markedly. In contrast to GluN2D,

expression of GluN2B remains high following birth and peaks in the first postnatal week. GluN3C is expressed later in development around postnatal day 10 and remains confined to the cerebellum and the olfactory bulb. GluN3 isoforms also show differential expression. GluN3A is expressed in early postnatal development and then declines over time; while GluN3B expression increases slowly throughout development, leading to high levels of expression in motor neurons of the adults. Overall, differential expression patterns result in high levels of GluN2B, GluN2D and Glu3A subunits in early development, suggesting their involvement in synaptogenesis and synaptic maturation. On the other hand, high levels of GluN2A and GluN2B in the adult CNS point to the importance of these isoforms in synaptic function and plasticity.

Expression of NMDAR subunits in zebrafish has been investigated by Cox et al (2005). Zebrafish express two paralogs of each of the GluN1 and GluN2 genes (Table 1). The GluN1 paralogs share about 90% amino acid identity to the corresponding human subunit. The transmembrane domains and C-terminus regions show the most similarity while the N-terminus region is more divergent. One important difference between zebrafish and human GluN1 subunits is that the majority of the zebrafish transcript contains the canonical motif for binding PDZ proteins, whereas it is not encoded in most of the mammalian GluN1 subunits. Because they lack this protein binding motif, mammalian GluN1 subunits depend on the PDZ motif containing GluN2 subunits for protein-protein interactions in the postsynaptic density (PSD) (Kornau et al., 1995; Niethammer et al., 1996). It is therefore suggested that zebrafish GluN1 subunits can directly interact with PDZ proteins (Cox et al., 2005). The transmembrane domain

regions of GluN2 subunits are also 90% conserved between zebrafish and human isoforms, while the N- and C- terminals are somewhat divergent. Zebrafish GluN2 subunit C-terminus is also longer than that found in mammals and contains several sequence repeats. Like their human counterparts, all zebrafish GluN2 subunits contain a PDZ binding motif. Expression of zebrafish *grin1* paralogs, which encode the GluN1 subunit (Table 1.1) is observed from early embryonic development of 24 hpf and becomes stronger by 48 hpf. Expression of *grin2* genes in the CNS differs significantly, with *grin2c* paralogs being absent throughout the development between 24-96 hpf, and *grin2ba* appearing at 96 hpf. The other *grin2* genes appear in the CNS within 24 to 48 hpf. There has been no study on the expression pattern of *grin3* paralogs in zebrafish.

Physiology and function

Activation of NMDARs requires simultaneous binding of both glutamate and glycine, because GluN1 and GluN3 subunits bind to glycine (or D-serine) and GluN2 subunits bind to glutamate. The ion channel is also subjected to a voltage dependent block by extracellular Mg^{2+}. As a result the receptor acts as a coincidence detector, sensing postsynaptic depolarization and release of glutamate at the same time. NMDARs are highly Ca^{2+} permeable. Activation of NMDARs generates a current with slow rise and slow decay time compared to AMPARs. The decay of NMDAR excitatory postsynaptic currents (EPSCs) is mainly governed by the identity of GluN2 subunit, with decay time of GluN1/GluN2A, GluN1/Glu2B or GluN2C and GluN1/GluN2D receptors being 40, 300 and 2000 ms respectively (Paoletti et al., 2013). During early postnatal development, NMDA receptors undergo a developmental switching of subunits whereby GluN2A

containing receptors predominates GluN2B containing receptors. This developmental change in receptor subunit composition is evolutionarily conserved, and accompanied by functional change of the receptors. In developing zebrafish, a developmental trend of increasing amplitude of NMDAR containing synapses has been observed between 1.2 to 3 dpf embryos (Ali et al., 2000a). The deactivation phase of NMDAR mediated synaptic currents of these embryos were best fitted with a biexponential function, which did not vary much during the development, indicating that maturation of NMDAR synapses in zebrafish probably occurs before 28 hpf. The role of NMDARs in synaptic plasticity has been studied extensively. In hippocampus, a brief high-frequency stimulus to CA1 pyramidal cells leads to long-lasting strengthening of synaptic transmission. Induction of this form of LTP is critically dependent on the activation of NMDARs, which subsequently increases intracellular Ca^{2+} and trafficking of AMPARs to the postsynaptic membranes. NMDAR dependent LTD has been also reported at many synapses.

1.3.3.3 $GABA_A$ receptor

Subunit composition and structure

$GABA_A$ receptors ($GABA_ARs$), like other Cys-loop ligand-gated chloride channels (LGICs) including GlyRs, are heteropentameric assemblies (Figure 1.3). All $GABA_A$ receptor subunits have a structural arrangement that is common to all group I LGICs, with a large N-terminal extracellular domain, four transmembrane domains, a long intracellular loop connecting transmembrane domain 3 and 4, and a short C terminus (Corringer et al., 2000). A stretch of disulfide-bond rich 15 amino acids (Cys loop) in extracellular domain is conserved throughout all LGICs. It provides binding sites for

glycine, antagonists and allosteric modulators whereas the transmembrane domain 2 from five neighboring subunits forms the chloride channel.

$GABA_AR$ subunits are encoded by 19 different genes in mammals that fall into eight subclasses based on sequence homology (α1–6, β1–3, γ1–3, δ, ε, θ, π, ρ1–3) (Table 1.1). Assembly of different combinations of the subunits gives rise to a large number of structurally and functionally distinct $GABA_ARs$, although majority of the receptors abundant in brain combine 2 α, 2 β and a single γ or δ subunits (Farrant and Nusser, 2005). In general, two populations of $GABA_ARs$ are found in the CNS; those that are localized at postsynaptic densities and the others that are at extrasynaptic sites. The synaptic receptors largely consist of α1-3, β2-3 and γ2 subunits; although their localization in postsynaptic specializations is not exclusive, as these receptors are also found in extrasynaptic sites. The γ2 subunit is essential for postsynaptic clustering of $GABA_ARs$ (Essrich et al., 1998). In developing postnatal brain, γ3 functionally substitute γ2 (Baer et al., 1999). Receptors that contain α4-6 along with β and δ subunits are mostly or exclusively distributed extrasynaptically. The lack of γ subunits in these receptors probably lead to their failure to localize at synapses.

Physiology and function

GABAergic transmission during early embryonic development is primarily mediated through extrasynaptic $GABA_ARs$ that contain α5 and δ subunits, as well as β2/3 and γ subunits (Deidda et al., 2014). These receptors show higher agonist affinity and capable of binding ambient GABA, producing long lasting "tonic" currents in young neurons.

GABA is depolarizing and excitatory during early development due to high intracellular chloride concentration (Ben-Ari et al., 2012). Thus, activation of extrasynaptic $GABA_A$Rs leads to persistent depolarization of immature neurons, which is critical for cell migration, proliferation, neurite growth and synapse formation. As synapses develop, $GABA_A$Rs with α2 and α3 subunits, characterized by long-lasting currents become widely expressed (Deidda et al., 2014). These subunits gradually become downregulated and receptors with α1 become prevalent, resulting in faster decay time course allowing for fine synaptic integration and network synchronization. Synaptic receptors mediate the phasic $GABA_A$R response.

1.3.3.4 Glycine receptor

Subunit composition and structure

Glycine receptors (GlyRs), which mediate fast inhibitory synaptic currents are group I ligand-gated ion channels (LGICs) that belong to the Cys loop receptor family, which also include $GABA_A$ receptors ($GABA_A$Rs). GlyRs are heteropentameric assemblies of two subunits, GlyRα and GlyRβ, with a tightly bound cytosolic scaffolding protein, gephyrin (Figure 1.3) (Lynch, 2004). Four vertebrate genes (*Glra1-4*) encode GlyRα and a single gene encodes GlyRβ (Grenningloh et al., 1990a; Grenningloh et al., 1990b). GlyRα subunits have more than 80% sequence homology and form functional homomeric receptors in heterologous expression system. GlyRα subunits contain the critical determinants of the ligand binding sites. By contrast GlyRβ subunits, which has less than 50% sequence similarity to GlyRα subunits do not form functional receptors when expressed alone in heterologous systems. This subunit also contributes to ligand

binding, provides binding sites for gephyrin, and plays essential roles in trafficking and postsynaptic clustering of the GlyRs. All GlyR subunits share the common structural features of other Cys-loop family of receptors.

Expression, physiology and function

GlyRs are expressed throughout the brain in a spatiotemporally regulated manner (Malosio et al., 1991). The α2 subunit is the most widely expressed isoform in the brain throughout embryonic development while mRNA for the β subunit is expressed in the cortex during early development. Expression of other GlyRs has not been identified in embryonic brain. Postnatally, expression of α2 and β transcripts shows a dynamic change, with α2 expression being greatly reduced and progressively restricted to cortical layer VI and dentate gyrus (Malosio et al., 1991). In contrast, β transcripts show widespread expression in all cortical layers, hippocampus, olfactory bulb, thalamus and cerebellum. In rats and mice, transcripts for α1 and α3 subunits become detectable in the CNS only after second postnatal week of development. α1 is the most prevalent GlyR subunit in the adult CNS, where it is highly expressed in the hypothalamus, brainstem and spinal cord. Synaptic α2 has been identified in different adult CNS regions, including spinal cord, brainstem, midbrain, olfactory bulb and retina. α3 transcripts are expressed later in development and are associated with regions that are involved in sensory and motor functions (Dutertre et al., 2012). Distribution pattern of GlyR subunits in adult zebrafish is generally consistent with that of mammalian CNS (Imboden et al., 2001).

The properties of GlyRs depend on the subunit composition of the receptors; therefore, a shift from α2 subunits to α1 subunits during early postnatal development is accompanied by a shift in GlyR channel kinetics. For example, the decay time of spontaneous GlyR currents (mIPSCs) in hypoglossal motoneurons becomes smaller during the first two postnatal weeks, from a mean value of 14.2 ± 2.4 ms to 6.3 ± 0.7 ms, concomitant with a developmental switch from fetal α2 subunit to adult α1 subunits (Singer et al., 1998). A developmental speeding of GlyR kinetics has also been observed in zebrafish M-cells (Ali et al., 2000b; Legendre, 1998), where GlyR mIPSCs were first observed in 26-29 hpf embryos at very low frequency, which increased several hundred folds by the time of hatching at around 48 hpf. The mIPSCs had characteristic decay time courses with two components (τ_{fast} and τ_{slow}), which progressively became faster throughout embryonic development. During this developmental period, glycinergic postsynaptic potentials shift from depolarizing in young embryos, to hyperpolarizing in larvae (Reynolds et al., 2008; Saint-Amant and Drapeau, 2000). An excitatory depolarizing effect of GlyR at early embryonic development plays important role in synaptogenesis (Drapeau et al., 1999). It has been shown that GlyR transmission at these early developmental stages induce activation of voltage-gated Ca^{2+} channels, which are crucial for postsynaptic clustering of GlyRs (Kirsch and Betz, 1998). Additionally, activation of presynaptic GlyRs is necessary for depolarization of nerve terminals and glutamate release during early postnatal development (Turecek and Trussell, 2001).

1.3.4 Calcium/calmodulin dependent protein kinase 2 (CaMKII)

Calcium/calmodulin dependent protein kinase 2 (CaMKII) is a multifunctional serine/threonine kinase that is highly abundant in the brain, constituting 1–2% of the total protein. It is enriched at synapses and is the main protein of the postsynaptic density (PSD). Neuronal CaMKII regulates important neuronal functions such as neurotransmitter synthesis and release, modulation of ion channel activity, cellular transport, cell morphology and neurite extension, synaptic plasticity and gene expression. In zebrafish (*Danio rerio*), the activity of CaMKII can be detected as early as 2 hpf and increases 100-fold by 3 days of development.

1.3.4.1 Expression profile of CaMKII genes in developing zebrafish brain

CaMKII is encoded by seven genes in zebrafish: one α gene (*camk2a1*), two β genes (*camk2b1*), two γ genes (*camk2g1* and *camk2g2*), and two δ genes (*camk2d1* and *camk2d2*) (Rothschild et al., 2007b). In situ hybridization of 72 hpf zebrafish reveals relatively small amounts of *camk2a1* mRNA in the forebrain compared with β1 (*camk2b1*), which is highly expressed in the forebrain and midbrain by 72 hpf. γ1 expression is reduced by 48 hpf, but then reappears strongly in the mid- and hindbrain by 72 hpf, while γ2 has been detected in the mid- and hindbrain at 48 and 72 hpf. Expression of δ1 mRNA is very weak in the brain, whereas δ2 is strongly expressed in the midbrain at 48hpf and in mid- and hindbrain at 72hpf. The distribution pattern of CaMKII isoforms in zebrafish demonstrates that these isoforms are expressed in a spatiotemporally regulated manner in the CNS.

1.3.4.2 Structure and regulatory mechanism

The CaMKII holoenzyme is a homo- or hetero-oligomeric complex of 12 subunits (Gaertner et al., 2004). Each subunit has three distinct domains: a C-terminal association domain, an N-terminal catalytic domain, and a regulatory domain in between (Figure 1.4). The catalytic domain contains the ATP- and substrate-binding sites, as well as sites for interaction with anchoring proteins, and inherently capable of catalyzing the phosphotransferase reaction. The sequence of amino acids 282–300 within the regulatory domain is known as the autoinhibitory domain which resembles protein substrates. This pseudosubstrate region interacts with the catalytic domain to block the ATP binding site, and inhibits the kinase activity of the enzyme. The amino acid sequence 293–310 binds calcium/calmodulin and partially overlaps with the autoinhibitory domain. Binding of calcium/calmodulin to the calmodulin binding site disrupts the interactions between the autoinhibitory and catalytic domains, activates the enzyme and exposes Thr286 on the autoinhibitory domain. The exposed Thr286 can now be phosphorylated by a neighboring subunit.

Autophosphorylation of Thr286 has two primary consequences: (1) the subsequent dissociation of bound Ca^{2+}/CaM is decreased by several folds, thereby prolonging its activation, and (2) even after full dissociation of Ca^{2+}/CaM, the kinase retains partial (30%–60%) activity (i.e., Ca^{2+}-independent or constitutive/autonomous activity). Thus, transient elevations of intracellular [Ca^{2+}] can result in prolonged CaMKII activity until protein phosphatases dephosphorylate Thr286 (Colbran, 2004a). Moreover, the extent of CaMKII autonomous activity can be dictated by the frequency of Ca^{2+} oscillations. This

mechanism is thought to be critical in several physiological situations, especially potentiation of synaptic transmission during learning and memory (Lisman et al., 2002). Once CaMKII is in the autonomous state, other sites within the calmodulin binding domain (Thr305/6) are available for phosphorylation. When these sites are phosphorylated, calmodulin can no longer bind to CaMKII and the activity of the enzyme becomes insensitive to changes in calcium/calmodulin.

CaMKII is present in the neuron as a soluble protein, which localized to the postsynaptic region in an activity dependent manner. Importantly, CaMKII constitutes the major protein of the postsynaptic density (PSD) in dendritic spines where it interacts with several proteins (Colbran, 2004b). Interaction of CaMKII with the PSD is dynamic and is regulated by binding of Ca^{2+}/CaM and the phosphorylation status of CaMKII. For instance, autophosphorylation of Thr286 promotes and stabilizes CaMKII binding to the PSD whereas autophosphorylation of Thr305/306 suppresses this interaction.

1.3.4.3 CaMKII and Synaptic plasticity

Synaptic plasticity is a property of vertebrate brain that refers to the modification of strength of synapses depending on their recent level of activity. Depending on the specific pattern of stimulation, individual synapses can increase or decrease the strength of their transmission. Short term synaptic plasticity, lasting from several milliseconds to few minutes, has been proposed to play important roles in short-term adaptations to sensory inputs, transient changes in behavioral states and short lasting memory (Citri and Malenka, 2008). A short burst of activity induces this type of synaptic plasticity by

causing transient increase of calcium in presynaptic nerve terminals. An increase in presynaptic calcium in turn activates the pathway for vesicle exocytosis, thereby increasing release probability. Several lines of study suggest that presynaptic CaMKII, predominantly associated with synaptic vesicles, regulates neurotransmitter release and short term synaptic plasticity (Wang, 2008).

The two prominent forms of long lasting synaptic plasticity, long-term potentiation (LTP) and long-term depression (LTD), have been considered as a cellular model for the process of learning and memory formation. LTP is triggered by the activation of N-methyl-D-aspartate (NMDA) receptors (NMDARs) followed by the trafficking of α-amino-3-hydroxy-5-methyl-4-isoxazole propionic acid (AMPA) receptors (AMPARs) into the postsynaptic membrane. At resting potential, AMPARs provide the majority of fast excitatory current of sodium and potassium ions whereas NMDARs become permeable only at a depolarized membrane potential due to its magnesium block that occludes the channel at resting potential. Upon activation, NMDARs allow sodium as well as calcium ions to flow into the postsynaptic cell. Several lines of study have shown that CaMKII is activated by the NMDA-receptor-mediated Ca^{2+} elevation which triggers the induction of LTP (Lisman et al., 2002). Extracellular or intracellular application of CaMKII inhibitors such as KN-62 and AIP, blocks LTP (Ito et al., 1991). Conversely, application of constitutively active CaMKII to CA1 hippocampal pyramidal cells increases AMPA receptor mediated synaptic transmission and prevents further LTP induction (Lledo et al., 1995). A specific subunit of AMPAR (GluR1) can be phosphorylated at Ser831 by CaMKII. Although phosphorylation of Ser831 enhances

channel function, it is not necessary for AMPARs trafficking. It has been proposed that the stable binding of autophosphorylated CaMKII to the NMDA receptor leads to the organization of a structural process that incorporates AMPA-receptor-binding proteins into the PSD, and subsequently anchors additional AMPA receptors (Lisman 2001).

CaMKII has also been implicated in the regulation of plasticity and synaptic transmission of inhibitory synapses containing type A (ionotropic) γ-aminobutyric acid ($GABA_A$) receptors. Application of constitutively active CaMKII increases the amplitude and prolongs the duration of β3 subunit-containing $GABA_A$ receptor mediated IPSCs in rat cerebellar granule neurons (Houston and Smart, 2006). The potentiation is a consequence of altered channel kinetics following phosphorylation of the receptor. On the other hand, CaMKII induced increase in $GABA_A$ IPSC in the hippocampus has been proposed to be the result of recruitment of new receptors to the cell surface (Wei et al., 2004).

1.3.4.4 Regulation of neuronal morphology by CaMKII

Neurite extension, branching, stabilization and maturation are important neuronal plasticity events that can lead to the addition of synaptic contacts in developing neurons, and changes in the number of synapses on mature neurons. CaMKII regulates dendritic arborization and maturation of dendritic branches (Fink et al., 2003; Wu and Cline 1998). For instance, inhibition of CaMKII by the specific CaMKII inhibitor, KN-93, leads to a rapid reduction in filopodial motility and small dendritic branching, and a longer-term decrease in the degree of dendritic arborization (Fink et al., 2003). Knockdown of

CaMKII-β expression by RNAi reduced dendritic arborization and synapse formation, whereas overexpression increased the number of synapses. CaMKII-a appeared to have opposing effect on dendritic arborization, which decreased branching and increased stabilization when overexpressed in Xenopus tectum (Wu and Cline, 1998). Together, these data suggest that CaMKII play important roles in the regulation of neuronal morphology.

1.4 Research Objectives and Aims

As previously mentioned, my research objective is to understand the role of CaMKII in synaptic development. My studies were guided by 2 main aims as presented below:

Aim 1: To characterize the expression profile of CaMKII isoforms in zebrafish Mauthner cells at the time of hatching. **Rationale:** In zebrafish, seven CaMKII genes (α, β1, β2, δ1, δ2, γ1, γ2) have been identified which are expressed in a spatio-temporally regulated manner during the early development of 24 to 72 hpf (Rothschild et al., 2009; Rothschild et al., 2007). Therefore, identifying the CaMKII isoforms expressed in Mauthner cells is a prerequisite for determining the function of different isoforms in the neurodevelopment of M-cells. **Hypothesis:** I hypothesize that M-cells at 48 hpf express *camk2a* and *camk2b*, considering their prominent expression in mammalian central nervous system (CNS) (Tobimatsu and Fujisawa, 1989).

Aim 2: To determine the role of CaMKII in the development of synaptic currents associated with M-cells. **Rationale:** The role of α and β CaMKII in neuronal

development and plasticity has been studied previously (Lisman et al., 2002; Wayman et al., 2008). However, the majority of the published literature is based on studies utilizing ex vivo preparations. While much is known about the role of CaMKII in synaptic plasticity, less is known about the role of CaMKII in synaptic development. Therefore, investigating the function of CaMKII isoforms in embryonic zebrafish will advance our understanding of its role in synaptic current development in vivo. Moreover, my research may demonstrate how development of synaptic receptors affects the excitability properties of M-cells. **Hypothesis:** Based on the existing literature, I hypothesize that CaMKII plays a role in the development of both excitatory and inhibitory synaptic currents in embryonic zebrafish.

The research in this thesis focuses on synaptic development. I present novel findings on the function of CaMKII-α in a developing organism and set the stage for future studies that aim to delineate the specific role of CaMKII-α in the development of NMDAR-containing synapses.

Table 1.1 Excitatory and inhibitory ionotropic receptor subunits.

Receptor class	IUPHAR subunit nomenclature	Zebrafish orthologs	Longest splice variant in zebrafish (amino acids)	ZFIN Accession # (followed by ZDB-GENE-)
AMPA	GluA1	*gria1a*	914	020125-1
		gria1b	917	020125-2
	GluA2	*gria2a*	917	020125-3
		gria2b	897	020125-4
	GluA3	*gria3a*	886	020125-5
		gria3b	883	030616-53
	GluA4	*gria4a*	898	020125-7
		gria4b	904	030131-8013
NMDA	GluN1	*grin1a*	966	051202-1
		grin1b	937	051202-2
	GluN2A	*grin2aa*	1460	070424-129
		grin2ab	1445	070424-223
	GluN2B	*grin2ba*	-	090821-2
		grin2bb	1770	061207-27
	GluN2C	*grin2ca*	1400	070822-3
		grin2cb	1328	100308-2
	GluN2D	*grin2da*	1916	041008-124
		grin2db	1959	100920-7
	GluN3A	*grin3a*	-	130530-780
	GluN3B	*grin3ba*	1156	070912-354
		grin3bb	961	131122-77
Glycine	α1	*glra1*	459	991117-1
	α2	*glra2*	448	090407-1
	α3	*glra3*	450	020402-1
	α4	*glra4a*	457	010410-3
		glra4b	537	020402-2
	β	*glrba*	498	010410-2
		glrbb	494	040801-106
$GABA_A$	α1	*gabra1*	459	061013-194
	α3	*gabra3*	294	091204-365
	α5	*gabra5*	491	081104-30
	α6	*gabra6a*	435	040426-1692
		gabra6b	444	080815-1
	β2	*gabrb2*	519	030131-8196
	β3	*gabrb3*	532	101102-2
	γ2	*gabrg2*	469	091118-65
		gabrg3	-	070718-5
	δ	*gabrd*	469	081105-170

Receptor class	IUPHAR subunit nomenclature	Zebrafish orthologs	Longest splice variant in zebrafish (amino acids)	ZFIN Accession # (followed by ZDB-GENE-)
$GABA_A$	π	*gabrp*	464	081028-62
	ρ1	*gabrr1*	466	040724-212
	ρ2	*gabrr2a*	475	060825-164
		gabrr2b	464	041014-174
	ρ3	*gabrr3a*	472	080722-20
		gabrr3b	308	131120-131

Figure 1.1

A

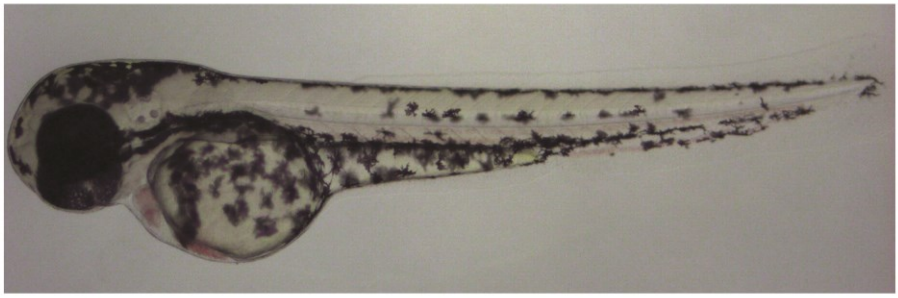

B

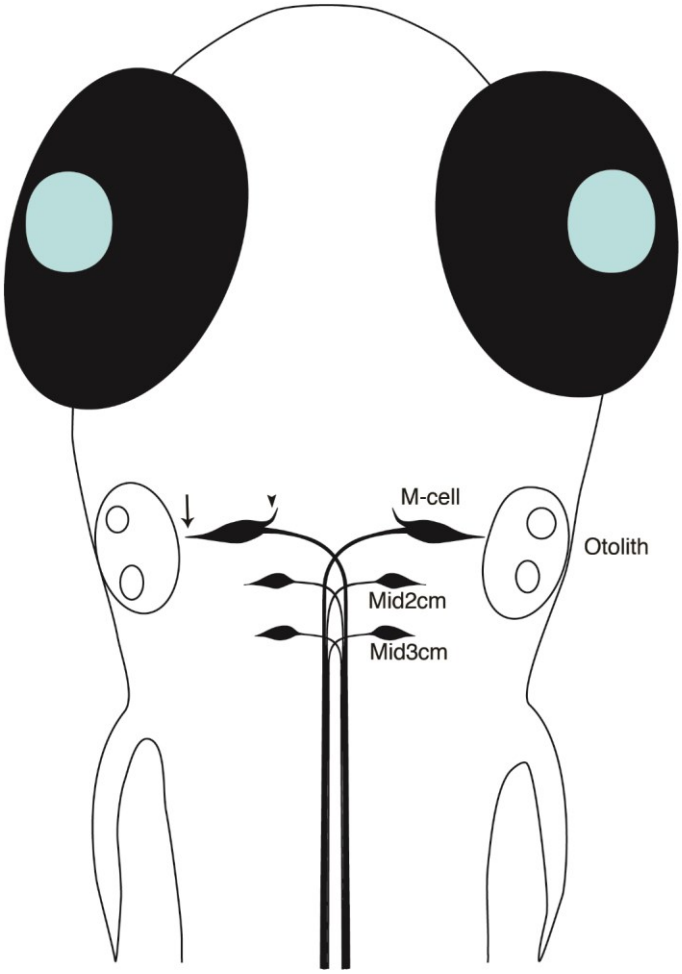

Figure 1.1 Two days post fertilization (dpf) zebrafish embryo. (A) Face view photograph. (B) Schematic representation of the zebrafish hindbrain showing the location of the Mauthner cells (M-cells), and their homologs Mid2cm and mid3cm. Arrowhead indicates ventral dendrite, arrow indicates lateral dendrite (not to sale).

Figure 1.2

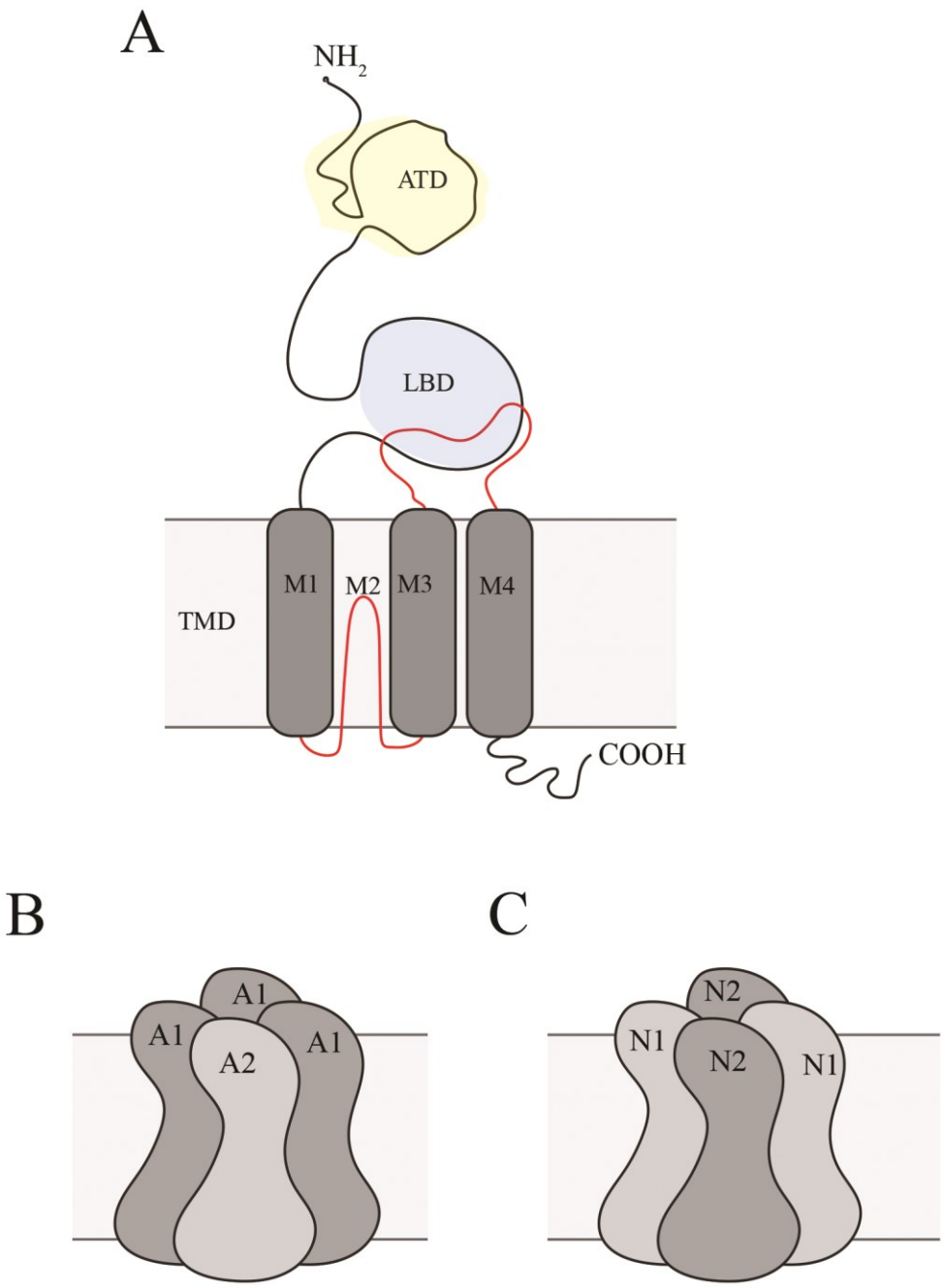

Figure 1.2 Structure and topology of excitatory ionotropic glutamate receptors. (A) Glutamate receptor subunits share common structural features, including extracellular amino-terminal domain (ATD), ligand-binding domain (LBD), the transmembrane domain (TMD), and an intracellular carboxyl-terminal (CTD). The ATD plays important roles in subunit assembly and receptor trafficking. The LBD provides the binding pocket for the receptor agonists. The TMD is composed of M1, M3, M4 transmembrane helices and M2 reentrant helix. (B) Schematic drawing of a heteromeric AMPA receptor containing GluA1 and GluA2 subunits. AMPARs with edited GluA2 exhibit low Ca^{2+} permeability and low single channel conductance. (C) Schematic drawing of diheteromeric NMDA receptors containing two obligatory GluN1 subunits and two GluN2 subunits.

Figure 1.3

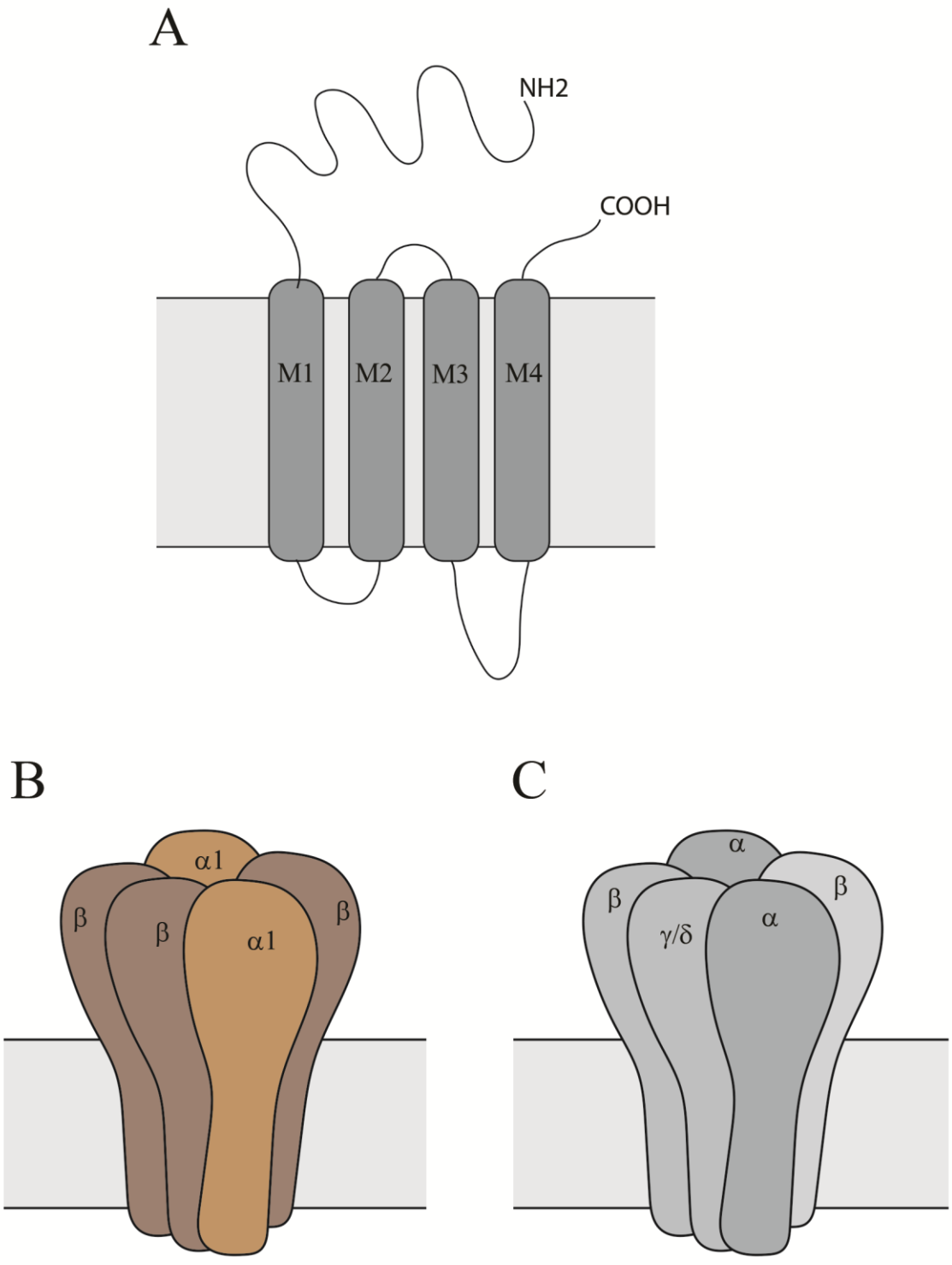

Figure 1.3 Structure and topology of glycine and $GABA_A$ receptors. (A) Topology of glycine and $GABA_A$ receptor subunits. Each subunit contains extracellular N- and C-terminus and four transmembrane domains (M1-M4). (B) Schematic drawing of a heteropentameric glycine receptor containing two $\alpha 1$ subunits and three β subunits. (C) Schematic drawing of a pentameric $GABA_A$ receptor containing α, β and δ or γ subunits.

Figure 1.4

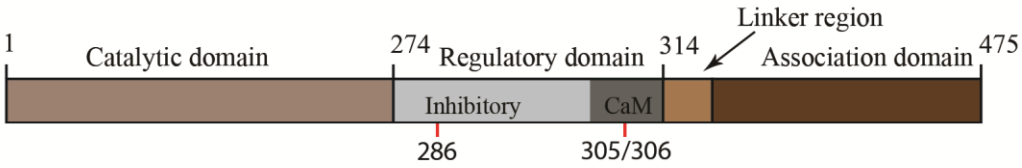

Figure 1.4 Structural organization of CaMKII subunit. Each subunit is comprised of a catalytic domain, a regulatory domain, a variable linker region and an association domain. The regulatory segment includes the autoinhibitory region (inhibitory) and calmodulin-binding region (CaM). Three critical phosphorylation sites lies in the regulatory domain: Thr 286 is located within the autoinhibitory segment, and Thr 305, Thr 306 are located within the CaM binding region (dark grey). The complete holoenzyme is composed of twelve subunits.

Chapter 2: Materials and Methods

2.1 Animals

Zebrafish wild-type AB line was obtained from the University of Oregon and raised in the aquatics facility in the Department of Biological Sciences at the University of Alberta according to established protocols (Westerfield, 2007). Embryos were raised at 28.5°C in Egg Water (60 µg/mL "Instant Ocean", United Pet Group, Cincinnati, OH, USA). Microinjected embryos were incubated in Embryo Medium (mM: 13.7 NaCl; 0.54 KCl; 0.025 Na_2HPO_4; 0.044 KH_2PO_4; 1.3 $CaCl_2$; 1.0 $MgSO_4$; 0.42 $NaHCO_3$; pH=7.2) containing Methylene Blue (Sigma-Aldrich, St. Louis, MO, USA; 0.003%) and PenStrep (Sigma; 10 mL/L). On the day of the experiment, the embryos were taken out of the incubator in the morning and kept at ambient room temperature (20-24°C) throughout the experimental procedures.

2.1.1 Dissection

Zebrafish embryos at 2 dpf were staged according to established procedures (Kimmel et al., 1995) and dissected for electrophysiology as described previously (Drapeau et al., 1999; Roy and Ali, 2013). In brief, the embryos were anesthetized in 0.02% tricaine (MS-222) (Sigma-Aldrich) and pinned through the notochord onto an electrophysiological recording chamber (Figure 2.1). After removal of the forebrain and rostral structures, the entire hindbrain was exposed to access the ventral surface (Figure 2.1B).

2.1.2 Identification of Mauthner cells

Mauthner cells were easily identified under Nomarski differential interface contrast (DIC) optics based on their morphology and location in rhombomere 4 of the hindbrain (Eaton and Farley, 1973). Occasionally, the cells were filled with 0.1% Lucifer Yellow (Sigma-Aldrich) to further confirm their identity during electrophysiological recording (Figure 2.1D).

2.2 RT-PCR

RNA was extracted from 40 whole 2 dpf embryos into 25 µl nuclease-free water using the MasterPure RNA purification kit (Epicentre Biotechnologies, Madison, MI, USA). In order to remove genomic DNA, the prepared RNA was treated with DNase I (Life Technologies, Carlsbad, CA, USA). RNA concentration was measured with a NanoDrop 1000 spectrophotometer (Thermo Fisher Scientific, Wilmington, DE, USA) and quality was confirmed by gel electrophoresis. Reverse transcription was carried out with a Maxima First strand cDNA synthesis kit (Thermo Fisher Scientific), according to manufacturer's instructions. To PCR amplify target cDNA sequences, primer pairs for each gene (Table 2.1) were designed using the Primer-BLAST program (Ye et al., 2012). The PCR reactions were carried out in a total volume of 50 µl containing 5 µl 5 µM primers, 1 µl 10 mM dNTP mix, 2.5 µl first strand cDNA, 10 µl 5X buffer and 0.5 µl Phusion high fidelity DNA polymerase (Thermo Fisher Scientific). The thermal profile was 98ºC for 30s followed by 40 cycles of amplification (98ºC for 15s, 60ºC for 30s, 72ºC for 30s) and a final amplification at 72ºC for 10 minutes. Amplified products were analyzed on a 2% agarose gel.

2.3 Single-cell RT-qPCR

2.3.1 Collection of Individual Mauthner cells

Patch-clamp pipettes with tip diameters of 0.2-0.4 μm were pulled from thin-walled borosilicate glass capillaries and backfilled with 4 μl resuspension buffer (Invitrogen, Carlsbad, CA, USA) containing RNase inhibitor and 0.1% Lucifer Yellow. The whole-cell configuration onto an M-cell was achieved and the resuspension buffer was allowed to permeate the cell for 1 minute before the cell was pulled out of the brain by visual guidance of the pipette. The cell was collected by breaking the pipette tip at the bottom of a 0.2 ml PCR tube after applying a small amount of positive pressure into the pipette. The cell was discarded if it was broken or if surrounding cells were attached to the pipette tip. The PCR tube was immediately transferred to a container filled with dry ice to prevent breakdown of cellular components. For long-term storage, the tubes were transferred to -80˚C freezer. As a contamination control, 2 μl of the perfusate surrounding the M-cell was collected in separate tubes and processed along with the single cell samples.

2.3.2 cDNA Synthesis from single cells

I used the Superscript III CellsDirect cDNA synthesis kit (Invitrogen) was used to synthesize cDNA directly from single cells into a final volume of 16.5 μl according to the manufacturer's instructions except that we reduced the recommended reaction volumes by half. Prior to the cDNA synthesis steps, samples were treated with 2.5 μl DNase I and 0.8 μl buffer at room temperature for 5 minutes to remove genomic DNA. The reaction was stopped by adding 0.6 μl of 25 mM EDTA and incubating at 70ºC for 5 minutes. cDNA synthesis was carried out using Oligo$(dT)_{20}$ primers (1 μl 50 mM primer, 0.5 μl 10

mM dNTP mix, 3 µl 5X RT buffer, 0.5 µl RNaseOUT, 0.5 µl Superscript III RT and 0.5 µl 0.1 M DTT) for 50 minutes at 50ºC followed by 5 minutes at 85ºC. Samples were then incubated with 0.5 µl RNase H (2U/µl) at 37ºC for 20 minutes to remove the starting RNA and stored at -80ºC until preamplification.

2.3.3 Construction of real-time PCR standards

Gene-specific standard curves for seven CaMKII genes, and EF1-α were prepared to quantify absolute cDNA copy number in single cell samples. Reverse transcription-PCR products were purified with QIAquick gel extraction kit (Qiagen, Maryland, USA), cloned into TOPO Vector (Life Technologies) and verified by sequencing. After transformation, plasmids were purified using the QIAprep spin miniprep kit (Qiagen) from overnight cultures, linearized and gel verified before making a serial dilution from 2 to 10^7 copies per 16.5 µl in 9 steps and stored in -80ºC freezer until needed.

2.3.4 Preamplification

A multiplex preamplification of the target genes was carried out on the single cell cDNA and plasmid DNA standards. TaqMan assays for all the genes were pooled together to give a final concentration of 1.75 µM for each primer. The preamplification reactions were carried out by combining 1 µl of the assay mix with 16.5 µl of cDNA or plasmid DNA sample, and 17.5 µl of 2X TaqMan PreAmp Mastermix (Applied Biosystems, CA, USA) and running 1 cycle of 95ºC for 10 minutes followed by 14 cycles of 95ºC for 15 s and 60ºC for 4 min. Preamplified products were diluted to 1:10 for downstream application.

2.3.5 Quantitative real-time PCR

The quantitative real-time PCR assays were designed by using the Universal ProbeLibrary Assay Design Center (Roche Diagnostics GmbH, Mannheim, Germany) and carried out with the 7500 Fast system (Applied Biosystems). qPCR Primers (Table 2.2) were designed so that they were separated by an intron. Each reaction (10 µl) contained 2.4 µl of cDNA, 2.5 µl of 1.6 µM forward and reverse primer mix, 0.1 µl of probes (Roche Diagnostics) and 5 µl of 2X FastStart TaqMan Probe Master (Rox) (Roche Diagonstics). The thermal profile included an initial cycle of 95ºC for 10 min followed by 45 cycles of 95ºC for 30 s, and 60ºC for 1 min. The standards were run in triplicate, single cell samples in duplicate, and the threshold cycle (Ct) was determined automatically by SDS software (Applied Biosystems). Ct values were averaged and 1 cycle was subtracted from the measured Ct values of the samples because the standards were double-stranded molecules. Data were presented as the absolute number of cDNA molecules per cell, which represent the lower limit estimate of the actual mRNA molecules in the cell (Stahlberg et al., 2011). I determined the limit of detection (LOD) as the Ct value for the lowest copy number standard in which all three replicates were positive. All data points below the LOD were removed from analysis.

2.4. Morpholino oligonucleotide mediated knockdown of *camk2a*

2.4.1 Morpholino design

Two separate antisense morpholino oligonucleotides (MO), obtained from Gene Tools LLC (Philomath, Oregon, USA) were used to knockdown *camk2a* expression. The translation-blocking MO, 5'-GCCATCCTGGAAGCGTGTGCGCCTC-3' was

previously used and validated for its specificity in zebrafish (Francescatto et al., 2010). The splice-blocking MO, 5'-GCTGATCTGAGCACCTACCCCGAGT-3', was designed to target the splice junction between exon 2 and intron 2 of *camk2a* pre-mRNA. A fluoresceinated MO, 5'-CCTCTTACCTCAgTTACAATTTATA-3', targeted against human beta-globin gene that does not bind to any known mRNA sequence in zebrafish was used as a standard negative control. MOs were diluted in sterile water to make a stock solution of 1 mM and stored at 4°C.

2.4.2 Microinjection

MO stock solutions were diluted and injected according to established guidelines (Bill et al., 2009). In brief, MO stocks were diluted in 1x Danieau solution (mM: 58 NaCl, 0.7 KCl, 0.4 MgSO4, 0.6 $Ca(NO_3)_2$, 5.0 HEPES, pH 7.6) containing 0.05% Phenol Red. Each MO was injected in three different concentrations – 1, 2 and 4 ng/nL to determine the highest dosage. Most MOs show specific knockdown at a dose of 5 ng or less, while injection of 6 ng or more sometimes can cause off-target effects (Bill et al., 2009). Therefore, I limited the highest dose to 4 ng in my experiments. None of the three MOs showed toxicity or mortality at 4ng/nL. This concentration was therefore chosen for subsequent experiments. MOs were delivered into one to four cell stage embryos using a Picospritzer II (General Valve Corporation, Fairfield, NJ, USA) Microinjection System calibrated to eject 1 nL solution consistently from microinjection needles.

2.4.3 Knockdown assessment

RT-PCR was performed to assess the level of knockdown by the splice blocking morpholino using a forward primer TCTCTCAGGGCAAGAGTATGC, and a reverse primer AAGATGAGGTAGTGGTGGCCT. Blot densities were measured using ImageJ software (Rasband, 1997-2014). Embryos at 2 dpf were used for RNA extraction and cDNA synthesis as previously described.

2.4.4 Western blot

Adult zebrafish brains or whole larvae (1.5, 2 and 3 dpf) were rapidly dissected in ice-cold physiological saline, placed in either sucrose buffer (in mM: 320 sucrose, 0.01 EDTA, 10 Tris–HCl, pH 7.4) or Tissue-PE LB buffer (G Biosciences, St. Louis, MO, USA) containing protease inhibitors (3mM PMSF, 40 μM leupeptin, 4 μM pepstatin A, 0.4 mg/ml aprotinin) and immediately placed on dry ice. We found no difference in the protein content of tissue homogenized in either of these two buffers. Whole brains were homogenized by hand with a Dounce tissue homogenizer and centrifuged at 13,000 X g for 5 min. The supernatant was removed to quantify the protein content and the pellet was discarded. Protein quantification was performed using the Lowry Protein Assay (Bio-Rad, Hercules, CA), and 50 μg of zebrafish homogenate was loaded per lane. Samples were subjected to SDS-PAGE (10%) and transferred to nitrocellulose membranes using a semi-dry transfer apparatus (Bio-Rad). Membranes were blocked in blocking buffer (5% skim milk powder, 0.1% Tween-20 in TBS) for 1 h at room temperature and incubated in rabbit polyclonal anti-CaMKII (pan) (Cell Signaling Technology, Danvers, MA, USA; 1:1000), or anti-Actin (Sigma-Aldrich, 1:2000) primary antibody overnight at 4°C.

Membranes were washed 5 times in TBS-T and incubated in secondary antibody coupled to horseradish peroxidase (HRP; 1:50,000 goat anti rabbit IgG, Santa Cruz Biotechnology) for 1 h at room temperature on a shaker. An enhanced HRP substrate (SuperSignal West Pico, Pierce, Rockford, IL) was added to the membrane and the resulting chemiluminescent signal was captured on X-ray film. Negative controls were performed whereby the primary antibody was pre-incubated with recombinant full length human CaMKII-α in a ratio of 1:5 overnight. This incubation mixture was then used as the primary antibody.

2.5. Electrophysiology

2.5.1 Recording solutions

Following dissection, the preparation was moved to a recording set-up and the chamber was continuously perfused with an aerated recording solution at room temperature (20-24^{o}C) that contained 15 μM D-tubocurarine (Sigma–aldrich), but lacked tricaine. Unless otherwise stated, synaptic currents were recorded at a holding potential of -60 mV, which approximate the normal resting membrane potential of M-cells of 2dpf zebrafish (Table 4.1). The extracellular recording solution contained (in mM) 134 NaCl, 2.9 KCl, 2.1 $CaCl_2$, 1.2 $MgCl_2$, 10 HEPES, and 10 glucose, with osmolarity adjusted to 285 mOsm, pH 7.8. $MgCl_2$ was excluded from extracellular recording solution for NMDA miniature excitatory postsynaptic potential (mEPSC) recording. Tetrodotoxin (TTX, 1 μM) was included in all recordings to block action potentials. Patch-clamp electrodes were pulled from borosilicate glass and had resistances of 3-5 MΩ when filled with a CsCl solution. The CsCl intracellular solution was composed of (in mM)

140 CsCl, 2 $MgCl_2$, 10 HEPES, 10 EGTA, 4 Na_2ATP, 0.4 LiGTP, osmolarity adjusted to 295 mOsm, pH 7.4.

2.5.2 Isolation of receptor-specific miniature postsynaptic currents

Different combinations of the following drugs were used to isolate receptor-specific currents: kynurenic acid (1 mM), strychnine (5 μM), picrotoxin (100 μM), APV (50 μM) and NBQX (0.1 μM) to block Glycine, GABA, NMDA and AMPA receptor mediated currents respectively. Effective concentration of NBQX for blocking synaptic AMPAR mEPSCs was determined empirically by varying its concentration in the recording solution in the following order (in μm): 2, 1, 0.5 and 0.1.

2.5.3 Neuronal depolarization by a 10 mM K^+ depolarizing medium

Whole cell configuration was achieved using the previously described recording solution in voltage clamp configuration. After recording baseline synaptic activity, the configuration was switched to I=0 mode and depolarization of the Mauthner cell was induced by applying a 5-minute bath of 10 mM K^+ depolarizing medium that contained (in mM): 125 NaCl, 10 KCl, 2.1 $CaCl_2$, 0.3 $MgCl_2$, 10 HEPES, and10 glucose, osmolarity adjusted to 285 mOsm, pH 7.8. To reduce Ca^{2+} buffering capacity of the CsCl internal solution, EGTA concentration was lowered to 0.2 mM in all experiments involving depolarization of the M-cell. Depolarization of the M-cell and increased synaptic activity was monitored throughout the 5-minute period. At the end of the depolarization, the cell was allowed to return to the normal resting potential by switching to regular extracellular recording solution. Synaptic activity was recorded again in voltage clamp mode.

2.5.4 Data Acquisition

Whole cell currents were recorded using an Axopatch 200B amplifier (Molecular Devices, Sunnyvale, CA, USA) and were low-pass filtered at 5-10 kHz (-3 dB) and digitized at 50 kHz. After establishing whole-cell recording mode, series resistance was compensated by 60-85 % using the amplifier's compensation circuitry. Data was discarded if series resistance changed by more than 20 % or when membrane potentials were more positive than -45 mV. The liquid junction potential after going whole cell was not corrected.

2.5.5 Analysis of spontaneous miniature postsynaptic currents

Synaptic activity was monitored using pClamp 8.1 software (Molecular Devices). Synaptic events were detected using the template function for events >3 standard deviations above the basal noise and analyzed with Axograph X (AxoGraph Scientific, Sydney, Australia). The software detected all events that could be recognized visually. All events were then inspected visually, and those with uneven baselines or overlaying events were discarded. Identified events from a single recording trace were averaged and analysis was carried out on the averaged events unless otherwise stated. The rise times were defined as the time from 20 to 80% of the miniature current amplitude. The presence of one or two exponential components during the decay phase of the miniature currents was tested by visually comparing the single and double exponential fits over the entire range of the decay. For events with double exponential fits, single exponential fits over the fast and slower decay regions were compared. Lastly, the sum of the squared

errors of the single and the double fits were compared using Student t-tests to determine the best exponential fit of the decay phase.

2.6 Immunohistochemistry

Zebrafish 2 dpf embryos were fixed in 2% paraformaldehyde for 1–2 h. Tissues were washed several times in PBS and permeabilized for 30 min in 4% Triton-X 100 containing 2% bovine serum albumin (BSA) and 10% goat serum. Following permeabilization, tissues were incubated in the primary antibodie anti-3A10 (Developmental Studies Hybridoma Bank, University of Iowa, Iowa, USA, 1:250) for 48 h at 4°C on a shaker. Tissues were then washed several times in PBS over a 24 h period, and then incubated in the secondary antibodies conjugated with Alexa 488 (Molecular Probes, Carlsbad, CA, 1:1000) for 4–6 h at room temperature. Animals were washed in PBS several times, de-yolked, cleared in 70% glycerol and mounted. Z-stack images were photographed using a Zeiss LSM 510 confocal microscope equipped with a 63X oil immersion objective, and compiled using Zeiss LSM Image Browser software. The z-stack fluorescent images were deconvolved using Huygens Essential (Scientific Volume Imaging, Hilversum, The Netherlands) software, and 3D rendering of the cell body and dendritic arborizations were carried out using Imaris software package (Bitplane Scientific Software, South Windsor, CT, USA).

2.7 Behavioral assay

Video observation of 2 dpf zebrafish embryos was performed using an AOS video camera (AOS S-PRI 1995; 1250 FPS; shutter speed: 800 μs; 2700 frames per sequence)

mounted on a dissecting microscope. Embryos were immobilized for behavioural observation in 2% low-melting point (26-30°C) agarose (LMPA) dissolved in embryo medium (2-Hydroxyethylagarose, type VII low gelling temperature, Sigma–Aldrich). The LMPA was made up in 50 mL aliquots and left to dissolve in a 66°C water bath for approximately one hour. After the LMPA was fully dissolved, 10-12 embryos were transferred to a 35 mm petri dish in a small amount of embryo medium and the LMPA was cooled to 32°C in an ice bath. The embryo media was replaced with approximately 2 mL of LMPA and was then left to solidify. To observe embryo movements, the LMPA was cut away from the embryo's tails while leaving the heads embedded in the gel. Embryo media was added to the petri dish to ensure that the larvae remained immersed in solution. Embryo stimulation was performed using a pulse of basic 2% phenol red (Sigma-Aldrich) dissolved in egg water ejected from a Picospritzer II (General Valve Corporation); the pulse lasted approximately 15-20 milliseconds (ms) with a pressure of approximately 35-55 pounds per square inch (psi) of pressure. The pipette was positioned close to the otolith without contacting the embryo. Borosilicate glass micropipettes (Sutter Instrument; O.D.: 1.2 mm, I.D.:094 mm, 10 cm length) were pulled using a Flaming/Brown Sutter Instrument pipette puller (model P-97; heat: 459, Vel: 70, Time: 200). The video-recordings were transferred and analyzed using a Motion Analysis Software, ProAnalyst® (Xcitex Inc, Cambridge, MA, USA).

2.8 Statistical analysis

All data values are given as means ± SEM. Correlations were calculated with the use of a least-squares linear regression analysis. Significance was determined using paired

and unpaired t-test. One-way analysis of variance with the Student Newman-Keuls Method of post-hoc testing was used for multiple comparisons of normally distributed, equal variance data. Kruskal–Wallis ANOVA and Dunn's method of comparison were used for non-normal distributions.

Table 2.1 List of primer pairs designed for RT-PCR of cDND from 2 dpf zebrafish embryos.

Gene	**GenBank Accession No.**	**Primer Sequence (5'→3')**	**Length (bp)**
camk2a	NM_001017741.2	CCAGTCCGAAGAGACACGAATC	181
		CCAATGGAGTTCAAGGAAACGA	
camk2b1	NM_001271393	TACCTGTCCCCCGAGGTGCTG	522
		TGCCTCCAGTGCAGGAGAGGG	
camk2b2	XM_001338641.2	TGTGCGAAACTCAGCACGGGT	863
		CTGCCCACGGAGAAGTTGCG	
camk2d1	NM_001114708.2	CTCCACTGCCACCAGATGG	272
		CAGAAAGGAGGGTAACCCACAA	
camk2d2	NM_001002542.1	CGGCTGTTAAGCTTGCTGACT	173
		CAGCAGAATGTAGAGGATCACACC	
camk2g1	NM_001030125.1	AGCAGCAGAGGCATCGACCCC	581
		AACCAGGTGTCCCAGCAAAACCAAA	
camk2g2	XM_001332303.2	CCGGAGACACCACAGAGGCGA	868
		GGAGCGTTGGCAGACCCATGG	
ef1a	NM_131263.1	CCCTGCCAATGTAACCACTGA	263
		CGATGTGAGCAGTGTGGCA	

Table 2.2: List of qRT-PCR primers.

Gene	UPL Probe No.	Primer Sequence (5'→3')	Amplicon Length (bp)
camk2a	78	TGGCAGATAGTCCATTTCCAC	78
		CCTGCGACTGTTTTCAACTG	
camk2b1	78	CTTTCTGGGACGAGGATCAG	78
		CCCATTCTGGAGATGGAAAA	
camk2b2	78	AACACCAAGAAGCTCTCAGCTC	72
		TTTTAGCAGACGGCAGATCC	
camk2d1	94	GTACAGGGAGACCAGCAAGC	96
		TACGGGTTTGCCATAAGGTT	
camk2d2	94	TTGGTTTGGCCATTGAGGTC	110
		CGGTTTGCCATAAGGATCTTTC	
camk2g1	133	CGACCAGGTTTACGGACGAG	98
		TTCCTGGCCAGTGGATTTTT	
camk2g2	78	TGAGGACCAGCACAAACTGT	67
		CCACTCTGGAGAGGGAAAATC	
ef1a	94	ACATCCGTCGTGGTAATGTG	94
		GGGTGGTTCAGGATGATGAC	

Figure 2.1

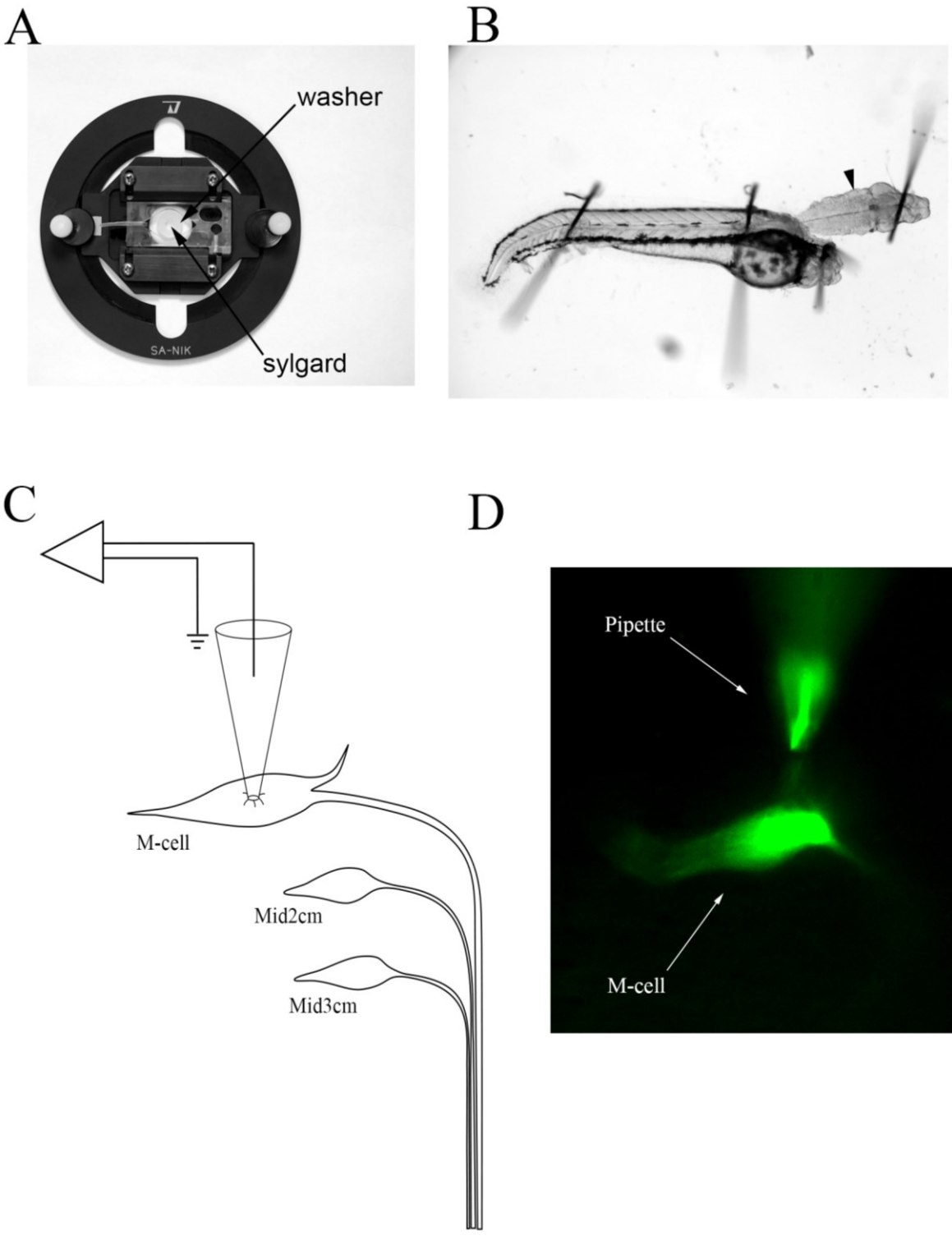
A
washer
sylgard
SA-NIK
B
C
M-cell
Mid2cm
Mid3cm
D
Pipette
M-cell

Figure 2.1 Setup for electrophysiological recording from zebrafish M-cells. (A) Dissecting and recording dish obtained from WPI. A thin washer is carefully sealed onto the glass slide at the bottom of the dish and Sylgard is applied to the well. (B) 48 hpf hindbrain-spinal cord preparation. The ventral surface of the hindbrain is facing up and the M-cell is located just beneath the surface of the tissue at the level of the arrowhead. (C) Diagram outlining whole-cell patch clamp recording setup. (D) Fluorescent image of a Mauthner cell of a 2 dpf embryo. The image was taken after recording spontaneous excitatory synaptic activity from the M-cell. The cell was filled with lucifer yellow during the experiment.

Chapter 3: Expression of the *camk2a* gene and its regulation of dendritic branching in embryonic zebrafish Mauthner cells [1]

3.1 Introduction

The temporal and spatial distribution patterns of *camk2* genes have been reported in many organisms including rat, mouse, zebrafish and drosophila (Bayer et al., 1999; Rachidi et al., 1999; Rothschild et al., 2007; Takaishi et al., 1992; Tobimatsu and Fujisawa, 1989). In zebrafish seven genes, namely α, β1, β2, γ1, γ2, δ1, and δ2, encode CaMKII. Using in situ hybridization of whole mount zebrafish Rothschild et al (2007) demonstrated expression of these genes at varying degrees in embryonic zebrafish brain. For example, during 24 to 72 hpf development expression of α gene (*camk2a1*) appears to be low in zebrafish brain while β1 (*camk2b1*) mRNA is present in the forebrain at 48 hpf and in mid- and forebrain by72hpf. Expression of γ1, γ2 and δ2 transcripts was also detected in varying degree in different brain areas during this developmental stage. CaMKII activity increases progressively throughout development. While the activity was stable between 4 and 12 hpf, it increased 100-fold by 3 dpf, and gradually levelled off around 6 dpf. These studies provided valuable information about which CaMKII transcripts are expressed in the hindbrain at 2 dpf, the developmental stage that is the focus of my study. But individual cells, even in a seemingly homogenous tissue, show cell-to-cell variation in mRNA and protein expression (Blake et al., 2003; Cai et al.,

[1] A version of this chapter has been published: Roy, B., Ferdous, J., and Ali, D.W. (2015). NMDA receptors on zebrafish Mauthner cells require CaMKII-α for normal development. *Developmental Neurobiology* 75(2):145-62.

2006; Elowitz et al., 2002). Therefore, I set out to determine the isoforms of *camk2* that are expressed specifically in M-cells of embryonic zebrafish at the time of hatching.

Normal expression of CaMKII is required for proper neuronal development. Neurons are dynamic cells whose dendrites change structures throughout the lifespan. Dendritic architecture specification is driven primarily by cell intrinsic genetic control mechanisms during early development, while input-specific activity-dependent mechanisms take over during later development and maturation stages (Metzger, 2010). Dendritic growth is rapid during early development, with frequent addition and removal of dendritic branches. As development progresses, dendritic growth slows and the branches become stable and mature. CaMKII plays important roles in dendritic stabilization and maturation. For example, Wu and Cline (1998) demonstrated that in *Xenopus* retinotectal neurons, dendritic arborization slowed down with the onset of CaMKII expression. Overexpression of constitutively active CaMKII reduced dendritic growth in young neurons, and stabilized dendritic structures in more mature neurons, while inhibition of CaMKII activity led to increased dendritic growth, neurite complexity and branch dynamics (Wu and Cline, 1998; Zou and Cline, 1999). Similarly, CaMKII regulates dendritic branching and maturation in rodent dorsal horn interneurons (Pattinson et al., 2006). For example, mice expressing a mutant version of CaMKII had significantly greater dendritic branching, while synaptic maturation of these neurons required autophosphorylation of CaMKII-α. The role of CaMKII-α in stabilizing dendritic processes is also conserved in adult brain, where conditional deletion of CaMKII-α from neural progenitor cells led to adult born granule cells with increased dendritic complexity

and a reduction in the number of mature synapses (Arruda-Carvalho et al., 2014). In line with altered morphological development, the newly generated granule cells also showed impaired hippocampus-dependent learning. A mouse strain that harbors a heterozygous null mutation for CaMKII-α shows profound abnormalities in brain structures and behaviour (Yamasaki et al., 2008). For example, these mice had impaired neuronal development in the dentate gyrus, where the number of immature neurons increased significantly. These mice also exhibited behavioral deficits such as severe working memory deficit and exaggerated infradian rhythm. Together, these data suggest that CaMKII-α is necessary for the stabilization and maturation of dendritic branches and development of normal behaviour. Therefore, following the determination of *camk2* expression in 2 dpf M-cell, I knocked down the expression of the predominant transcript to investigate its roles in the development of M-cell dendrites and the touch response of zebrafish embryos.

3.2 Results

3.2.1 Expression of camk2 genes in zebrafish 2 dpf embryos

I began by identifying the *camk2* genes that are expressed in 2 dpf whole embryos by reverse-transcription PCR. RNA from whole zebrafish embryos was reverse transcribed and the cDNA was PCR amplified with gene-specific primer pairs (Table 2.1). Zebrafish elongation factor 1 alpha (*ef1a*) was used as a positive control for successful RNA extraction and cDNA synthesis. I found that 2 dpf zebrafish embryos express all seven *camk2* genes (Figure 3.1). PCR products were detected as single bands at the expected molecular weights ranging from 100 to 900 base-pairs (bp) except for the *camk2b1* PCR product, which was detected as multiple bands, possibly due to non-specific amplification. I sequenced the amplified PCR products of the expected molecular weights and found that the primers were amplifying the intended sequences of all seven isoforms.

3.2.2 Mauthner cell-specific expression of camk2 genes

Next, I used quantitative real-time PCR to determine the expression of these seven genes in M-cells at the time of hatching. To make the calibration curves for real-time PCR, I prepared specific DNA standards for each gene by cloning the reverse transcription PCR products and serially diluting them to 2, 10, 10^2, 10^3, 10^4, 10^5 and 10^6 copies. To maintain the integrity of the standards over the entire period of the study, I used the cloned reverse transcription PCR products to construct the standards instead of directly using the purified PCR products (Dhanasekaran et al., 2010). The plasmid was linearized before making the serial dilution to prevent copy number overestimation (Hou et al., 2010). The resulting standard curves had high coefficient of determination ($R^2 \geq$

0.993) and obtained PCR efficiencies ranging from 91% to 105% (Table 3.1). I then plotted the input copy number of the standards against output copy numbers and calculated 95% confidence intervals, illustrating a high level of detection sensitivity over the entire range (Figure 3.2).

I used qPCR to analyze 19 single M-cells for *camk2* expression. Ubiquitously expressed *ef1a* was used as an indicator for successful single cell processing. *ef1a* was not detected in 3 of the 19 cells and expression of *camk2* was only detected in cells where *ef1a* was also detected (Figure 3.3). The control sample, which consisted of extracellular solution taken from a region surrounding the M-cells (ECS in Fig 3.3), showed no detectable amplification. I found that none of the cells expressed CaMKII-β1, β2, γ1 or γ2 genes at detectable levels. Only one of the 16 cells expressed *camk2d1* at a calculated copy number of 12 copies. The gene for *camk2a* showed the highest level of expression, which was detectable in 14 cells (87.5% of the cells). The calculated copy numbers of *camk2a* and *ef1a* are shown in box plots in Figure 3.4A. The expression followed a log-normal distribution as is commonly seen in biological samples (Figure 3.4B) (Bengtsson et al., 2005). The copy number of *camk2a* in a single M-cell varied widely, from a low value of 3 to a high of 155, with a geometric mean of 8 copies per cell. Thus, my results suggest that the primary CaMKII isoform present in M-cells at the time of hatching is CaMKII-α.

3.2.3 Morpholino knockdown of CaMKII-α

To investigate a possible role of CaMKII-α during development, I knocked down its expression in zebrafish embryos using two different morpholinos. The first morpholino was a translation-blocking CaMKII-α morpholino that had been previously validated by CaMKII peptide assay (Francescatto et al., 2010), while the second was a splice-blocking morpholino designed to remove exon 2 from the transcript, which encodes part of the CaMKII-α catalytic domain. I reasoned that if the enzyme was involved in excitatory neurodevelopment, then its reduction might lead to alterations in cell morphology, synaptic activity and behavior (Wu and Cline, 1998; Yamasaki et al., 2008). Injection of 4 ng/nl of either morpholino resulted in embryos that were smaller than controls and which sometimes exhibited curved tails (Figure 3.5). I performed RT-PCR on whole embryos to confirm that the splice-blocking morpholino reduced the levels of CaMKII-α mRNA (Figure 3.6) and found that there was a 57% reduction in the levels of CaMKII-α mRNA in morphants compared with uninjected embryos and a 47% reduction compared with control injected embryos (Figure 3.6; $n=5$; $p<0.001$, one-way ANOVA, multiple comparison with Student-Newman-Keuls Method), confirming the knockdown of CaMKII-α.

To determine the extent of knockdown at the protein level, I attempted to perform SDS PAGE and immunoblotting with a pan-CaMKII antibody (Figure 3.7). Mouse brain lysate (15 mg/lane) was used as a positive control. A polyclonal antibody raised against N-terminal region of human CaMKII detected a 50 kDa band, the expected size for CaMKII-α, in both mouse tissue and in the adult zebrafish CNS tissue (Figure 3.7a, left

panel) (Barria et al., 1997a). A 60 kDa band, possibly corresponding to CaMKII-β, was also detected in the adult zebrafish CNS tissue (Figure 3.7a). A negative control was performed by preincubating the primary antibody with recombinant human CaMKII-α and then using the mixture as the primary antibody. No protein band was detected in these pre-absorbtion controls (Figure 3.7a, right panel). Unfortunately protein bands were not detected with tissue samples from whole embryos (1.5-3 dpf), although loading control experiment with anti-actin antibody on the same membrane following stripping of anti-CaMKII showed similar bands in all zebrafish samples (Figure 3.7b). Therefore, I was not able to determine the reduction in protein levels in the morphant embryos.

3.2.4 Dendritic branching on Mauthner cells is altered in camk2a morphants

De-regulation or reduction of CaMKII activity increases dendritic arborization in other vertebrates (Cline, 2001; Pattinson et al., 2006; Zou and Cline, 1999). To determine if this was also the case in zebrafish, I immunolabelled M-cells with an antibody targeted against the neurofilament 3A10 and examined the M-cells of morphants and controls for evidence of altered dendritic branching. Because 3A10 identifies many neuronal structures in addition to the M-cells, z-stack confocal images were deconvolved and a three-dimensional rendering of the M-cell was constructed to distinguish its morphological features from other CNS structures. Determination of M-cell dendritic branching was carried out on the 3D rendering using Imaris software package. I found that morphants had an increased number of dendritic branches on ventral dendrites compared with control-injected fish (Figure 3.8; $p= 0.029$, Mann-Whitney U test). For instance, in 48 hpf control embryos there were no additional branches emanating from the

ventral dendrites or cell bodies, but in the splice-blocked morphants we found several additional branches projecting from both the ventral dendrites and the cell soma. Evidence of dendrites branching from the M-cell soma is unusual and was only present in the morphants.

3.2.5 CaMK2–α is required for normal development of zebrafish escape response

Since the M-cells are involved in escape responses, and it appeared that the reduction in CaMKII-α altered M-cell morphology, I performed a behavioral analysis of the c-start escape response following a touch stimulus to assess the effect of CaMKII–α knockdown. I embedded fish in agar but then cut away the agar surrounding the trunk and tail of the embryo, as well as a small section of agar on one side of the head in order to stimulate the fish. I then pico-spritzed a jet of fluid onto the head near the otolith, which produced an escape response of the embryo. The responses were recorded and analyzed from the initiation of the response. I compared various parameters of the first major bend of the trunk, which represents the c-bend, as well as the second bend that represents the onset of swimming following the c-start (Figure 3.9). I found no difference in the maximum angle of the c-start (Figure 3.10A) but the translation-blocked morphants took a longer time to reach the maximum bend angle compared with controls (Figure 3.10B; $p<0.05$, Kruskal-Wallis ANOVA, multiple comparison test with Dunn's method). Furthermore, the second bend of the trunk took a significantly longer time to occur in both morphants compared with the controls (Figure 3.10C; $p<0.001$ for translation blocked morphants, and $p<0.05$ for splice blocked morphants, Kruskal-Wallis ANOVA, multiple comparison test with Dunn's method). In the control injected fish the time of the second bend was 30.1 ± 1.5 ms (n=18), while it was 74.1 ± 11.5 ms (n=14) in the

translation blocked morphants and 42.9 ± 2.3 (n=13) in the splice-blocked morphants. In addition, I found that of the splice-blocked morphants, 13 of 26 fish displayed abnormal responses by bending once during the c-start, and then stopping their movement, or by not responding to the stimulus at all. Additionally, 5 of 19 fish in the translation-blocked group, and 2 of the 14 fish in the splice-blocked group responded abnormally by turning towards the stimulus, while 1 of 19 control injected fish and 1 of 15 uninjected fish responded abnormally (Figure 3.10D; p= 0.221, Chi-square test). These data indicate that knockdown of CaMKII-α resulted in abnormal escape response.

Table 3.1 Characteristics of the real-time PCR standard curves.

Gene	**Slope**	**Y Intercept**	**R^2**	**PCR Efficiency (%)**
camk2a	-3.24318	29.89442	0.995368	103.3947
camk2b1	-3.56875	34.58887	0.994586	90.6383
camk2b2	-3.25046	29.53241	0.995697	103.0716
camk2d1	-3.2969	30.17769	0.993664	101.0552
camk2d2	-3.21457	28.42632	0.998021	104.6839
camk2g1	-3.3246	29.742	0.9985	99.8886
camk2g2	-3.24705	29.29339	0.995874	103.2228
ef1a	-3.32544	30.22648	0.993261	99.8538

Figure 3.1

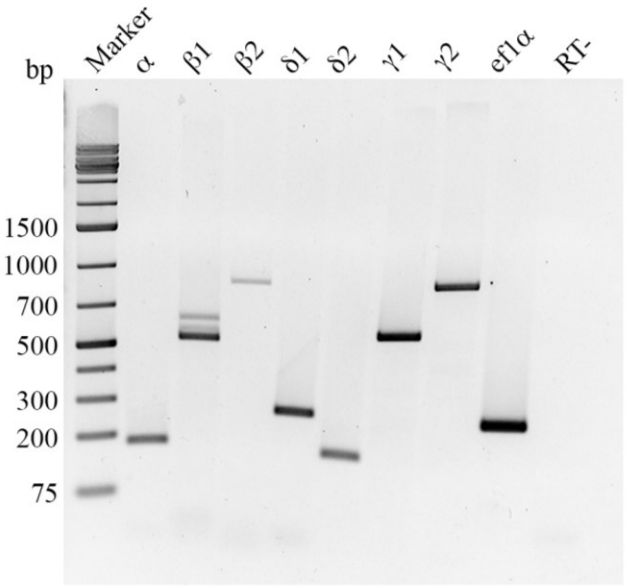

Figure 3.1 Two dpf zebrafish embryos express all seven CaMKII genes. RNA from 40 embryos were extracted, reverse transcribed and PCR amplified with eight gene-specific primer pairs. Zebrafish elongation factor 1 alpha (EF1-α) was used as a positive control. RT-: no reverse transcriptase in the reaction.

Figure 3.2

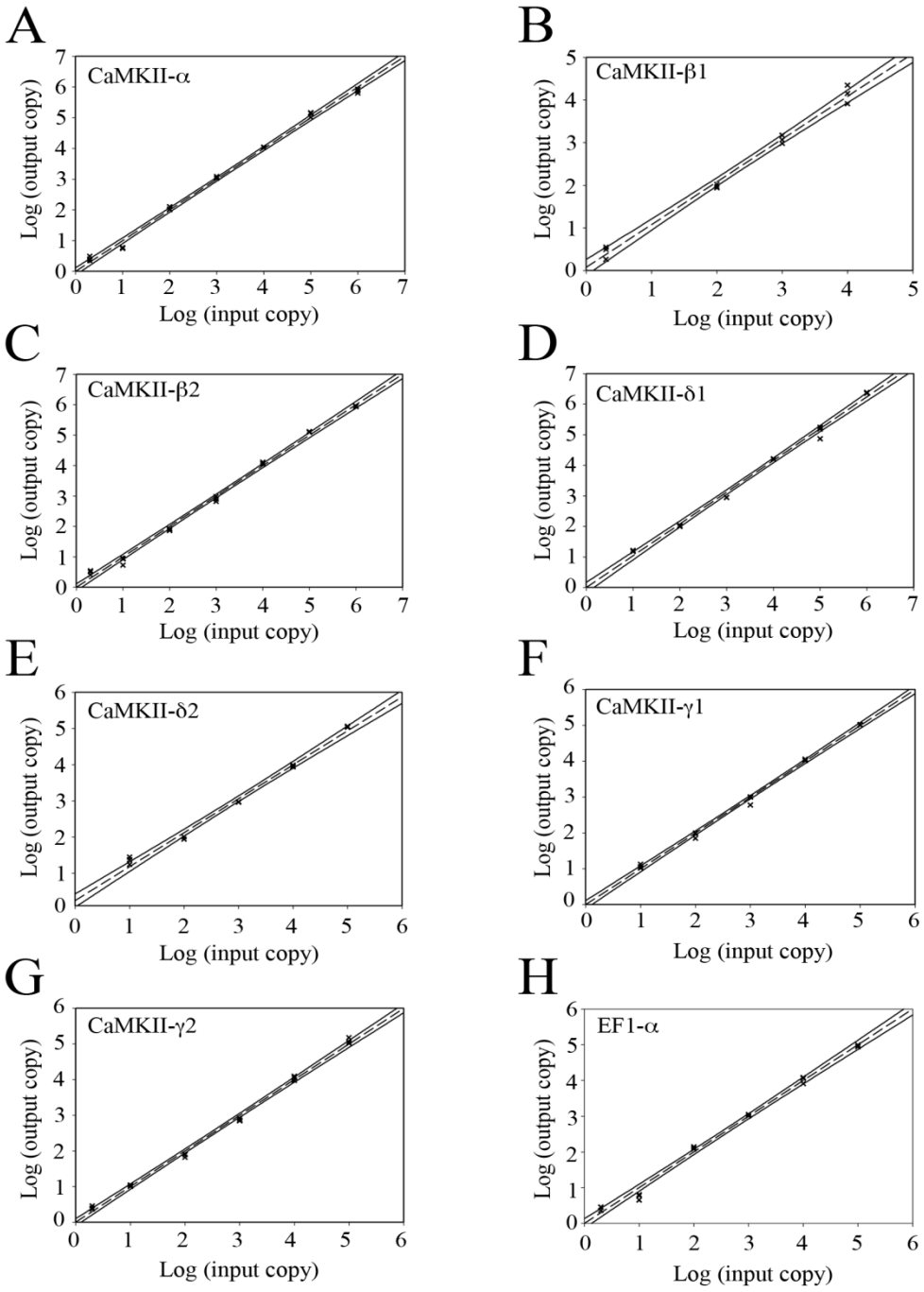
A
CaMKII-α
B
CaMKII-β1
C
CaMKII-β2
D
CaMKII-δ1
E
CaMKII-δ2
F
CaMKII-γ1
G
CaMKII-γ2
H
EF1-α
Log (output copy)
Log (input copy)

Figure 3.2 Measurement of output copy numbers for an input of pre-amplified DNA standards of known copy numbers ranging from 2 to 10^6. Linear regression lines and 95% confidence intervals are shown. Each data point was measured in triplicate.

Figure 3.3

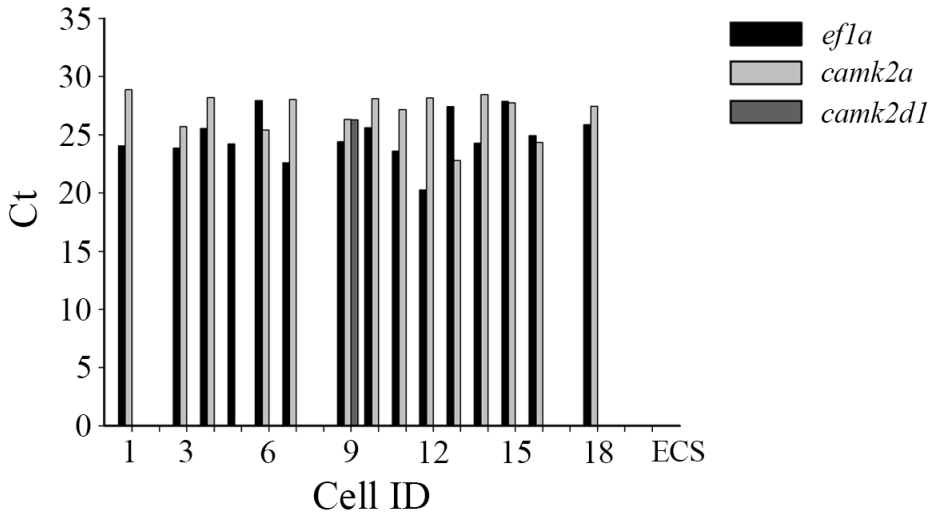
35
30
25
20
15
10
5
0
Ct
1
3
6
9
12
15
18
ECS
Cell ID
ef1a
camk2a
camk2d1

Figure 3.3 Zebrafish M-cells express primarily *camk2a* transcripts. Expression of housekeeping gene *ef1a* indicates successful cell processing. An arbitrary Ct value of 0 was assigned when any particular gene was undetectable. Note that only one cell (ID: 9) expressed CaMKII-δ1 at detectable level. The control sample consisted of extracellular fluid (ECS) taken from a region surrounding the M-cell.

Figure 3.4

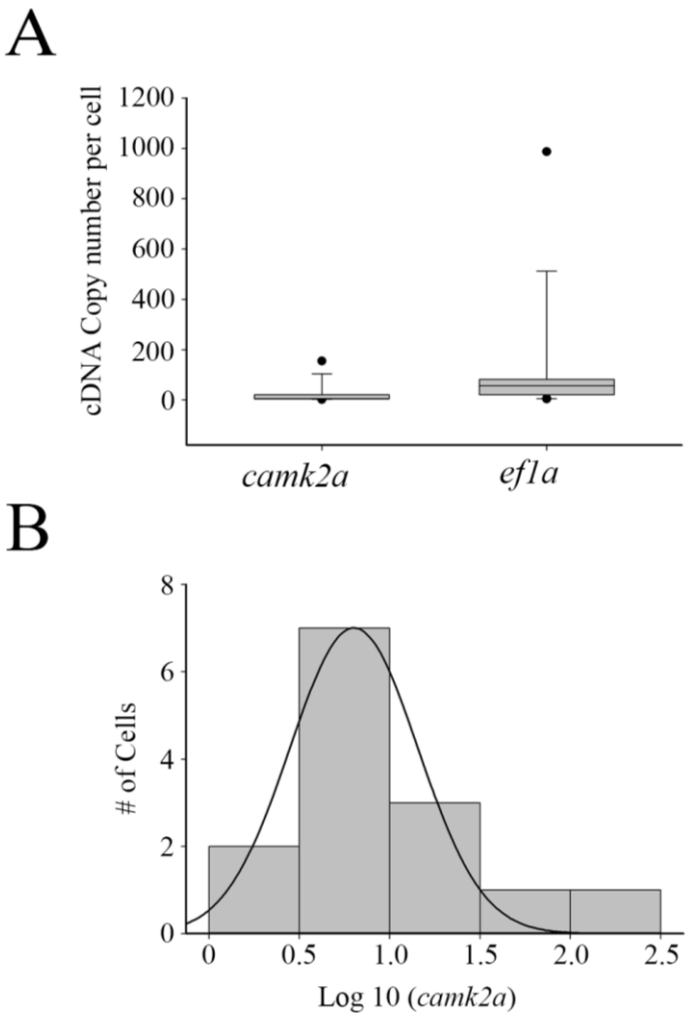
A
cDNA Copy number per cell
1200
1000
800
600
400
200
0
camk2a
ef1a
B
# of Cells
8
6
4
2
0
0
0.5
1.0
1.5
2.0
2.5
Log 10 (camk2a)

Figure 3.4 Quantification of *camk2a* cDNA copy number. (A) Box plot of quantified copies of *camk2a* and *ef1a cDNA* in single M-cells. The median and 10, 25, 75 and 90 percentiles are plotted. (B) Log-normal distribution of *camk2a* cDNA.

Figure 3.5

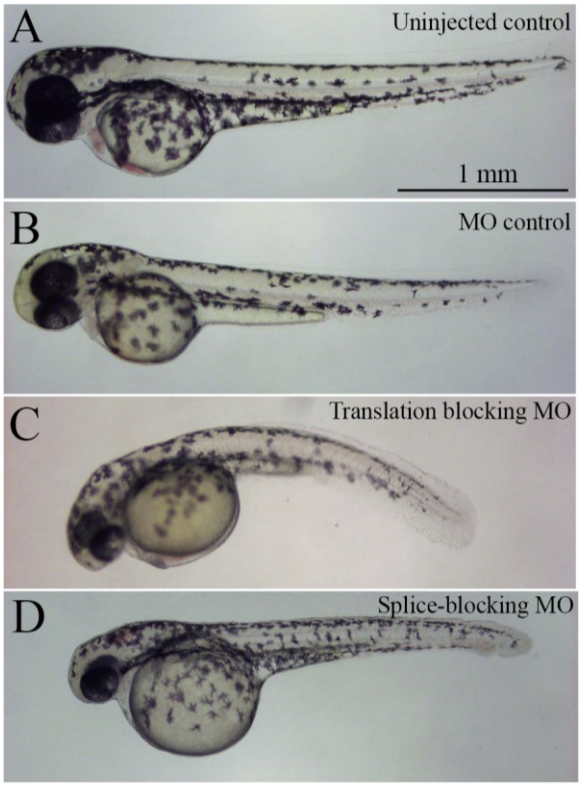
A
Uninjected control
1 mm
B
MO control
C
Translation blocking MO
D
Splice-blocking MO

Figure 3.5 Images of 2 dpf zebrafish. (A) uninjected controls, (B) embryos injected with 4 ng of control morpholino, (C) embryos injected with 4 ng of a translation-blocking CaMKII-α morpholino, and (D) embryos injected with 4 ng of a splice-blocking morpholino.

Figure 3.6

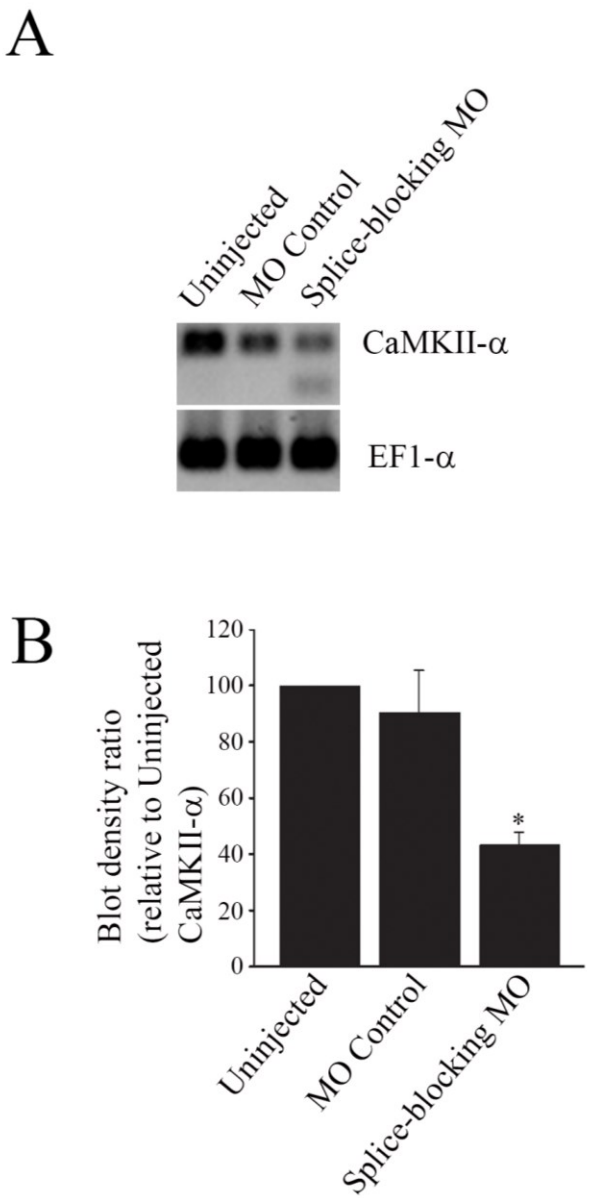
A
Uninjected
MO Control
Splice-blocking MO
CaMKII-α
EF1-α
B
Blot density ratio
(relative to Uninjected
CaMKII-α)
120
100
80
60
40
20
0
*
Uninjected
MO Control
Splice-blocking MO

Figure 3.6 Knockdown of CaMKII-α mRNA by splice-blocking morpholinio. (A) RT-PCR blots of CaMKII-α knockdown assessment. EF1-α was used as a loading control. (B) Quantification of blot densities (n=5 experiments).

Figure 3.7

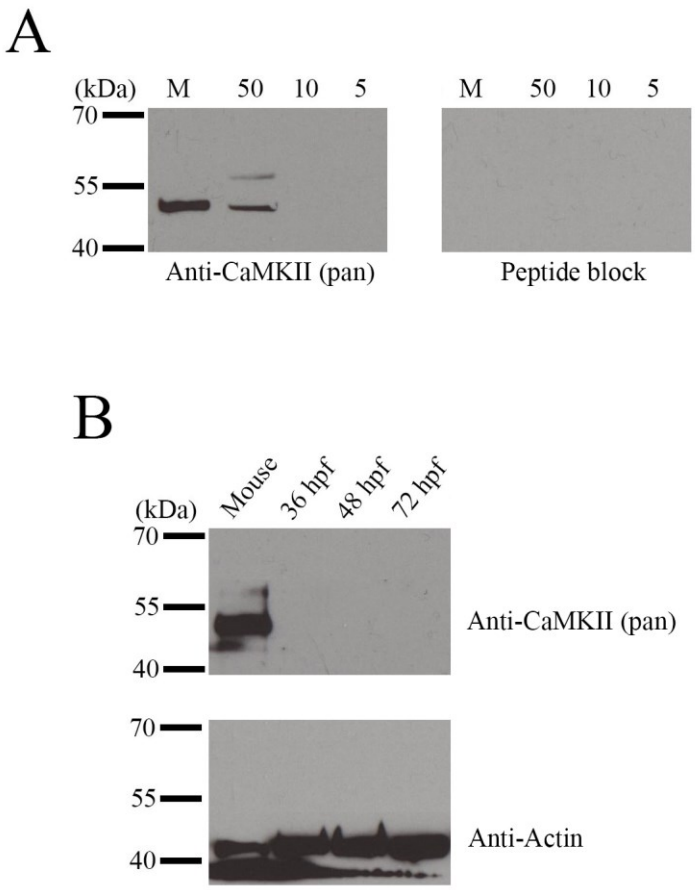
A
(kDa)
M
50
10
5
70
55
40
Anti-CaMKII (pan)
M
50
10
5
Peptide block
B
(kDa)
Mouse
36 hpf
48 hpf
72 hpf
70
55
40
Anti-CaMKII (pan)
70
55
40
Anti-Actin

Figure 3.7 Immunoblot of zebrafish CaMKII-α protein (n = 3). Lanes were loaded with either mouse brain lysate or zebrafish homogenate. Proteins were transferred to nitrocellulose membranes and incubated in either anti-CaMKII (pan), or anti-CaMKII (pan) preabsorbed with recombinant human CaMKII-α at a ratio of 1:5, or anti-Actin. Protein standards ranging from 40 kDa to 700 kDa are indictaed to the left of each immunoblot. (A) Lanes were loaded with either 15 mg mouse brain lysate or 5-50 mg adult zebrafish brain homogenate as indicated. Right panel shows negative control with preabsorbed anti-CaMKII (pan). (B) Lanes were loaded with either 15 mg mouse brain lysate or 50 mg embryonic zebrafish homogenate, and probed with anti-CaMKII (pan) (upper panel) or with anti-Actin (lower panel) after stripping the same membrane.

Figure 3.8

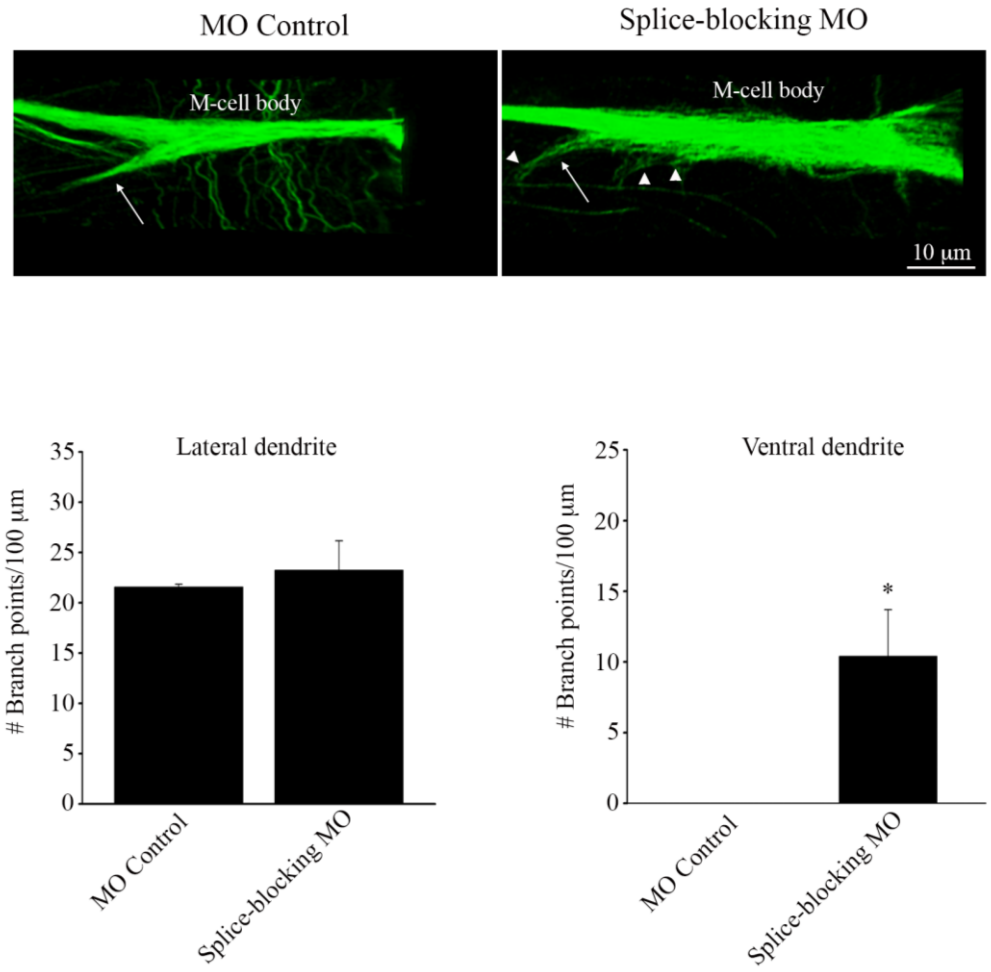
MO Control
Splice-blocking MO
M-cell body
M-cell body
10 µm
Lateral dendrite
Branch points/100 µm
35
30
25
20
15
10
5
0
MO Control
Splice-blocking MO
Ventral dendrite
Branch points/100 µm
25
20
15
10
5
0
*
MO Control
Splice-blocking MO

Figure 3.8 Immunohistochemical images of the M-cell labeled with anti-3A10, from control injected and splice-blocking morphants. (A) The M-cell of MO control-injected fish. Arrow points to the ventral dendrite. (B) The M-cell of a splice-blocked embryo. Arrow points to the ventral dendrite. Arrowheads point to dendritic arborizations present on the cell body and ventral dendrite. Quantification of the number of branch points per 100 μm, emanating from the lateral dendrites (C) and the ventral dendrites (D). * Significantly different from MO controls, $p<0.05$.

Figure 3.9

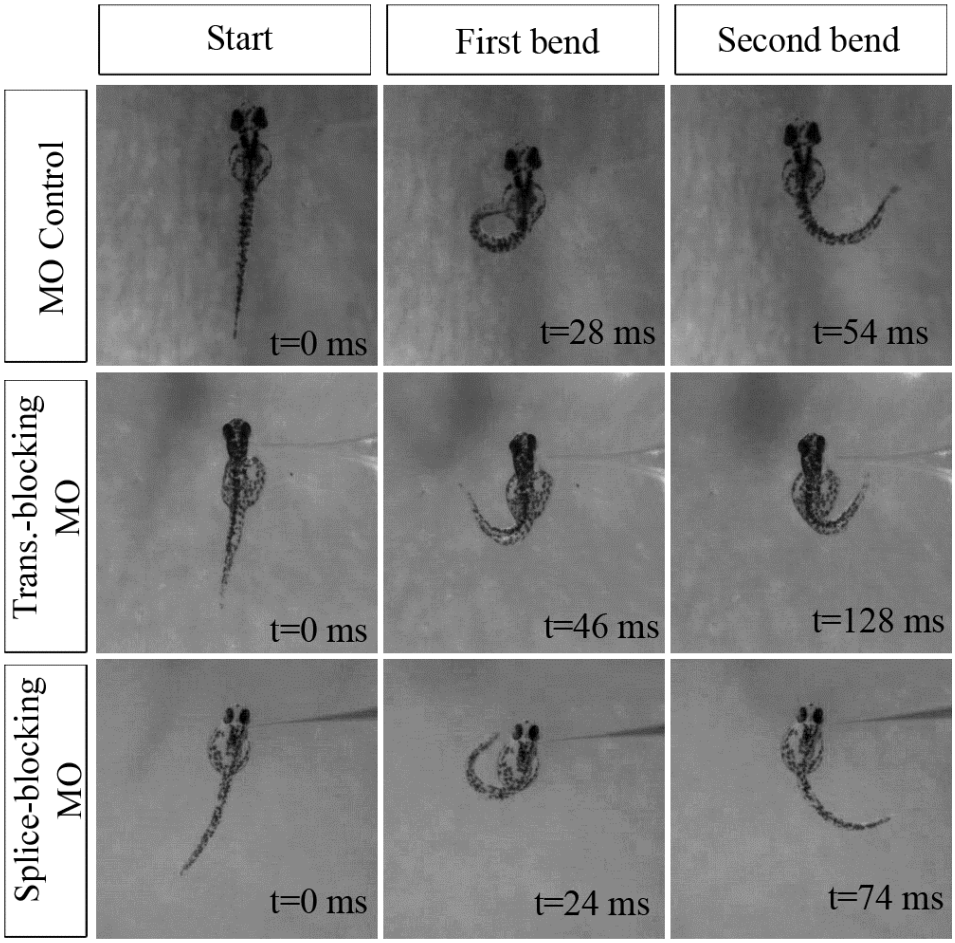
Start
First bend
Second bend
MO Control
t=0 ms
t=28 ms
t=54 ms
Trans.-blocking MO
t=0 ms
t=46 ms
t=128 ms
Splice-blocking MO
t=0 ms
t=24 ms
t=74 ms

Figure 3.9 Locomotor behaviour of zebrafish in response to tactile stimuli. Agar-restrained embryos were given a pulse of water jet around the otolith and response was recorded using a high-speed video camera. The times shown on the figures indicate the time from the start of the response at t=0 ms.

Figure 3.10

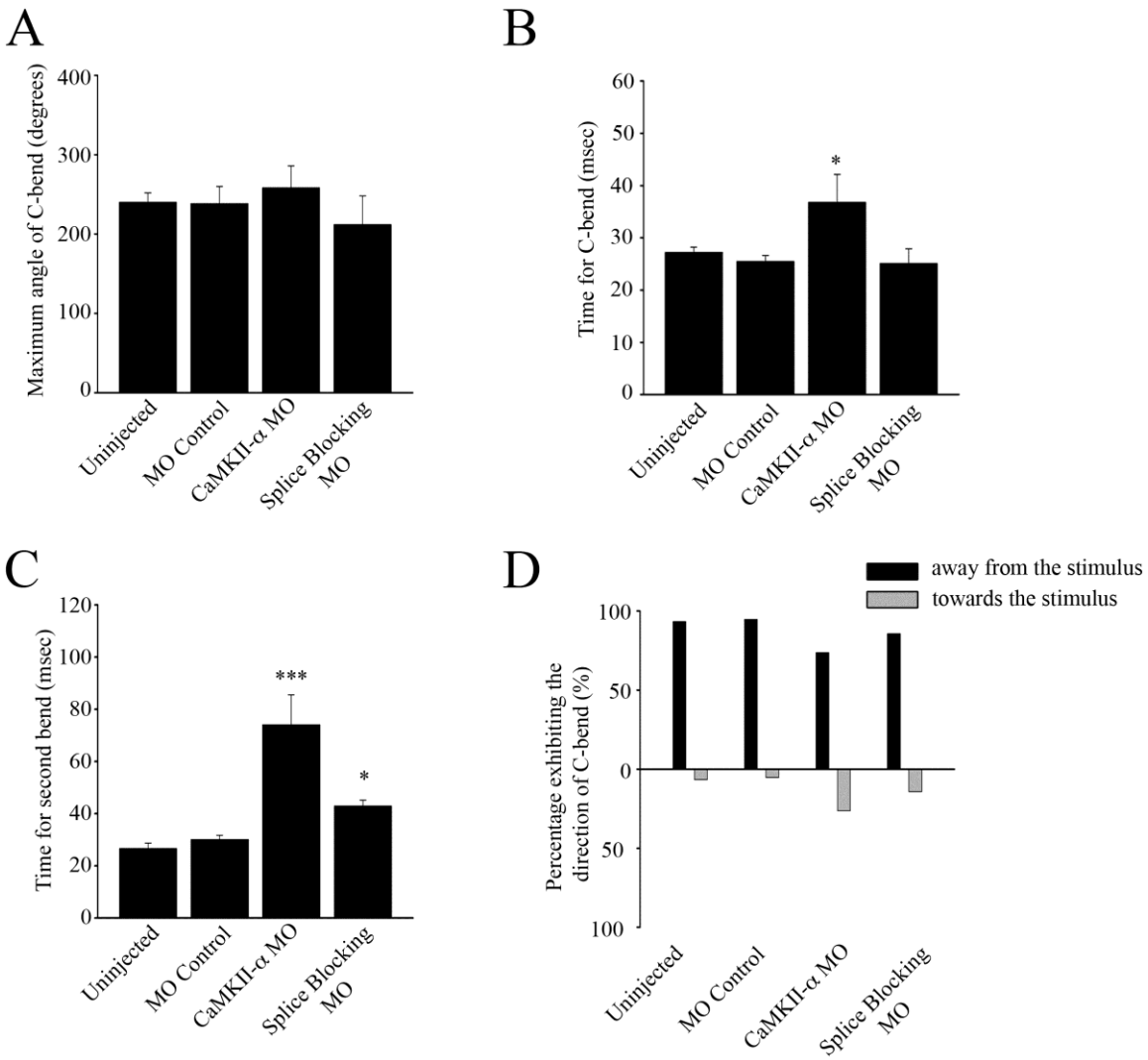
A
Maximum angle of C-bend (degrees)
400
300
200
100
0
Uninjected
MO Control
CaMKII-α MO
Splice Blocking MO
B
Time for C-bend (msec)
60
50
40
30
20
10
0
*
Uninjected
MO Control
CaMKII-α MO
Splice Blocking MO
C
Time for second bend (msec)
120
100
80
60
40
20
0
***
*
Uninjected
MO Control
CaMKII-α MO
Splice Blocking MO
D
away from the stimulus
towards the stimulus
Percentage exhibiting the direction of C-bend (%)
100
50
0
50
100
Uninjected
MO Control
CaMKII-α MO
Splice Blocking MO

Figure 3.10 Touch responses of 2 dpf, agar-restrained embryos. (A) Angle of the c-bend ascertained by measuring the degree of rotation of the tail from the unstimulated, start position (t=0 ms) to the maximum bend angle. (B) Time for the c-bend to occur from the moment the fish starts to respond, to the maximum point of curvature of the tail. (C) Time taken for the tail to move from the end of the c-start to the second bend of the tail. (D) Direction of the movement of the tail relative to the stimulation. * Significantly different from MO controls, $p<0.05$, *** significantly different from MO controls, $p<0.005$.

Chapter 4: Regulation of AMPA and NMDA receptor development by CaMK2-α[2]

4.1 Introduction

Glutamatergic synapses mediate the majority of the excitatory synaptic transmission in the vertebrate CNS. AMPA and NMDA are the two principle types of ionotropic receptors in the glutamatergic synapses. During long-term potentiation, activation of NMDA receptors increases intracellular Ca^{2+} which activates CaMKII. Upon activation, CaMKII translocates from cytoplasm to the postsynaptic membrane, where it binds to NMDARs (Leonard et al., 1999; Shen and Meyer, 1999; Strack and Colbran, 1998). The GluN2B subunit of NMDARs contains several binding sites for CaMKII (Bayer et al., 2001). The amino acid S1303 in GluN2B binds to CaMKII that is not phosphorylated at T286 site. A second binding site on GluN2B between amino acids 839 and 1120 requires activated CaMKII that is phosphorylated at the T286 site. Binding of CaMKII to NMDAR locks the enzyme in an active state, which can persist for tens of minutes.

The active CaMKII in the postsynaptic membrane potentiates AMPAR mediated transmission. This is achieved by increasing the AMPAR conductance and also by increasing the number of receptors at the synapse. A number of studies have found that CaMKII phosphorylate the GluA1 subunit of AMPARs, thereby increasing the channel conductance during LTP (Barria et al., 1997b; Benke and Isaac, 1998; Lee, 2006). Synaptic increase of AMPA receptor number involves multiple steps, including insertion

[2] A version of this chapter has been published: Roy, B., Ferdous, J., and Ali, D.W. (2015). NMDA receptors on zebrafish Mauthner cells require CaMKII-α for normal development. *Developmental Neurobiology* 75(2):145-62.

of AMPARs from an intracellular pool to the extrasynaptic membrane, lateral diffusion of the receptors to synapse and subsequent stabilization of the receptors within PSD (Opazo and Choquet, 2011). CaMKII has been implicated in these steps. For example, CaMKII can phosphorylate extrasynaptic mobile AMPARs on their auxiliary protein stargazing which then traps the receptors at the PSD (Opazo et al., 2010). Although, the role of CaMKII has been studied in detail for activity-dependent plasticity mechanisms, its role in the synaptic development of glutamate receptors has not received comparable attention. Therefore, my goal in this study was to explore the roles of CaMKII-α in the development of ionotropic glutamate receptor mediated synaptic currents in embryonic zebrafish.

4.2 Results.

4.2.1 CaMKII-α does not affect AMPA receptor development

CaMKII affects AMPAR currents in mammalian systems. In particular, activation of CaMKII leads to an upregulation of AMPA currents through phosphorylation of the GluA1 subunit (Barria et al., 1997b; Kristensen et al., 2011). To determine if acute activation of CaMKII could affect AMPA mEPSCs in zebrafish, I incubated the preparation in an elevated K^+ solution to depolarize the cells and to increase synaptic activity as shown previously (Patten and Ali, 2009). This treatment should increase intracellular Ca^{2+} and CaMKII activity. AMPA mEPSCs were recorded in regular recording solution that included TTX (1 μM) to block action potentials, strychnine (5 μM) to block glycine, picrotoxin (100 μM) to block GABA, and APV (50 μM) to block NMDA receptors in the extracellular bath. All remaining events were blocked by NBQX (0.1 μM), confirming their identity (Figures 4.5). For elevated K^+ experiments, I recorded baseline AMPA mEPSCs in regular recording solution in voltage clamp mode and then switched to I=0 mode to allow the cells to depolarize for 5 minutes in 10 mM KCl containing solution that lacked the drugs. I used a low calcium buffering CsCl internal solution to allow calcium levels to rise throughout the elevated K^+ wash and continuously monitored the membrane potential. When 10 mM KCl was washed on to the preparation, the membrane potential typically depolarized to about -30 mV from an average resting membrane potential of about -65 mV. I also noted a significant increase in synaptic activity during the elevated K^+ wash. At the end of the depolarization period, the elevated K^+ solution was washed off with the regular recording solution that contained the above-mentioned drugs. I waited for 5 minutes to allow the drugs to fully block voltage gated

Na^+ channels and other receptors and then recorded AMPA mEPSCs again in voltage-clamp mode as shown in Figure 4.1A. Individual events in each recording traces were averaged and analysis done on the averaged mEPSCs. Analysis of mEPSCs indicated a significant increase in the amplitude of the events, from a control amplitude of 25.2 ± 1.4 pA to a mean of 30.3 ± 1.7 pA after elevated K^+ application (Figure 4.1B; n= 6 experiments; p=0.038, t-test). The increase in mEPSC amplitude was prevented by inclusion of 10 μM of the CaMKII blocker, KN 62, in the intracellular solution (Figure 4.1B; n=4 experiments; p=0.80, t-test). To confirm these results, I tested the ability of a second, more specific CaMKII blocker, AIP in the intracellular solution to prevent the elevated K^+ induced increase in AMPA mEPSC. I found that 1 μM AIP also prevented the increase in amplitude (Figure 4.1B; n=4 experiments; p=0.80, t-test).

Elevated K^+ also induced an increase in the frequency of AMPAR mEPSCs, which doubled from a control value of 9.6 ± 1.0 Hz in normal ESC to 20.1 ± 1.8 Hz following elevated K^+ wash (Figure 4.1C; $p<0.001$, t-test). The CaMKII blockers KN 62 and AIP had no effect on the elevated K^+-induced change in frequency (Figure 4.1C; p=0.04 and p=0.004 respectively, t-test), suggesting that CaMKII plays little or no role in the presynaptic release of glutamate.

To examine the mEPSCs in more detail, I constructed amplitude histograms for controls and for events obtained from elevated K^+ preparations (Figure 4.2A). There appeared to be a slight shift in the events such that there were a greater proportion of higher amplitude events following high K^+ solution incubation compared with controls.

Scatter plots of 20-80% rise time vs amplitude (Figure 4.2B) showed no correlation in these parameters, indicating no space clamping issues with my recordings.

An examination of the kinetics showed that incubation of 10 mM K^+ alone does not change mEPSC rise time (Figure 4.3A; p=0.23, t-test). Neither was there a change in the groups incubated in AIP, but curiously there was a significant increase in the rise time of high K^+ induced events compared with controls, in the KN 62 incubated group (Figure 4.3A, p= 0.0255, t-test). It is surprising that this occurred given the lack of effect in the AIP group; however, it should be noted that the control rise time was slightly smaller in the KN 62 group than in any of the other controls, while the rise time in the elevated K^+ group was actually not significantly different from any other elevated K^+ group (Figure 4.3A; p=0.495, one-way ANOVA).

An analysis of the decay time constants suggested that blocking CaMKII leads to a significant slowing of the mEPSC off kinetics as indicated by the increased decay time constant in the AIP treated group (Figure 4.3B; n=4, p= 0.0243, t-test). Here, the decay time constant increased from 0.28 ± 0.01 ms in baseline recording to 0.36 ± 0.03 ms following elevated K^+ application. These values were significantly different and represented a 28 % increase in the decay time. The decay time of the elevated K^+ treated group when incubated in KN 62 was not significantly different from its control (Figure 4.3B; p=0.114, t-test), but was trending towards higher values.

Taken together, these data suggest that CaMKII increase the amplitude of AMPA currents following cellular depolarization by elevated K^+ solution. These findings are similar to those in mammalian systems which show that activation of CaMKII phosphorylates AMPARs and induces insertion of new receptors to synapses, thus increasing AMPA current amplitudes (Poncer et al., 2002). I attempted to confirm these results by including an active form of CaMKII in the whole cell patch pipette, which would theoretically lead to a gradual increase in the amplitude of AMPA mEPSCs, and possibly a change in decay kinetics. For these experiments I used a mammalian form of CaMKII-α, that was made constitutively active and that has been shown to be effective in murine models (Lledo et al., 1995). However, I found that inclusion of active CaMKII-α (400 nM or 10 U/μl) in the pipette had no effect on mEPSC parameters as shown in Figure 4.4. It was difficult to maintain the whole cell patch for longer than 10 minutes and so all parameters are examined within the 10 minute time point. My results indicate that AMPA mEPSCs were unaffected by the active CaMKII. These findings were at odds with my previous data suggesting that CaMKII may indeed alter AMPA mEPSC properties, as has been shown in mammalian systems (Lledo et al., 1995), and could be due to my use of mammalian rather than zebrafish CaMKII, or that a longer period of time is required to see an effect. It is also possible that CaMKII may not actually be involved in the high K^+ induced upregulation of AMPA mEPSCs. Therefore, additional studies are required to shed more light on the acute effect of CaMKII-α activation on AMPARs. I should be clear that I did not directly measure the activity of CaMKII after the high K^+ wash, and therefore cannot confirm that high K^+ does indeed activate CaMKII. However, the similar effects of KN 62 and AIP, which employ different

mechanisms to block CaMKII, lead me to believe that CaMKII was activated by the elevated K^+ solution.

Since my primary aim was to determine if CaMKII-α is involved in the normal development of AMPA containing synapses, I sought to reduce the levels of CaMKII via morpholino knockdown as described in Chapter 3. Electrophysiological recordings were difficult to obtain from the morphants because they possessed fragile cell membranes that precluded stable, long-term recordings; however, basal electropohysiological parameters were similar between all of the groups (Table 4.1). Example traces are shown in Figure 4.5, along with averaged mEPSCs. To confirm that the events were indeed AMPA mEPSCs, I blocked their occurrence with NBQX (Figure 4.5). Surprisingly, I found little difference among the mEPSC parameters investigated. Amplitude distributions and 20-80% rise time vs amplitude scatter plots (Figure 4.6) show no obvious difference amongst the various groups. Similarly, bar graphs of mean amplitude and frequency indicate that the morphants exhibit AMPA mEPSCs that are similar to controls (Figure 4.7; $p>0.05$, one-way ANOVA, multiple comparison test with Student Newman–Keuls Method). Finally, an analysis of mEPSC kinetics (Figure 4.8) shows no change in the rise time of the events and only a small but significant increase in the decay time constant in the translation blocking morphants compared with uninjected controls (Figure 4.8B; $p<0.05$, one-way ANOVA, multiple comparison test with Student Newman–Keuls Method). However the decay time course of the AMPA mEPSCs obtained from the splice-blocking morphants were not significantly different from the control-injected embryos. Taken

together, these results suggest that knockdown of CaMKII-α has little or no effect on the development of AMPA currents on zebrafish M-cells.

4.2.2 Effect of *camk2a* knockdown on NMDA mEPSCs

To determine if CaMKII affects the development of NMDA-containing synapses, I isolated NMDA mEPSCs, by including TTX (1 μM), picrotoxin (100 μM), strychnine (5 μM) and NBQX (0.1 μM) in Mg^{2+} free extracellular recording solutions. Confirmation of their identity was obtained by blocking all remaining mEPSCs with APV (50 μM) (Figure 4.9). Due to the low frequency of NMDA events, I recorded mEPSCs for long period (~30 minutes) to capture a sufficient number of events for analyses. To confirm the stability of the mEPSC kinetics under my recording conditions, I compared the events captured between 6 to 15 minutes with events captured between 16 to 25 minutes (n = 3 uninjected embryos). I found that the frequency of NMDA events increased significantly over time from 0.06 ± .01 Hz in 6-15 minutes to 0.11 ± 0.01 Hz in 16-25 minutes (Figure 4.10A; $p<0.05$, t-test). However, the mean amplitude of the events and amount of charge transferred during synaptic currents were not different between the two groups (Figure 4.10B, C) confirming the general stability of the mEPSCs throughout the recording period.

I recorded NMDA mEPSCs from uninjected (n=7), control MO-injected (n=6), translation blocking MO-injected (n=5), and splice blocking MO-injected (n=5) 2 dpf embryos. There were no obvious differences between the uninjected controls and the MO controls; however, analysis of NMDA mEPSCs indicated that the mean mEPSC

amplitude was significantly smaller in the translation-blocking and splice-blocking morphants compared with control embryos (Figures 4.9 and 4.11A,). Specifically, I found that mean mEPSC amplitude of NMDA events was 83.7 ± 8.3 pA in uninjected controls, 80.6 ± 9.3 pA in MO controls, 49.7 ± 5.3 pA in the translation-blocking morphants and 58.0 ± 12.1 pA in the splice-blocking morphants (Figure 4.11A; p=0.003, one-way ANOVA, multiple comparison test with Student Newman–Keuls Method). There was no change in either the frequency or the 20-80% rise times of the NMDA mEPSCs between groups (Figure 4.11B, C).

An examination of the mEPSC decay component indicated that NMDA events decayed with a bi-exponential time course, and that the amplitude of the fast component did not differ between groups (Figures 4.9, 4.12, 4.13A). There was no difference in the time course of the fast exponential component (τ_{fast}), which was 34.9 ± 4.4 ms (n=5) in the translation-blocking morphants, 32.1 ± 8.8 ms (n=5) in the splice-blocking morphants, 25.9 ± 4.8 ms (n=6) in the control MO group and 25.2 ± 2.2 ms (n=7) in the uninjected embryos (Figure 4.13B; p=0.246, one-way ANOVA, multiple comparison test with Student Newman–Keuls Method). Additionally, there was no significant effect on the time course of the slow NMDA component (τ_{slow}) (Figure 4.13D); but importantly, the amplitude of the slow component was significantly reduced in both of the morphants compared with controls (Figure 4.13C; p=0.001, one-way ANOVA, multiple comparison test with Student Newman–Keuls Method). Specifically, the amplitude of τ_{slow} was 19.8 ± 2.7 pA (n = 5) in the translation-blocking morphants, 26.7 ± 5.8 pA (n = 5) in the splice-blocking morphants, 45.1 ± 4.6 pA (n = 6) in the MO injected controls and 45.4 ± 4.6 pA

(n = 7) in the uninjected embryos (Figure 4.13C). These results suggest that CaMKII-α is necessary for the normal development of NMDA-mediated currents in zebrafish M-cells.

4.2.3 Effect of acute activation or blocking of CaMKII-α on NMDA mEPSC decay kinetics

To confirm that the reduction of NMDAR mEPSC amplitude in CaMKII-α morphants resulted from a lack of developmental upregulation of NMDARs, and not from a deficiency in acute activity of CaMKII-α, I attempted to activate CaMKII-α in M-cells via a high K^+ solution as I had done for the AMPA mEPSCs. I used a bath solution that contained 10 mM K^+ to depolarize the neurons and activate CaMKII-α. Application of the depolarizing solution doubled NMDA mEPSC frequency in the control recordings from 0.12 ± 0.01 Hz to 0.23 ± 0.05 Hz (Figure 4.14A n = 4 recordings, p = 0.018, t-test). When the CaMKII blocker, AIP, was included in the recording pipette, the increase in frequency did not occur (n = 4 embryos; p=0.258, t-test). This result was a curious one and remains unexplained, as effects on mEPSC frequency are likely to be presynaptic in origin and were not expected to be affected by CaMKII inhibition in the postsynaptic cell.

High K^+ solution or acute inhibition of CaMKII-α did not change the amplitude, rise time, or decay kinetics of NMDA mEPSCs (Figure 4.14 B, C, 4.14A, C; p >0.05). Specifically, AIP did not affect the amplitude of the slow component of the NMDA decay (Figure 4.15D, control: 36.3 ± 6.5 pA before 10 mM K^+ bath, AIP: 34.5 ± 5.7 before 10 mM K^+ bath, p > 0.05). These findings suggest that acute block of CaMKII did

not have an effect on NMDA mEPSCs properties and that the main role of CaMKII was to regulate normal development of NMDAR-containing synapses.

Table 4.1 Electrophysiological parameters of M-Cells.

	Membrane Potential (mV)	Cell Capacitance (pF)	Membrane Resistance (MΩ)
Uninjected controls (n = 7)	-61.9 ± 2.5	24.1 ± 1.8	55.2 ± 8.3
MO controls (n = 6)	-63.4 ± 1.6	24.5 ± 1.7	57.9 ± 5.2
Translation-blocking MO (n = 5)	-60.7 ± 7.6	21.7 ± 0.6	63.9 ± 10.4
Splice-blocking MO (n = 5)	-65.2 ± 1.2	18.6 ± 1.4	53.5 ± 9.3

Figure 4.1

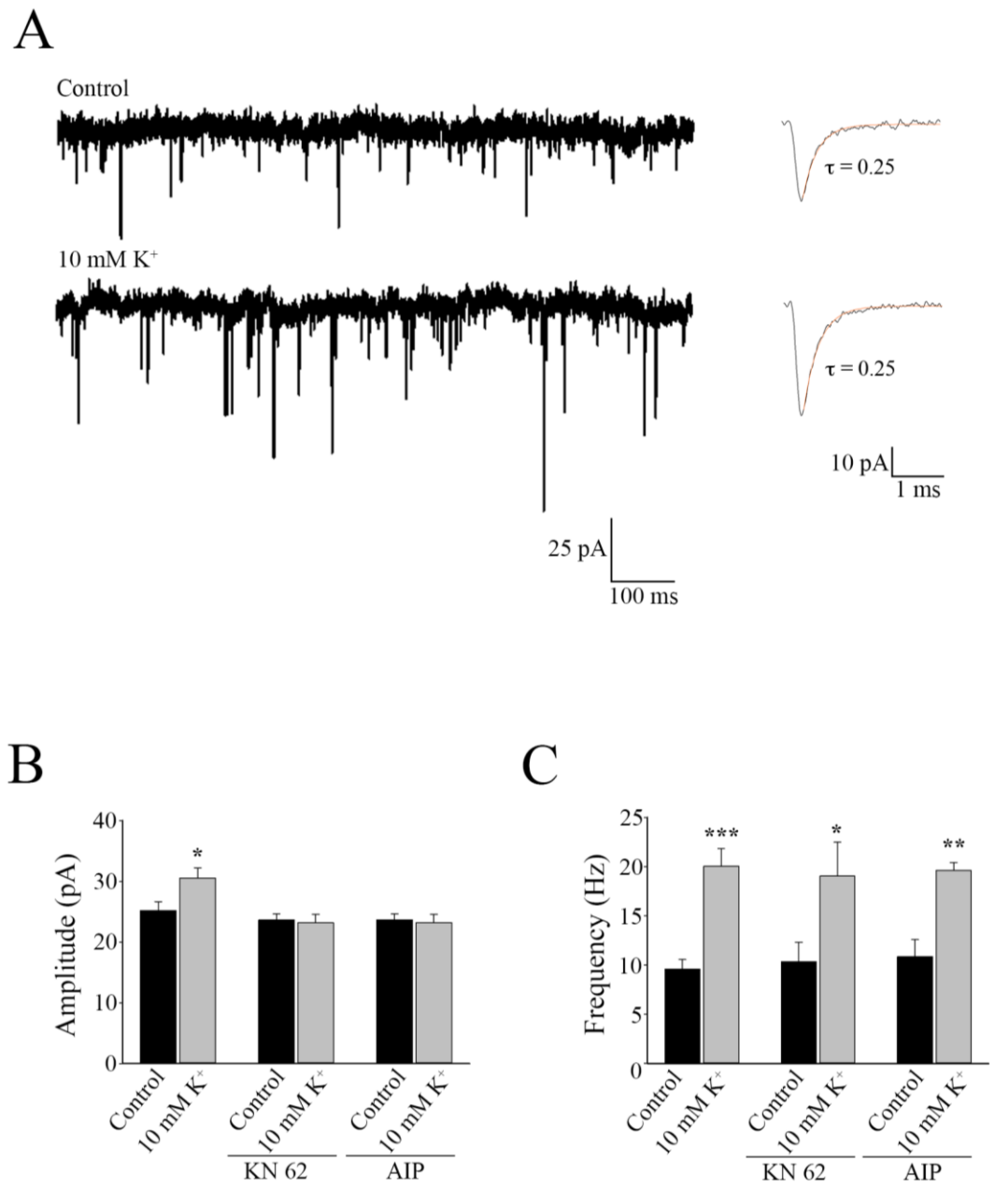
A
Control
10 mM K+
τ = 0.25
τ = 0.25
10 pA
1 ms
25 pA
100 ms
B
Amplitude (pA)
40
30
20
10
0
*
Control
10 mM K+
Control
10 mM K+
Control
10 mM K+
KN 62
AIP
C
Frequency (Hz)
25
20
15
10
5
0
***
*
**
Control
10 mM K+
Control
10 mM K+
Control
10 mM K+
KN 62
AIP

Figure 4.1 CaMKII inhibitors block upregulation of AMPAR mEPSCs. (A) Example traces of AMPAR mEPSCs recorded before (control) and after (10 mM K^+) 5-minute bath application of 10 mM K^+ containing depolarizing medium. Recordings were obtained from 6 different preparations. In separate experiments, two different CaMKII inhibitors, KN-62 (10 μM, n = 4 experiments) and AIP (1 μM, n = 4 experiments) were used in the intracellular solution to block CaMKII activity in the postsynaptic cell. Bar graphs comparing (B) amplitude and (C) frequency of averaged AMPA mEPSCs. * Significantly different from control, $p<0.05$, ** significantly different from control, $p<0.01$, *** significantly different from control, $p<0.001$.

Figure 4.2

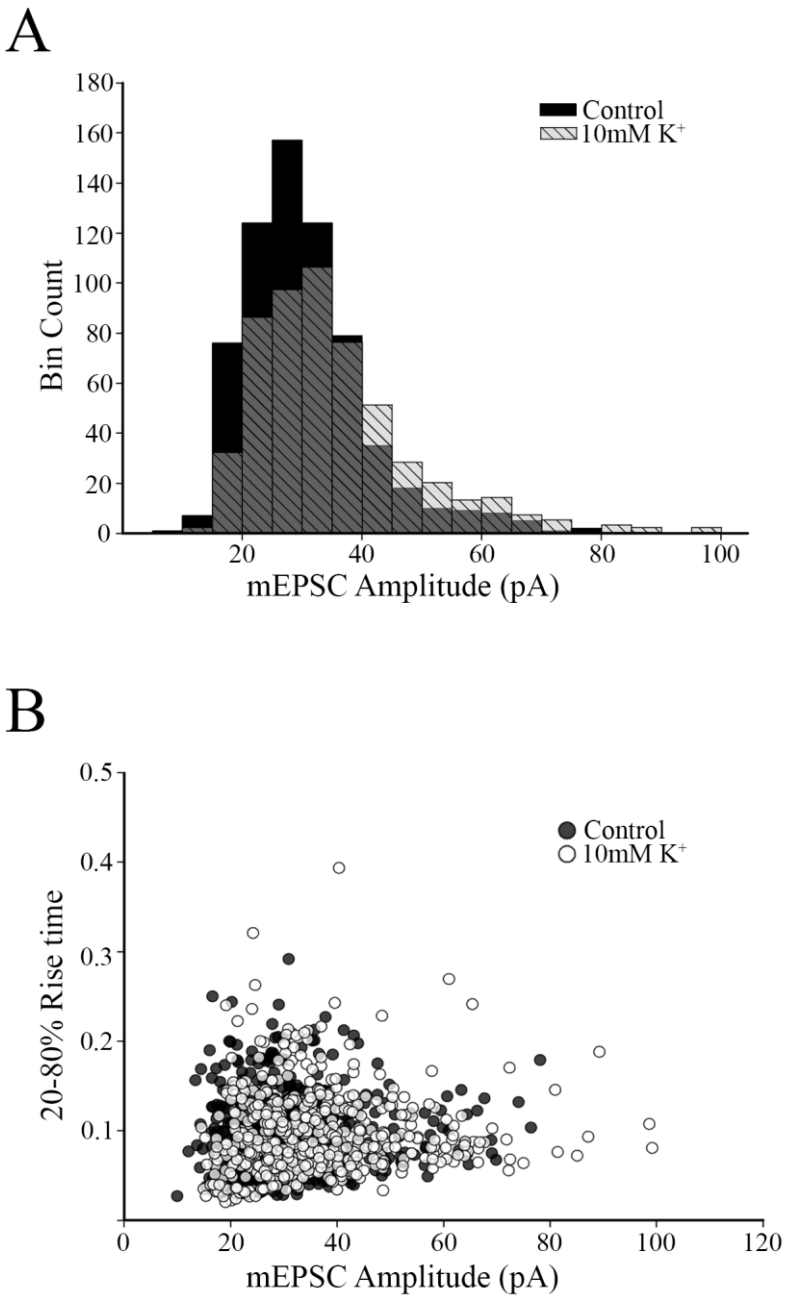
A
Control
10mM K+
Bin Count
mEPSC Amplitude (pA)
B
Control
10mM K+
20-80% Rise time
mEPSC Amplitude (pA)

Figure 4.2 Amplitude histogram and scatter plot of AMPA mEPSCs obtained from the M-cell of 48 hpf embryos, recorded in the presence of 1 mM TTX, 1 mM strychnine and 100 mM picrotoxin. mEPSCs recorded from control (normal ECS) are represented by the black bars while events recorded from elevated K (10 mM K^+) solutions are represented by the light grey, hatched bars. Dark grey, hatched bars represent overlapping regions. (B) Scatter plot of rise time vs mEPSC amplitude. Holding potential was -60 mV.

Figure 4.3

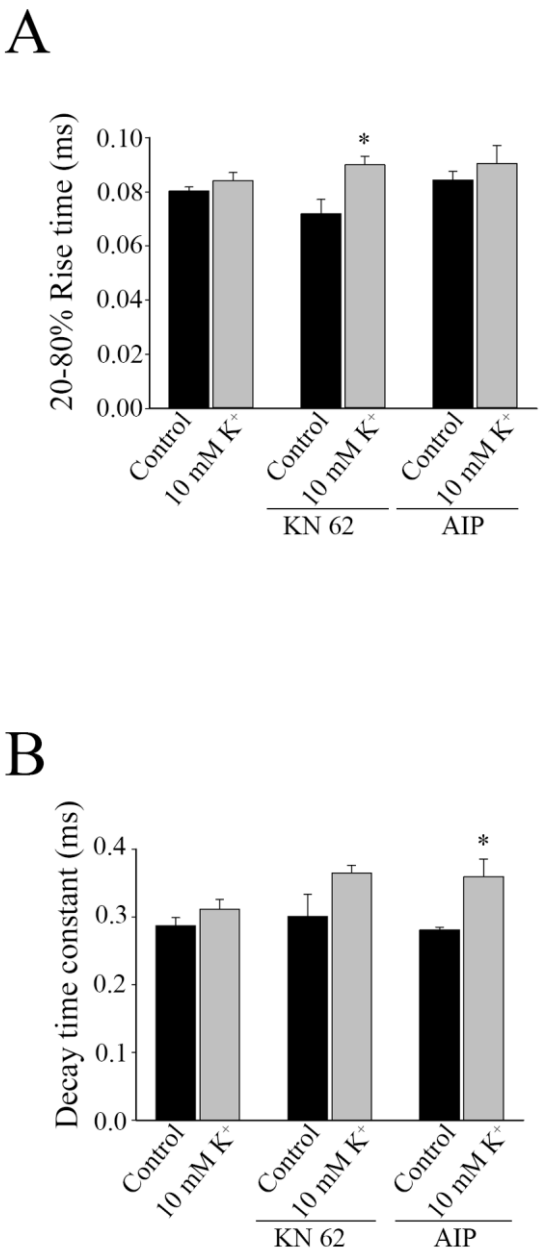
A
20-80% Rise time (ms)
0.10
0.08
0.06
0.04
0.02
0.00
*
Control
10 mM K+
Control
10 mM K+
Control
10 mM K+
KN 62
AIP
B
Decay time constant (ms)
0.4
0.3
0.2
0.1
0.0
*
Control
10 mM K+
Control
10 mM K+
Control
10 mM K+
KN 62
AIP

Figure 4.3 Kinetic properties of AMPA mEPSC recorded from 10 mM K^+ stimulated M-cells. Bar graph showing the (A) 20-80% rise time and (B) decay time constant of mEPSCs recorded in normal ECS and 10 mM K^+ solution illustrating the effect of the broad spectrum CaMKII blocker, KN62 and the more specific CaMKII blocker, AIP. * Significantly different from control, $p<0.05$.

Figure 4.4

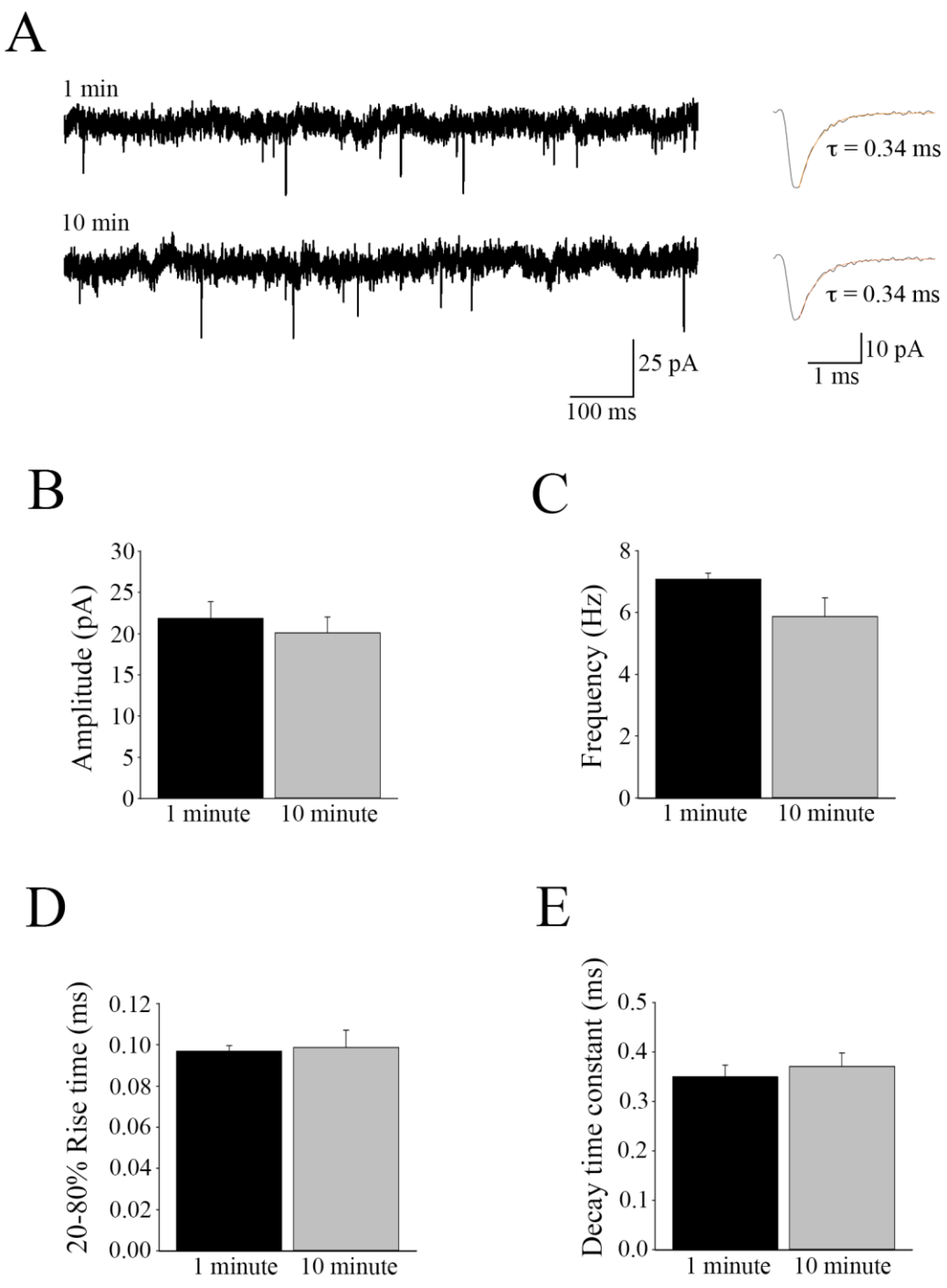
A
1 min
10 min
τ = 0.34 ms
τ = 0.34 ms
25 pA
100 ms
10 pA
1 ms
B
Amplitude (pA)
30
25
20
15
10
5
0
1 minute
10 minute
C
Frequency (Hz)
8
6
4
2
0
1 minute
10 minute
D
20-80% Rise time (ms)
0.12
0.10
0.08
0.06
0.04
0.02
0.00
1 minute
10 minute
E
Decay time constant (ms)
0.5
0.4
0.3
0.2
0.1
0.0
1 minute
10 minute

Figure 4.4 Acute effect of active CaMKII-α on AMPA mEPSCs. (A) 10 minute application of the active form of CaMKII-α (400 nM, or 10 U/μl) to the Mauthner cell cytosol had no apparent effect on AMPA mEPSCs. Bar graphs showing mEPSC (B) amplitude, (C) frequency, (D) 20-80% rise time and (E) decay time constant indicate no change in these parameters after 10 minute intracellular application of active CaMKII.

Figure 4.5

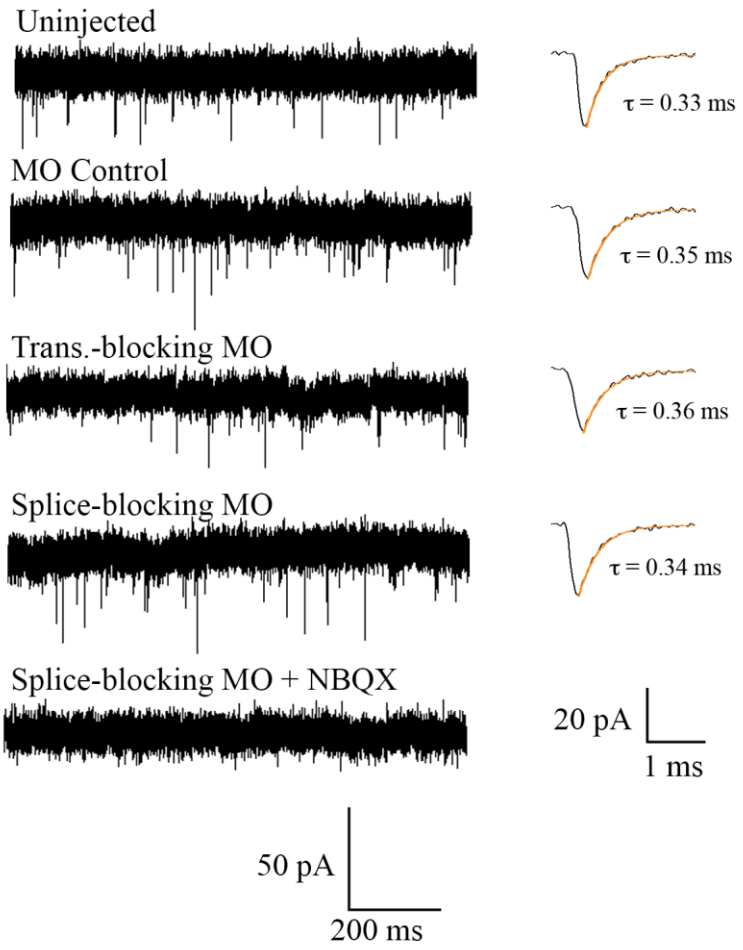
Uninjected
τ = 0.33 ms
MO Control
τ = 0.35 ms
Trans.-blocking MO
τ = 0.36 ms
Splice-blocking MO
τ = 0.34 ms
Splice-blocking MO + NBQX
20 pA
1 ms
50 pA
200 ms

Figure 4.5 Spontaneous synaptic AMPAR currents obtained from M-cells. Uninjected embryos (n = 7), control morpholino injected embryos (n = 8), translation-blocking morpholino injected embryos (n = 7) and splice-blocking morpholino injected embryos (n = 6) exhibit AMPAR currents at similar frequencies. The inclusion of NBQX (0.1 μM) confirmed the mEPSCs as AMPAR-mediated. Preparations were incubated in TTX (1 μm), strychnine (5 μM), picrotoxin (100 μM) and APV (50 μM) to block action potentials, glycine, GABA and NMDA receptors respectively. Average traces are shown to the right of each recording; each trace is an average of multiple events; 215 mEPSCs for the uninjected controls, 224 events for the MO controls, 174 events for the translation-blocking morphants and 276 events for the splice-blocking morphants.

Figure 4.6

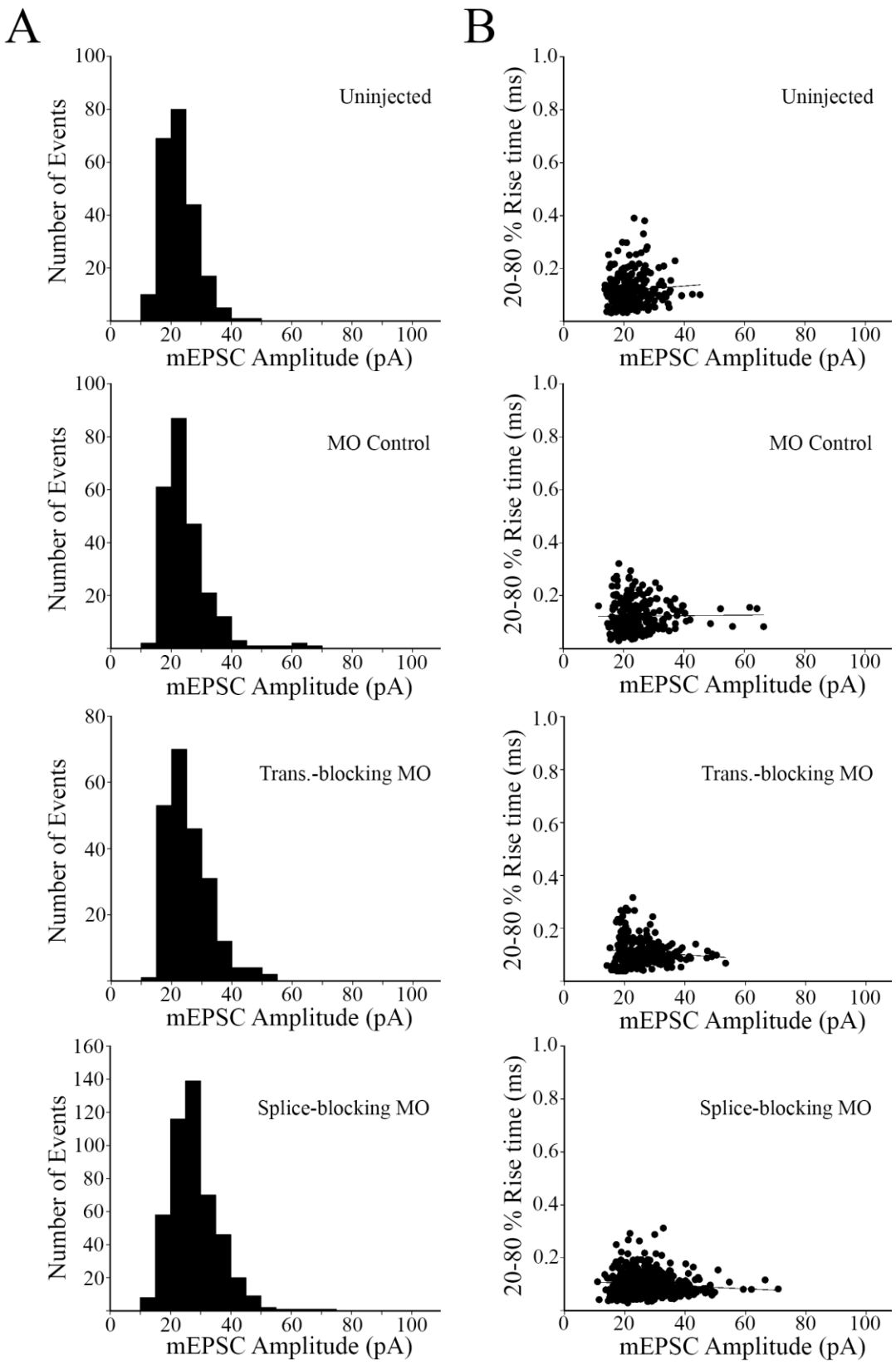
A
B
Uninjected
MO Control
Trans.-blocking MO
Splice-blocking MO
Number of Events
20-80 % Rise time (ms)
mEPSC Amplitude (pA)

Figure 4.6 AMPA mEPSC distributions. (A) Amplitude histogram of AMPA mEPSCs obtained from Mauthner cells and recorded from uninjected controls (n = 7), morpholino controls (n = 8), translation-blocking morphants (n = 7) and splice-blocking morphants (n=6). (B) Scatter plots of rise time versus amplitudes of mEPSCs captured from the cells in (A). For uninjected controls, r = 0.077; n = 227 events. For morphant controls, r = 0.014; n = 239 events. For translation-blocking morphants, r = 0.098; n = 223 events. For splice-blocking morphant, r = 0.095; n = 472 events.

Figure 4.7

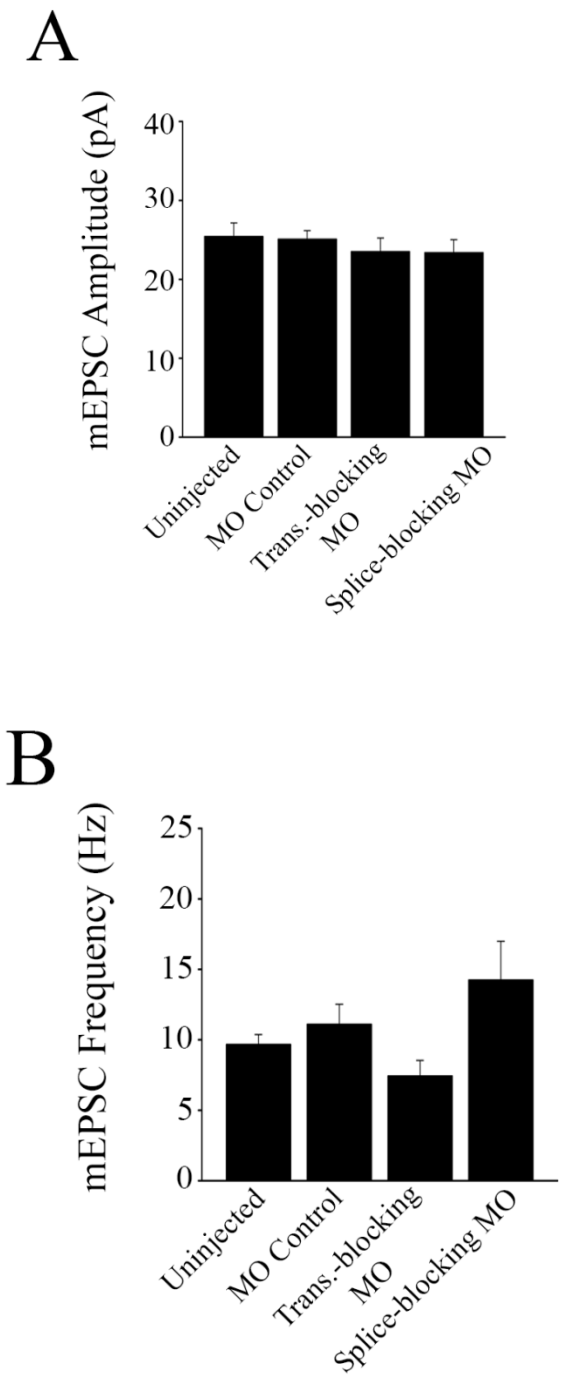
A
mEPSC Amplitude (pA)
40
30
20
10
0
Uninjected
MO Control
Trans.-blocking MO
Splice-blocking MO
B
mEPSC Frequency (Hz)
25
20
15
10
5
0
Uninjected
MO Control
Trans.-blocking MO
Splice-blocking MO

Figure 4.7 Properties of AMPA mEPSCs. Bar graphs showing the mean mEPSC amplitude (A) and frequency (B) of events recorded from uninjected controls, morpholino controls, translation-blocking morphants and splice-blocking morphants.

Figure 4.8

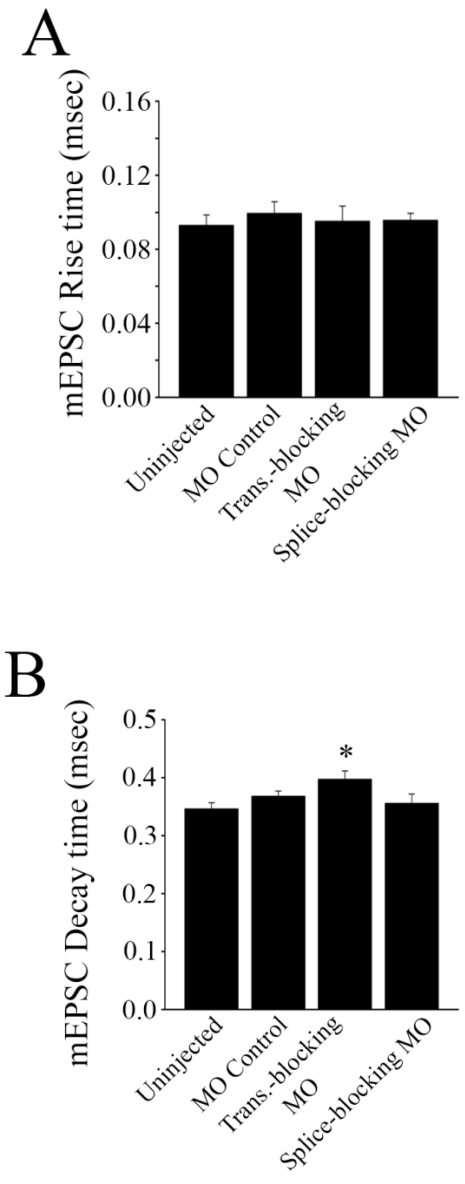
A
mEPSC Rise time (msec)
0.16
0.12
0.08
0.04
0.00
Uninjected
MO Control
Trans.-blocking MO
Splice-blocking MO
B
mEPSC Decay time (msec)
0.5
0.4
0.3
0.2
0.1
0.0
*
Uninjected
MO Control
Trans.-blocking MO
Splice-blocking MO

Figure 4.8 Kinetic properties of AMPA mEPSCs. Bar graphs showing the mean mEPSC rise time (A) and decay time constants (B) of events recorded from uninjected controls (n = 7), morpholino controls (n = 8), translation-blocking morphants (n = 7) and splice-blocking morphants (n = 6). * Significantly different from uninjected controls, $p<0.05$.

Figure 4.9

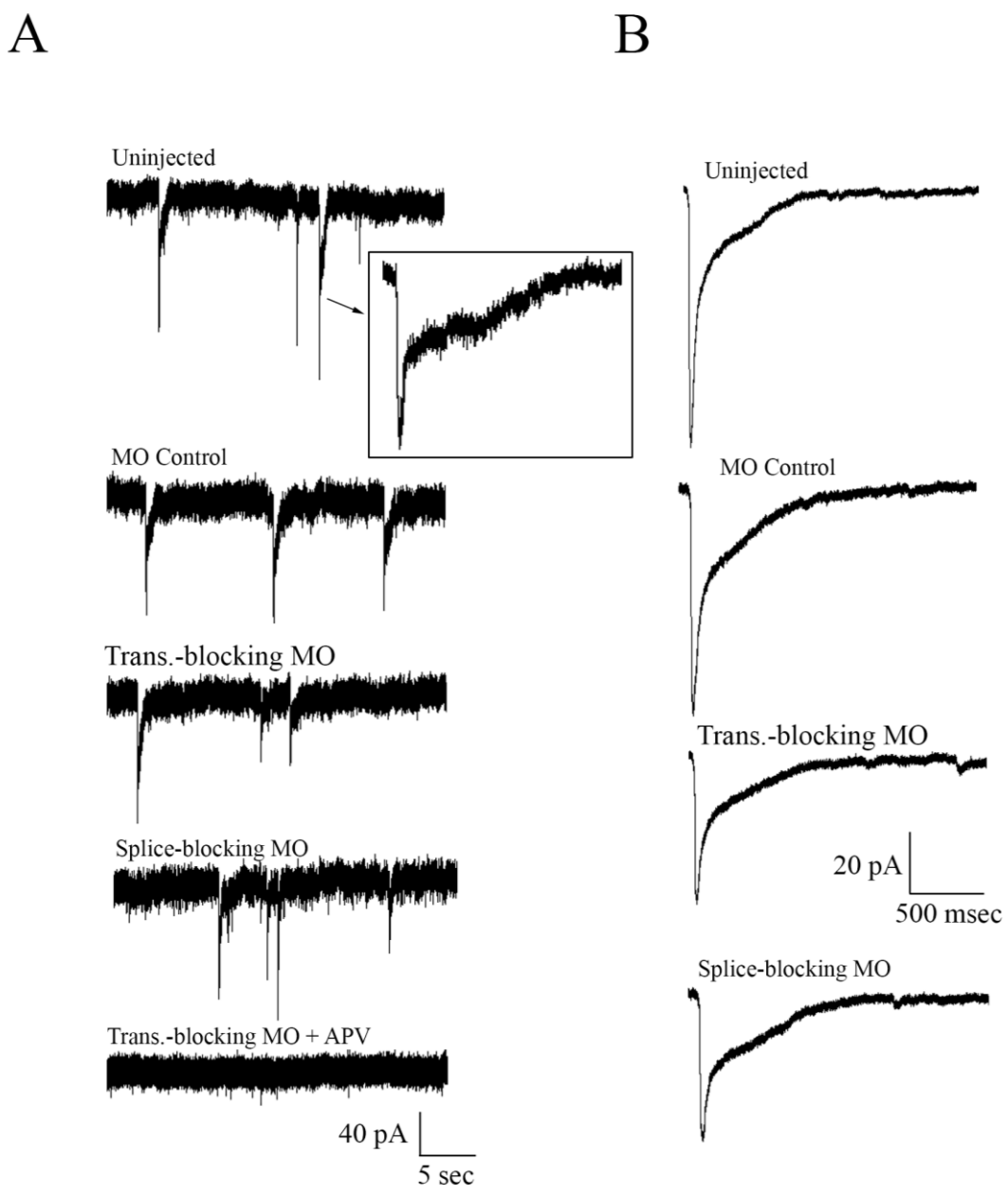
A
B
Uninjected
MO Control
Trans.-blocking MO
Splice-blocking MO
Trans.-blocking MO + APV
40 pA
5 sec
Uninjected
MO Control
Trans.-blocking MO
20 pA
500 msec
Splice-blocking MO

Figure 4.9 Spontaneous synaptic NMDAR currents obtained from M-cells. (A) Uninjected embryos, control morpholino injected embryos, translation-blocking morpholino injected embryos and splice-blocking morpholino injected embryos exhibit NMDAR currents at similar frequencies. The inclusion of APV (50 μM) confirmed the mEPSCs as NMDAR-mediated. Inset shows an example of an individual mEPSC on an expanded time scale. Note the biexponential decay phase of the individual event. Preparations were incubated in TTX (1 μm), strychnine (5 μM), picrotoxin (100 μM) and NBQX (0.1 μM) to block action potentials, glycine, GABA and AMPA receptors respectively. (B) Averaged mEPSCs recorded from M-cells of an uninjected control, a control MO injected embryo and translation-blocking morpholino injected embryo and a splice-blocking morpholino injected embryo. Each trace is an average of multiple events; 86 mEPSCs for the uninjected controls, 44 events for the MO controls, 58 events for the translation-blocking morphants and 22 events for the splice-blocking morphants.

Figure 4.10

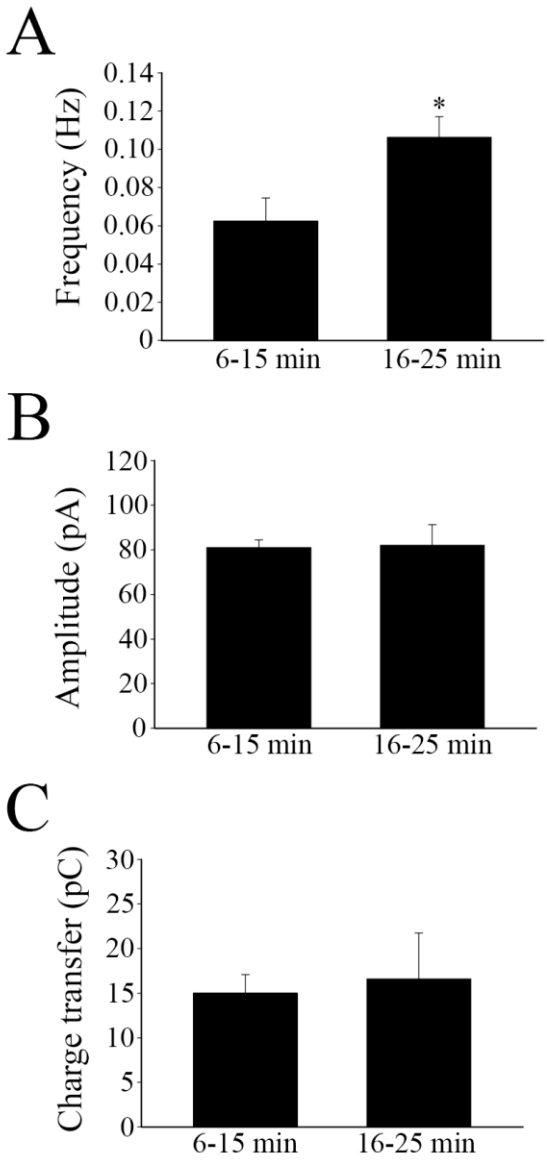
A
Frequency (Hz)
0.14
0.12
0.10
0.08
0.06
0.04
0.02
0
*
6-15 min
16-25 min
B
Amplitude (pA)
120
100
80
60
40
20
0
6-15 min
16-25 min
C
Charge transfer (pC)
30
25
20
15
10
5
0
6-15 min
16-25 min

Figure 4.10 Long-term stability of NMDA mEPSCs. Bar graphs comparing frequency (A), peak amplitude (B), and mean charge transfer (C) between events captured from 6 to 15 minutes and events captured from 16-to 25 minutes of recording. * Significantly different, $p < 0.05$.

Figure 4.11

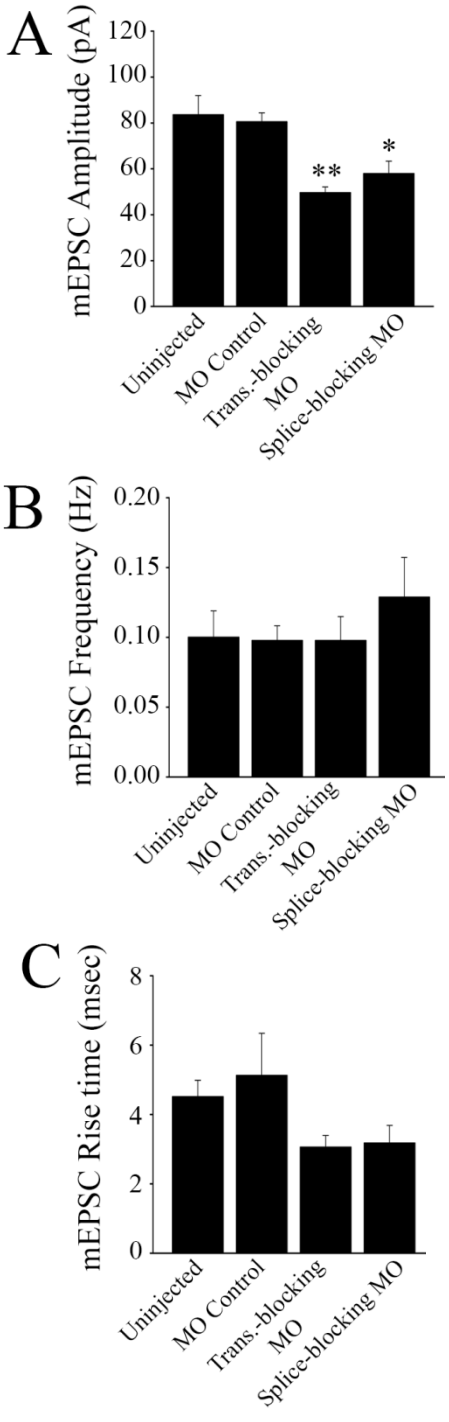
A
mEPSC Amplitude (pA)
120
100
80
60
40
20
0
**
*
Uninjected
MO Control
Trans.-blocking MO
Splice-blocking MO
B
mEPSC Frequency (Hz)
0.20
0.15
0.10
0.05
0.00
Uninjected
MO Control
Trans.-blocking MO
Splice-blocking MO
C
mEPSC Rise time (msec)
8
6
4
2
0
Uninjected
MO Control
Trans.-blocking MO
Splice-blocking MO

Figure 4.11 Properties of NMDA mEPSCs. Bar graphs comparing the peak amplitude (A), frequency (B) and 20-80% rise time (C) of averaged NMDA mEPSCs. * Significantly different from uninjected and MO controls, $p<0.05$, ** significantly different from uninjected and MO controls, $p<0.01$.

Figure 4.12

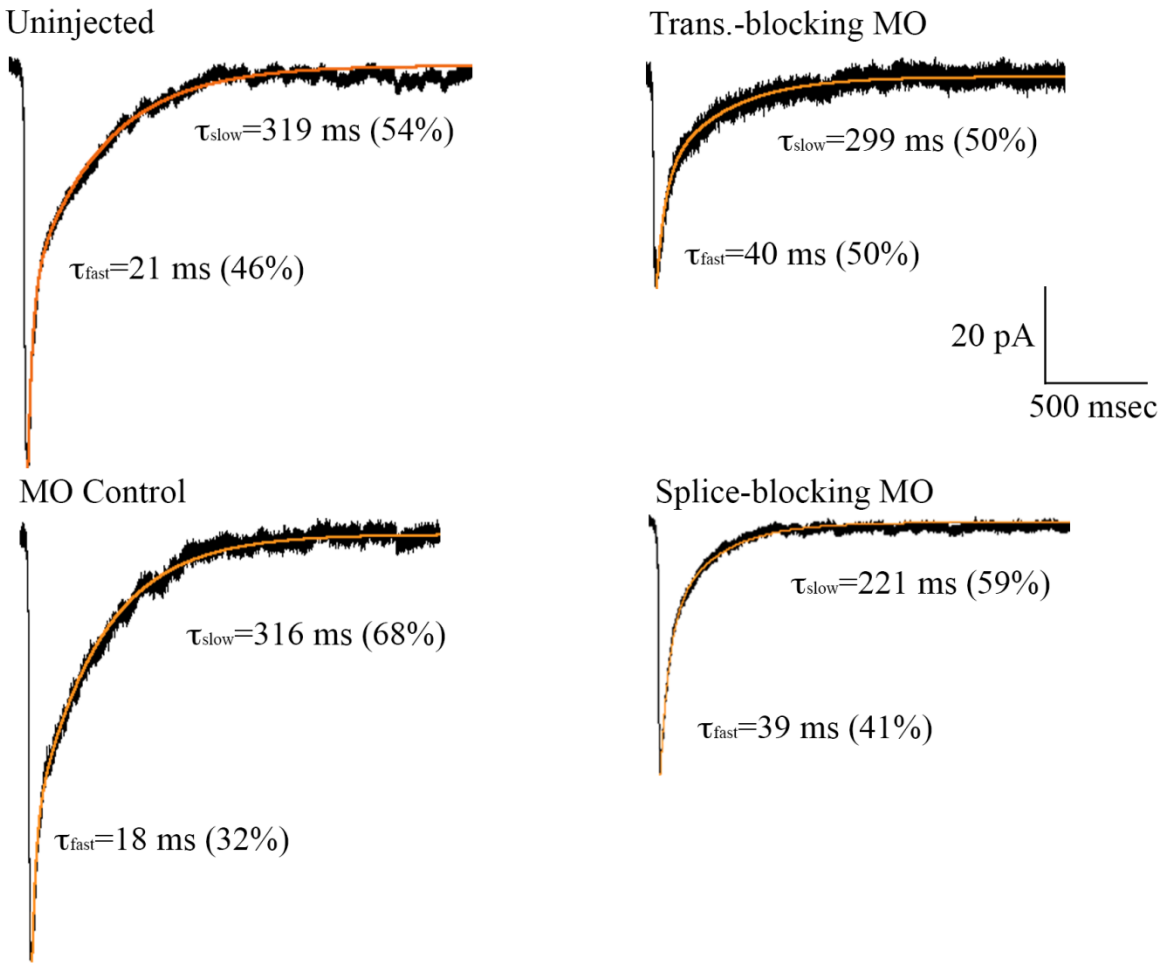
Uninjected
τslow=319 ms (54%)
τfast=21 ms (46%)
Trans.-blocking MO
τslow=299 ms (50%)
τfast=40 ms (50%)
20 pA
500 msec
MO Control
τslow=316 ms (68%)
τfast=18 ms (32%)
Splice-blocking MO
τslow=221 ms (59%)
τfast=39 ms (41%)

Figure 4.12 Averaged NMDA mEPSCs. The averaged traces had biexponential decay phases with τ_{fast}=21 ms and τ_{slow} =319 ms in the uninjected control, τ_{fast} =18 ms and τ_{slow}=316 ms in the MO controls, τ_{fast} =40 ms and τ_{slow}=299 ms for the translation-blocking morphants and τ_{fast}=39 ms and τ_{slow} =221 ms for the splice-blocking morphants.

Figure 4.13

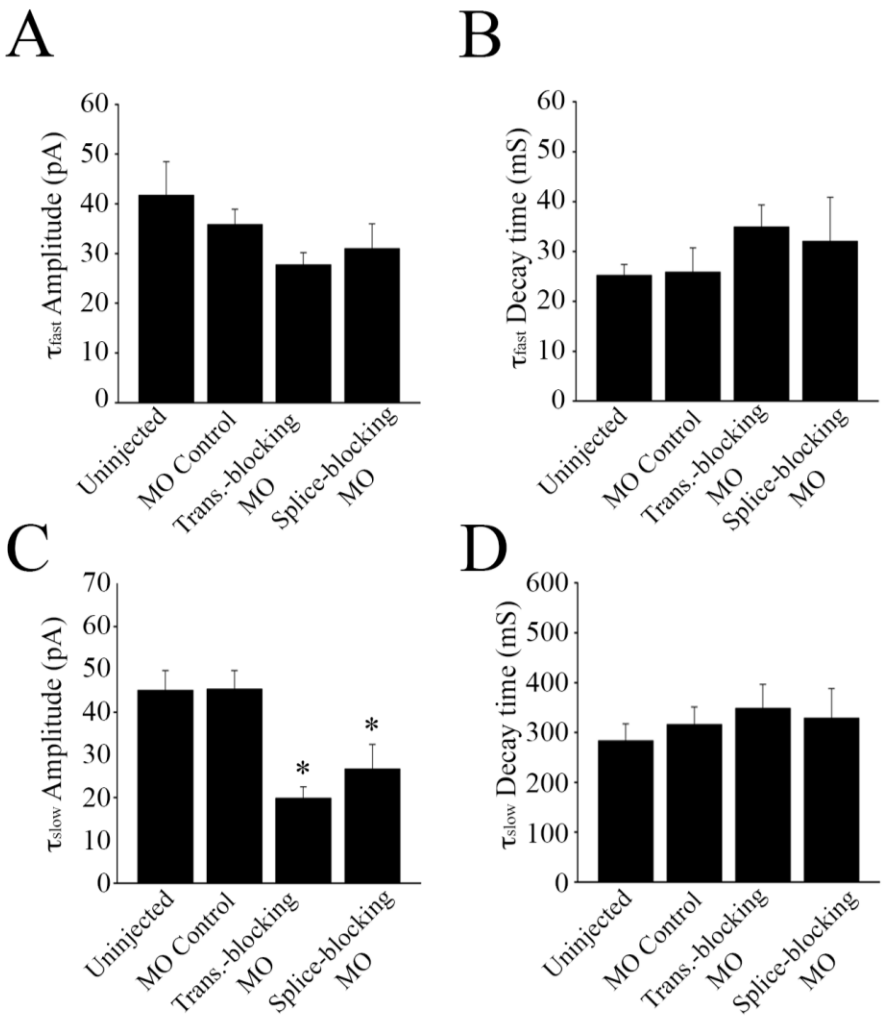
A
B
C
D
τfast Amplitude (pA)
τfast Decay time (mS)
τslow Amplitude (pA)
τslow Decay time (mS)
Uninjected
MO Control
Trans.-blocking MO
Splice-blocking MO
*
*

Figure 4.13 Decay kinetics of NMDA mEPSCs. Bar graphs comparing the amplitude of the fast component (A), the decay time constant of the fast component, τ_{fast} (B), the amplitude of the slow component (C), and the decay time constant of the slow component, τ_{slow} (D). * Significantly different from uninjected and MO controls, $p<0.05$.

Figure 4.14

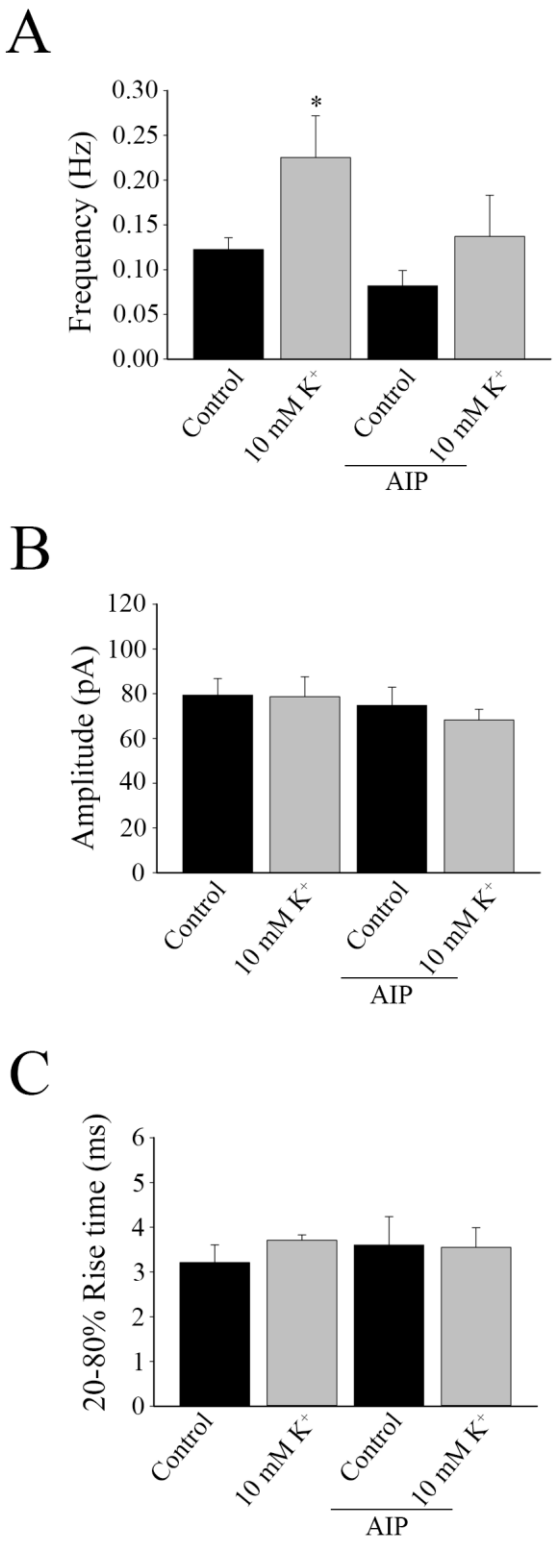
A
Frequency (Hz)
0.30
0.25
0.20
0.15
0.10
0.05
0.00
*
Control
10 mM K+
Control
10 mM K+
AIP
B
Amplitude (pA)
120
100
80
60
40
20
0
Control
10 mM K+
Control
10 mM K+
AIP
C
20-80% Rise time (ms)
6
5
4
3
2
1
0
Control
10 mM K+
Control
10 mM K+
AIP

Figure 4.14 NMDA mEPSC properties before and after acute activation or inhibition of CaMKII-α. Acutely activation of CaMKII-α was induced by a 5 minute bath of 10 mM K^+ containing recording solution (n = 4 experiments). A CaMKII-α specific inhibitory peptide, AIP (1 μM) was included AIP in the intracellular recording solution to block CaMKII-α activity (n = 4 experiments). Bar graphs comparing frequency (A), amplitude (B), and 20-80% rise time (C) of the averaged mEPSCs before and after acute activation or inhibition of CaMKII-α. * Significantly different than control, $p < 0.05$.

Figure 4.15

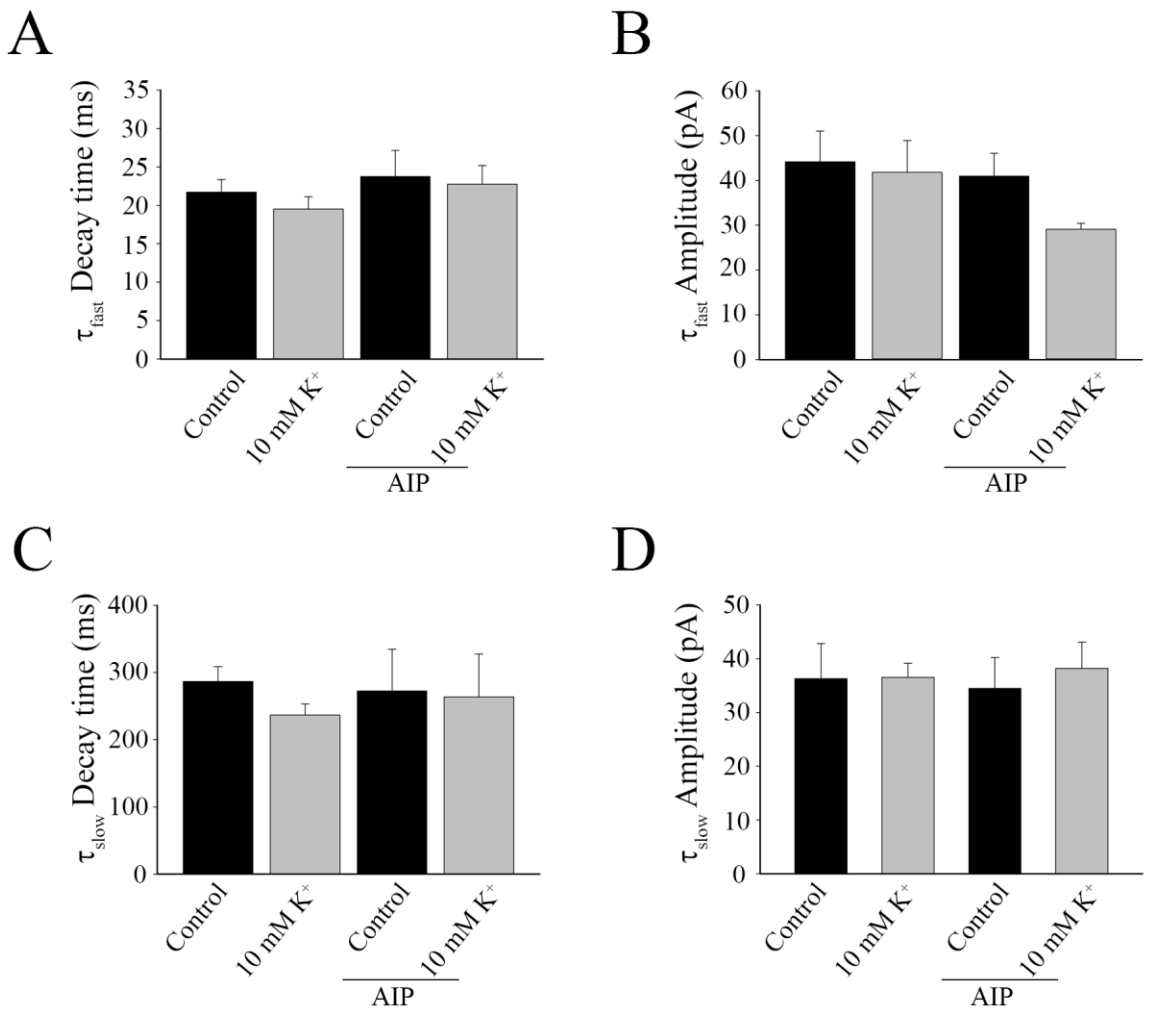
A
B
C
D
τ_{fast} Decay time (ms)
τ_{fast} Amplitude (pA)
τ_{slow} Decay time (ms)
τ_{slow} Amplitude (pA)
Control
10 mM K+
Control
10 mM K+
AIP

Figure 4.15 NMDA mEPSC decay kinetics following 10 mM K^+ stimulation. Bar graphs shows (A) the decay time constant of the fast component, τ_{fast} (B), the amplitude of the fast component, (C) the decay time constant of the slow component, τ_{slow}, and (D) the amplitude of the slow component.

Chapter 5: Effect of CaMKII-α on $GABA_A$ and Glycine receptor mediated inhibitory synaptic currents[3]

5.1 Introduction

γ-Aminobutyric acid (GABA) is a major inhibitory neurotransmitter in the vertebrate nervous system (Capogna and Pearce, 2011; Mody and Pearce, 2004; Roberts and Frankel, 1950, 1951; Rudolph and Mohler, 2014). It mediates fast, inhibitory synaptic transmission by binding to ionotropic $GABA_A$ receptors ($GABA_A$Rs), and slower, second messenger signaling via activation of metabotropic $GABA_B$ receptors. Ionotropic $GABA_A$Rs belong to the family of pentameric, fast ligand gated receptors and are composed of 5 individual subunits (α1-6, β1-3, γ1-3, δ, ε, θ, π, ρ1-3) with various stoichiometries (Laurie et al., 1992a; Laurie et al., 1992b; Wisden et al., 1992). Although $GABA_A$Rs can be composed of a wide diversity of subunits, the α1β2γ2 subunit combination appears to be the predominant form in the mammalian brain (Laurie et al., 1992a; Laurie et al., 1992b; Wisden et al., 1992).

The GABA system plays crucial roles in regulating and controlling neural networks and GABAARs are key targets for the treatment of disorders such as schizophrenia, autism, epilepsy and depression (Rudolph and Mohler, 2014). Thus, it is important to have a clear understanding of the properties, behavior and function of $GABA_A$Rs. Multiple studies have reported on the expression of GABA neurons in the zebrafish brain (Doldan et al., 1999; Mueller et al., 2006; Tabor and Friedrich, 2008), but an investigation into the

[3] A version of this chapter has been published: Roy, B., and Ali, D.W. (2014). Multiple types of GABAA responses identified from zebrafish Mauthner cells. *Neuroreport* 25(15):1232-6.

electrophysiological properties of $GABA_A$Rs in developing zebrafish has not been presented. In this section of the thesis I sought to determine the properties of synaptic $GABA_A$R associated with the M-cells in zebrafish. Additionally, I sought to determine if knockdown of CaMKII had an effect on the development of $GABA_A$Rs, since CaMKII potentiates $GABA_A$R currents in other organisms (Houston and Smart, 2006).

In addition to GABA synaptic activity, the M-cell receives a substantial amount of inhibition via Glycine receptors (GlyRs) (Ali et al., 2000b; Legendre and Korn, 1994). Like $GABA_A$Rs, GlyRs are pentameric receptors, with various combinations of α and β subunits. The α subunits are encoded by four different genes (Glra 1-4), while the β subunit is encoded by one gene (Glrb) in mammals. The α subunits contain the ligand binding sites for glycine, while the β subunit provides the binding site for gephyrin. The majority of synaptic GlyRs are heteromeric assemblies of α and β subunits, although homomeric receptors containing only α subunits can also form functional receptors that are mostly non-synaptic due to the lack of gephyrin binding sits on the α subunits. Expression of GlyRs in the CNS is developmentally regulated, with α2 being the most prominently expressed during embryonic development and α1 being the predominant form in the adult brain. Moderate expression of α3 transcript is also observed in the adult CNS (Malosio et al., 1991). The developmental changes of GlyRs are accompanied by changes in the biophysical and electrophysiological properties of the receptors (Betz and Laube, 2006). The development and maturation of GlyR synapses has been examined in zebrafish M-cells throughout the early developmental stages between 26 to 56 hpf (Ali et al., 2000b; Legendre, 1998; Legendre and Korn, 1994). Overall, spontaneous glycinergic

synaptic activity is detected as early as 26-29 hpf. The frequency of the mIPSCs increas progressively, presumably indicating accelerated synaptogenesis. Concomitant with the increasing frequency, the rise time and decay kinetics of the GlyRs become faster throughout the development, although the amplitude remains remarkably unchanged. It is proposed that the change in decay time reflects a transition from embryonic, slow GlyR to mature, fast GlyR subtypes during this time period. CaMKII plays an important role in the formation and maturation of glycinergic synapses (Charrier et al., 2010; Wang and Randic, 1996; Yamanaka et al., 2013). GlyRs are primarily inserted and removed from plasma membrane from non-synaptic sites. Single particle imaging techniques revealed that GlyRs diffuse freely on the plasma membrane and are trapped into synaptic sites by interaction with the scaffolding protein gephyrin (Dahan et al., 2003; Feng et al., 1998). Recently, adhesion protein integrins have been found to regulate the number of GlyRs at synapses indirectly by modulating gephyrin turnover at synaptic sites in a CaMKII dependent manner (Charrier et al., 2010). Inhibition of CaMKII decreases synaptic accumulation of GlyRs but did not affect GlyR mobility in the extrasynaptic membrane. Inhibition of CaMKII also impairs synaptic accumulation of GlyRs in embryonic zebrafish M-cells (Yamanaka et al., 2013), where application of a CaMKII inhibitor KN-93 to 1-3 dpf embryos or targeted expression of a CaMKII inhibitor peptide in zebrafish M-cell both reduce GlyR clustering. Given that CaMKII is involved in the clustering of the GlyRs, and the kinetic properties of these receptors change during embryonic development, I hypothesized that CaMKII-α may play a role in the development of GlyR currents.

5.2 Results

5.2.1 Characterization of GABAergic miniature inhibitory synaptic currents (mIPSCs) in Mauthner cell

To isolate $GABA_A$ mIPSCs, I recorded in the presence of TTX (1 μM), kynurenic acid (1 mM), and strychnine (5 μM). Bath application of the $GABA_AR$ antagonist, picrotoxin (100 μM), completely abolished all remaining mIPSCs, confirming their identity as $GABA_A$-mediated (Figure 5.1A). GABA mIPSCs were low in amplitude, averaging 27.2 ± 0.9 pA (Figure 5.2A; n = 271 events), and only occurred about once every 30 seconds. To examine mIPSC properties, I binned the event amplitudes and 20-80% rise times and plotted their distributions (Figure 5.2A, B). Both distributions were normal but were skewed towards larger values. Interestingly, the rise time distribution exhibited a main peak around 0.5 ms, and a second smaller peak around 2 ms (Figure 5.2B) indicating the possible presence of a sub-population of events that may represent activation of extrasynaptic receptors (Capogna and Pearce, 2011; Ferando and Mody, 2013). A scatter plot of 20-80% rise time versus amplitude showed that the longer rise time events clustered around the lower amplitudes, as might be expected for the activation of extrasynaptic events (Figure 5.2C).

To examine the mIPSC decay kinetics, I fitted the decay portion of individual events with an exponential function. Most events were well fit with a single exponential decay; with values ranging from ~10 ms to ~300 ms. Approximately 15% of the events were better fit with a double exponential decay rather than with a single exponent. I separated the events based on single or double exponential time courses and examined

them further. The distribution of mIPSCs with single decay kinetics was skewed towards larger values (Fig 5.3A) with a main peak around 40-60 ms and a second, smaller peak around 150 ms. A scatter plot of the single decay time constant versus peak amplitude indicated that the majority of the longer decaying events had smaller amplitudes in the range of 15 pA to 45 pA (Fig 5.3B). These results suggested that there might be two separate populations of events that decay with a single exponential time course: fast and slow mIPSCs. Therefore, we grouped the events into two groups: the first (group I) exhibited a single decay component less than 100 ms (peaking between 40 and 60 ms) and the second (group II) had decay time courses above 100 ms (peaking between 120-160 ms) (Fig 5.1B, 5.3C). Lastly, we placed the double exponential events in group III.

The mean time course of the fast component of the double decay events (τ_1= 28.7±2.5 ms, n = 42 events from 9 experiments) was shorter than the time course of the single exponential fast events (Fig 5.3C; τ_{Fast} = 54 ± 1.6 ms, n = 192 events; $p<0.001$ Mann- Whitney U test), while the time course of the slow component of the double decay (τ_2 = 153 ± 11 ms, n = 42 events) was similar to the time course of the single exponential slower event (τ_{Slow} = 151 ± 7 ms, n = 37 events) (Fig 5.3 C; p= 0.927, Mann-Whitney U test). Even though the mean values of the fast single decay events and the fast component of the double decay events were different, their distributions showed significant overlap, suggesting that they may indeed belong to the same population of receptors. Taken together, these results suggest the presence of 3 separate groups of events: single exponential fast, single exponential slow and double exponential events.

To further examine the properties of each of these 3 groups of mIPSCs, I compared their frequencies, amplitudes and rise times (Fig 5.4). The frequency of the fast single exponential events (τ_f) was several-fold greater than either the slow single decay (τ_s), or the double decay mIPSCs (Fig 5.4B; n = 9 experiments; p=0.001, one-way ANOVA, multiple comparison with Student-Newman-Keuls Method) suggesting that the majority of GABA synapses are of the fast type. The mean amplitude of the double decay events was significantly greater than either of the single decay groups (Fig 5.4A; $p<0.001$, Kruskal-Wallis One Way ANOVA, multiple comparison with Dunn's method). The amplitude of the fast component of the double exponential decay was 21.2 ± 2.4 pA (n = 42 events). Finally, there was no difference in mIPSC rise time between groups indicating that the longer rise time events (Figure 5.2B) were comprised of a mixture of events from all 3 group (Figure 5.4C; $p<0.05$; n=192 events for τ_{Fast}, n=37 events for τ_{Slow} and n=42 events for the double decay mIPSCs).

5.2.2 Effect of CaMK2-α on GABA receptor mediated mIPSCs

To determine the role of CaMKII-α on the GABA receptors, I recorded mIPSC from control MO-injected, and CaMKII-α translation blocking MO-injected embryos (n = 4 embryos in each group) as described in the previous section. Next, I assembled the events in three groups as described and analyzed the properties of each group of events. I detected very few events that fell in the double decay group (n = 6 events for control MO-injected embryos, and 7 for translation blocking morphants) and therefore excluded this group from further analysis. Comparison of single decay fast events between groups showed that there was no difference in the frequency, rise time or amplitude (Figure 5.5).

Interestingly, the decay time course of these fast events in translation blocking morphants (39.3 ± 1.7 ms, n = 130 events) was significantly smaller than control MO injected embryos (47.7 ± 1.7 ms, n = 146 events) (Figure 5.5D; $p < 0.05$, Mann-Whitney U test). Histograms of decay time distribution revealed that the fast events in translation blocking morphants were shifted towards lower values (Figure 5.6). The properties of slow mIPSCs were not significantly different between control morphants and translation blocking morphants (Figure 5.7).

5.2.3 CaMKII-α knockdown alters Glycine mIPSC decay kinetics

To determine if CaMKII-α is involved in the development of inhibitory synapses on zebrafish M-cells, I recorded glycine mIPSCs from control and morpholino injected embryos. I focused on the translation-blocking morphants for 2 reasons. First, when comparing the effects of the two different morpholinos thus far, I found no significant difference between them. Second, in the interest of time I was only able to investigate the effects a single morpholino and decided to use the translation-blocking morpholinos. To record Glycine currents from M-cells, I included TTX (1 μM) to block action potentials, kynurenic acid (1 mM) to block AMPA and NMDA receptors, and picrotoxin (100 μM) to block GABA receptors in the recording solution. All remaining currents were blocked by adding the glycine receptor antagonist, strychnine (5 μM) in the bath (Figure 5.8). Glycine mIPSCs were recorded from uninjected, control morpholino-injected, and CaMKII–α translation blocking morpholino-injected embryos. Amplitude histograms show no obvious differences between the three groups (Fig 5.9). Additionally, bar graphs

of the mean mIPSC amplitudes and frequencies showed no significant effect of knocking down CaMKII-a (Fig 5.9; p=0.782 and 0.508 respectively, one-way ANOVA).

Similar analysis revealed that the 20-80% rise times were normally distributed between groups (Fig 5.10A). Bar graphs of the mean rise times also indicated no significant differences between groups (Fig 5.10B, p=0.36, one-way ANOVA). Scatter plots of mIPSC rise times versus amplitudes showed no correlation between these parameters, suggesting that there were no space clamping issues in the recordings. Next, I examined the decay time constants of the mIPSCs. Glycinregic mIPSCs have been extensively investigated in the Ali lab and show double exponential decay time constants throughout development (Ali et al., 2000b; Legendre, 1998; Legendre and Korn, 1994). At the time of hatching (48-52 hpf) glycinergic mIPSCs associated with the M-cells of uninjected fish exhibit a fast component with a time course of 1.2 ± 0.1 ms (n=10), and a slow component of 5.0 ± 0.4 ms. The decay time constants of the control morphant group is similar with a fast component of 1.2 ± 0.1 ms and a slow component of 5.8 ± 0.5 ms (n=7) (Fig 5.11, 5.12). However, the decay time courses of the mIPSCs recorded from the translation-blocking morphants was significantly longer in duration than either of the controls (Fig 5.12, p=0.037, one-way ANOVA, multiple comparison with Student-Newman-Keuls Method). Specifically, I found that the fast decay component of the mIPSC was 1.6 ± 0.1 ms (n=6) and for the slow component it was 7.6 ± 0.6 ms (Fig 5.12). The relative amplitudes of the fast and the slow decay time constants were not significantly different from the uninjected controls or the morpholino control groups (Fig 5.11B).

Figure 5.1

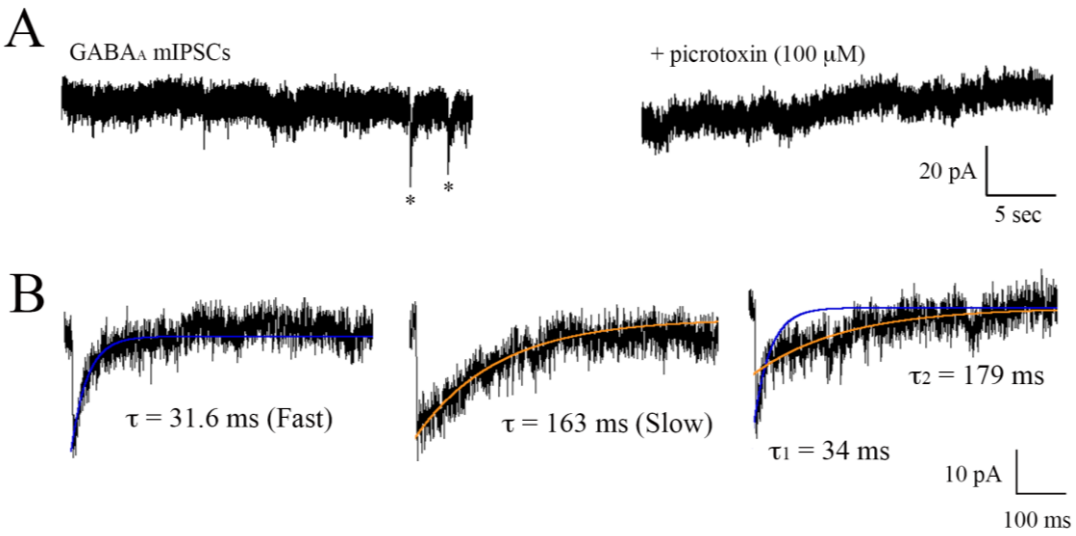
A
GABAA mIPSCs
+ picrotoxin (100 μM)
20 pA
5 sec
B
τ = 31.6 ms (Fast)
τ = 163 ms (Slow)
τ2 = 179 ms
τ1 = 34 ms
10 pA
100 ms

Figure 5.1 Isolation of GABA mIPSCs from M-cells of 2 dpf zebrafish embryos. (A) A 30 second trace showing the low frequency of mIPSCs (denoted by *) during bath application of 1 μM TTX, 1 mM kynurenic acid and 5 μM strychnine to block action potentials, AMPA, NMDA and glycine receptors respectively. Bath application of 100 μM picrotoxin blocks mIPSCs. (B) Individual mIPSCs recorded from 48 hpf embryos with a single decay time course (τ) of 31.6 ms, 163 ms, or a double exponential decay of τ_1 = 34 ms and τ_2 = 179 ms.

Figure 5.2

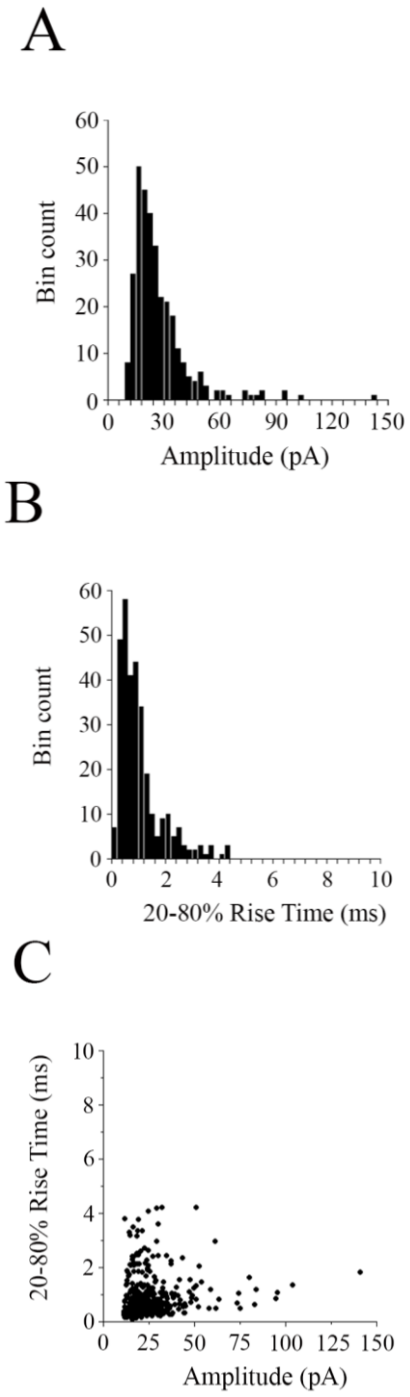
A
Bin count
Amplitude (pA)
B
Bin count
20-80% Rise Time (ms)
C
20-80% Rise Time (ms)
Amplitude (pA)

Figure 5.2 Properties of GABA mIPSCs. (A) Amplitude distribution of the mIPSCs obtained from 9 separate recordings (n= 271 events; binwidth = 3 pA). (B) 20-80% Rise time distribution of all mIPSCs (n = 271 events; binwidth = 0.2 ms). (C) Scatter plot of rise time vs. amplitude for all of the mIPSCs obtained from 9 separate recordings.

Figure 5.3

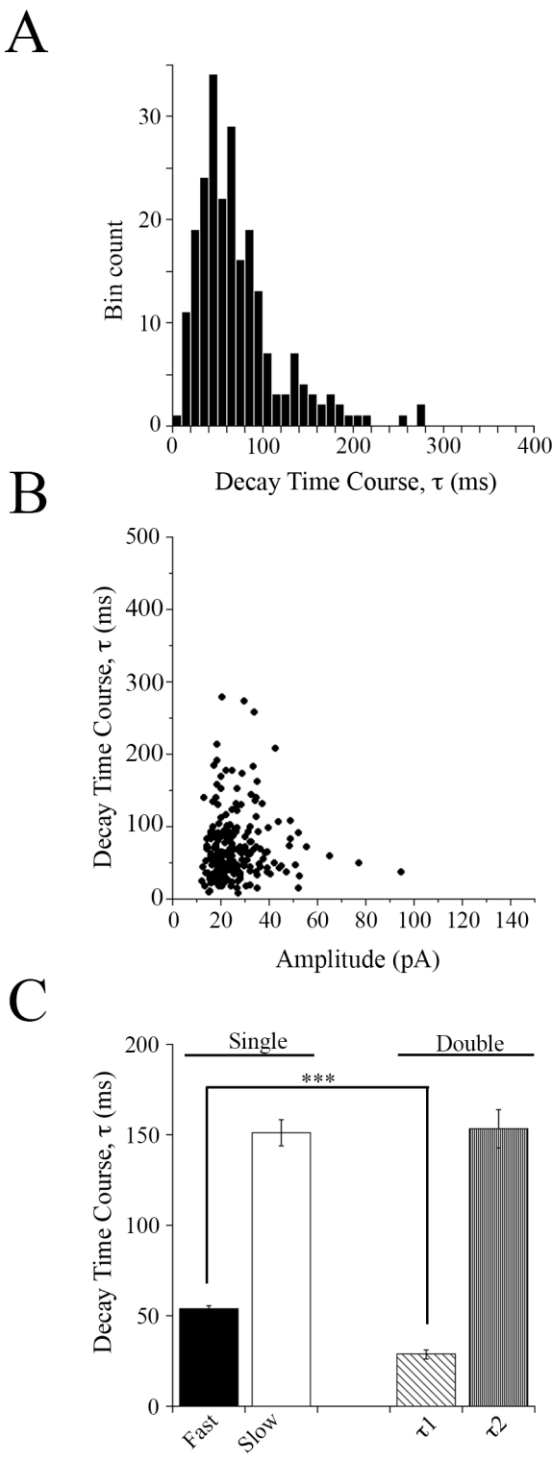
A
Bin count
Decay Time Course, τ (ms)
B
Decay Time Course, τ (ms)
Amplitude (pA)
C
Single
Double
***
Decay Time Course, τ (ms)
Fast
Slow
τ1
τ2

Figure 5.3 Decay kinetics of GABA mIPSCs. (A) Single exponential decay distribution of mIPSCs that were appropriately fit with a single exponential decay (n = 229 events; binwidth = 10 ms). (B) Scatter plot of single exponential decay vs. peak amplitude of mIPSCs. (C) Bar graph of the decay time constants for the single fit fast events (τ_f), single fit slow events (τ_s) and the fast (τ_1) and slow (τ_2) components of the double exponential fits. *** Significantly different from control, $p<0.001$.

Figure 5.4

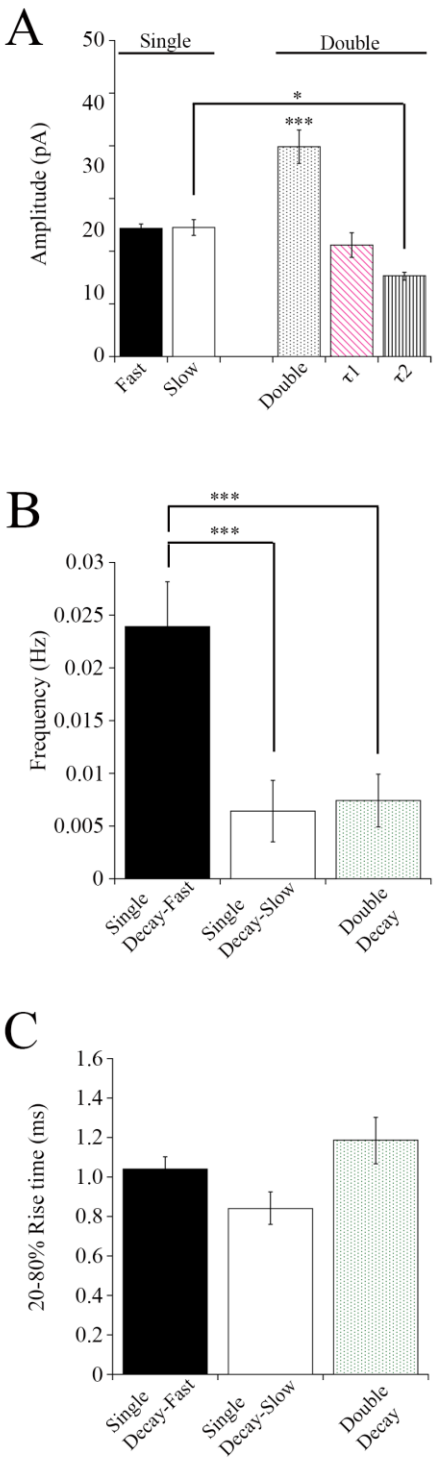
A
Single
Double
Amplitude (pA)
50
40
30
20
10
0
*
***
Fast
Slow
Double
τ1
τ2
B
***
***
Frequency (Hz)
0.03
0.025
0.02
0.015
0.01
0.005
0
Single Decay-Fast
Single Decay-Slow
Double Decay
C
20-80% Rise time (ms)
1.6
1.4
1.2
1.0
0.8
0.6
0.4
0.2
0
Single Decay-Fast
Single Decay-Slow
Double Decay

Figure 5.4 Comparison of GABA mIPSC properties. (A) Averaged amplitudes of events from group I (τ_f; n=192), group II (τ_s; n=37) and group III (n=42). Note that the fast and slow components of the double fits are shown individually for comparison with the single exponential decays. (B) Averaged frequencies of events from group I, group II and group III. (C) Averaged 20-80% Rise times of group I, group II and group III events. * Significantly different from control, $p<0.05$, *** Significantly different from control, $p<0.001$.

Figure 5.5

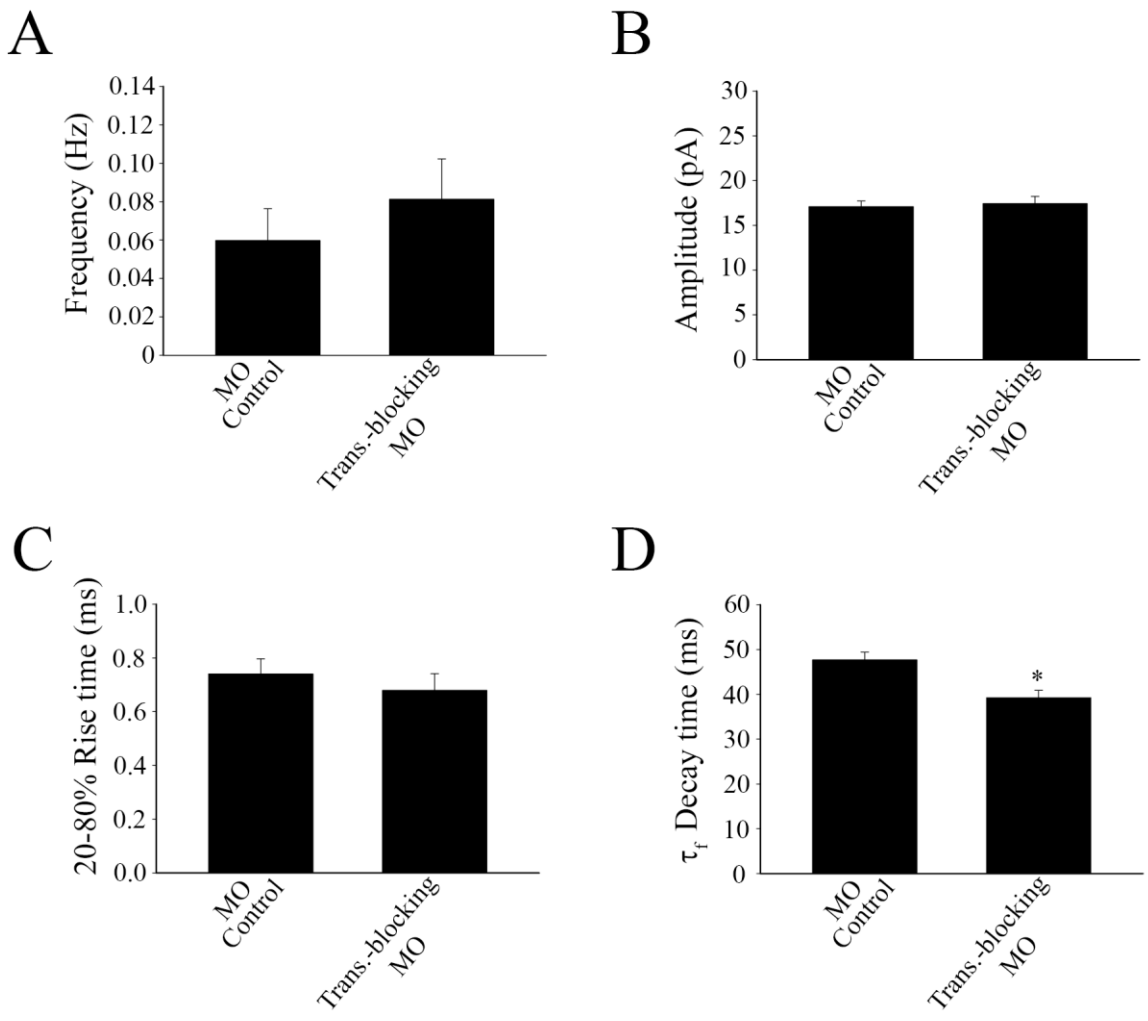
A
Frequency (Hz)
0.14
0.12
0.10
0.08
0.06
0.04
0.02
0
MO Control
Trans.-blocking MO
B
Amplitude (pA)
30
25
20
15
10
5
0
MO Control
Trans.-blocking MO
C
20-80% Rise time (ms)
1.0
0.8
0.6
0.4
0.2
0.0
MO Control
Trans.-blocking MO
D
τf Decay time (ms)
60
50
40
30
20
10
0
*
MO Control
Trans.-blocking MO

Figure 5.5 Properties of single decay fast (Group I) GABA mIPSCs in CaMKII-α morphant zebrafish. GABA mIPSCs were recorded from control morpholino injected (n = 4 embryos, 146 events) and translation-blocking morpholino injected (n = 4 embryos, 130 events). Bar graphs comparing (A) frequency, (B) amplitude, (C) 20-80% rise time, and (D) decay time course. * Significantly different compared to control, $p < 0.05$.

Figure 5.6

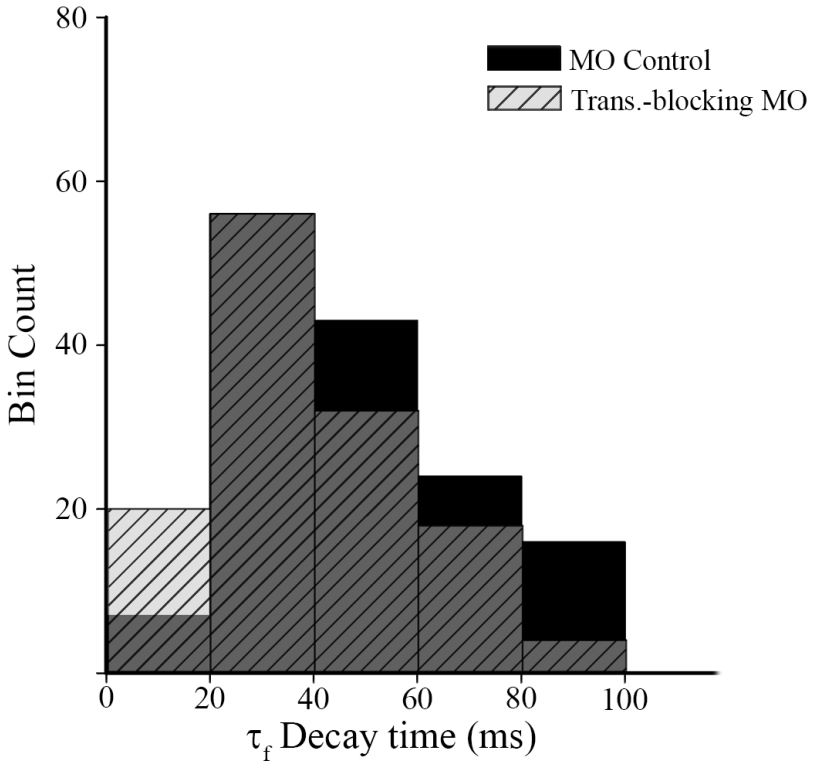
80
60
40
20
Bin Count
MO Control
Trans.-blocking MO
0
20
40
60
80
100
τf Decay time (ms)

Figure 5.6 Decay time course distribution of Group I events. Histograms showing decay time of single decay fast events from control morpholino injected embryos (n = 146 events, bin width = 20 ms), and translation blocked morphants (n = 130 events, bin width = 20 ms).

Figure 5.7

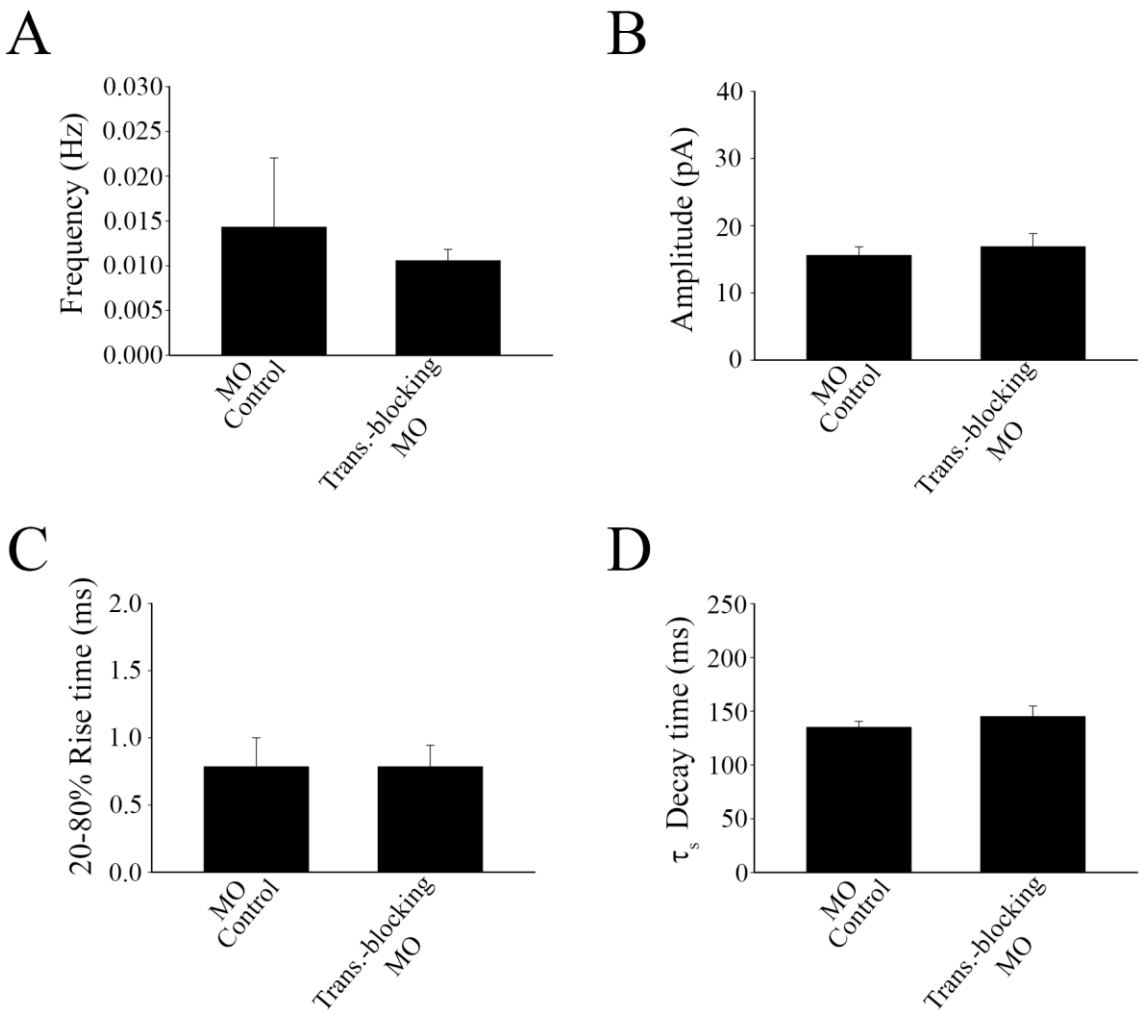
A
Frequency (Hz)
0.030
0.025
0.020
0.015
0.010
0.005
0.000
MO Control
Trans.-blocking MO
B
Amplitude (pA)
40
30
20
10
0
MO Control
Trans.-blocking MO
C
20-80% Rise time (ms)
2.0
1.5
1.0
0.5
0.0
MO Control
Trans.-blocking MO
D
τs Decay time (ms)
250
200
150
100
50
0
MO Control
Trans.-blocking MO

Figure 5.7 Properties of single decay slow GABA mIPSCs (Group II) in morphant embryos. Bar graphs comparing (A) frequency, (B) amplitude, (C) 20-80% rise time, and (D) decay time (n = 24 events for control MO injected, and 17 events for translation blocked morphants).

Figure 5.8

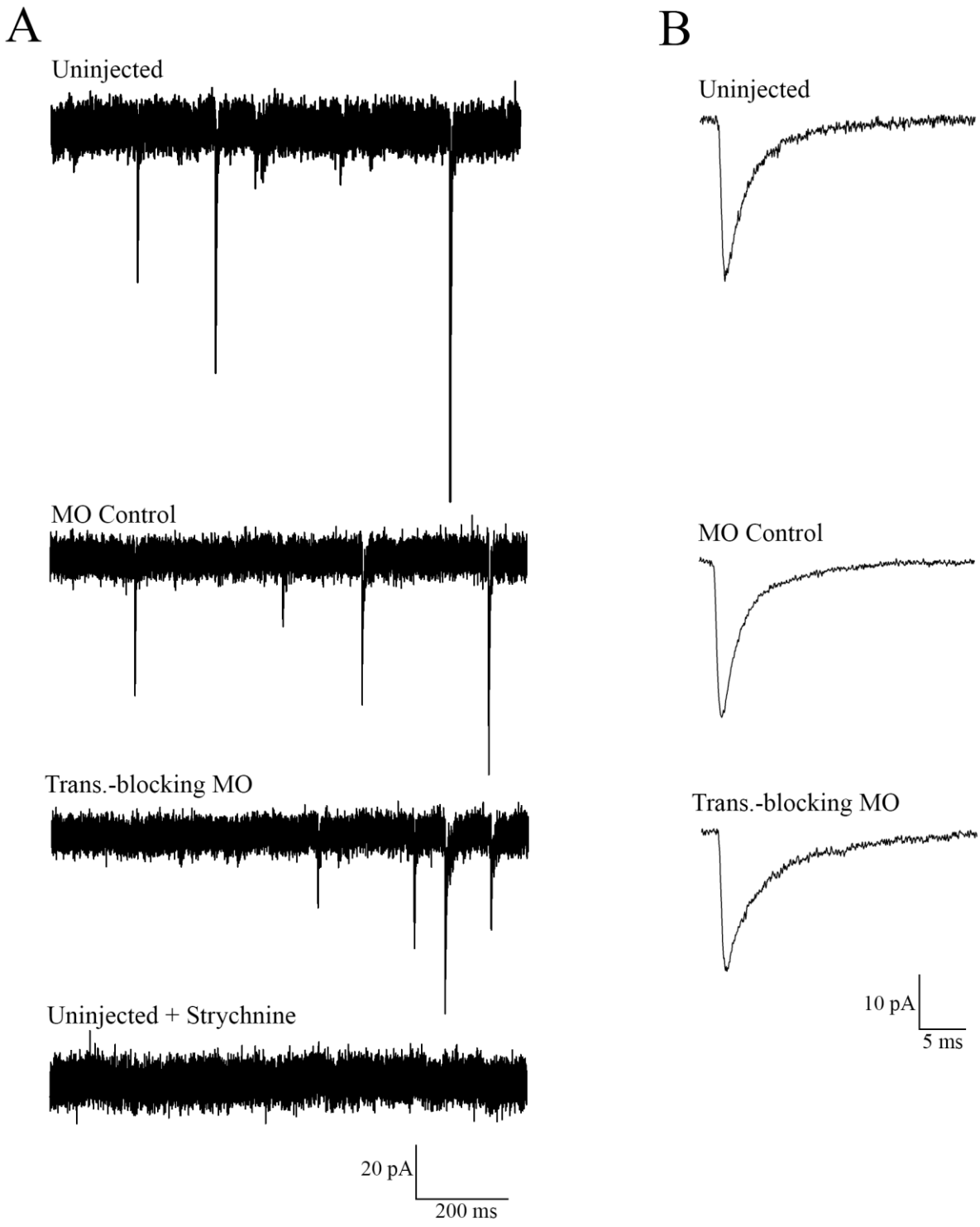
A
Uninjected
MO Control
Trans.-blocking MO
Uninjected + Strychnine
20 pA
200 ms
B
Uninjected
MO Control
Trans.-blocking MO
10 pA
5 ms

Figure 5.8 Spontenous synaptic GlyR currents recorded from 2 dpf zebrafish Mauthner cells. (A) Uninjected embryos (n=10), control morpholino injected embryos (n=7), and CaMKII-a translation blocking morpholino injected embryos (n=6) exhibit synaptic currents at comparable frequencies. Currents were recorded in the presence of 1 μM TTX, 1 mM kynurenic acid and 100 μM picrotoxin to block action potentials, ionotropic glutamate receptors and $GABA_A$ receptors respectively. The remaining currents were completely abolished by 5 μM strychnine incubation, confirming the identity of the synaptic currents as GlyR-mediated (B) Averaged GlyR mIPSCs. Each trace is an average of multiple events; 113 events for uninjected, 191 events for control morpholino injected and 114 events for translation blocking morpholino injected embryos

Figure 5.9

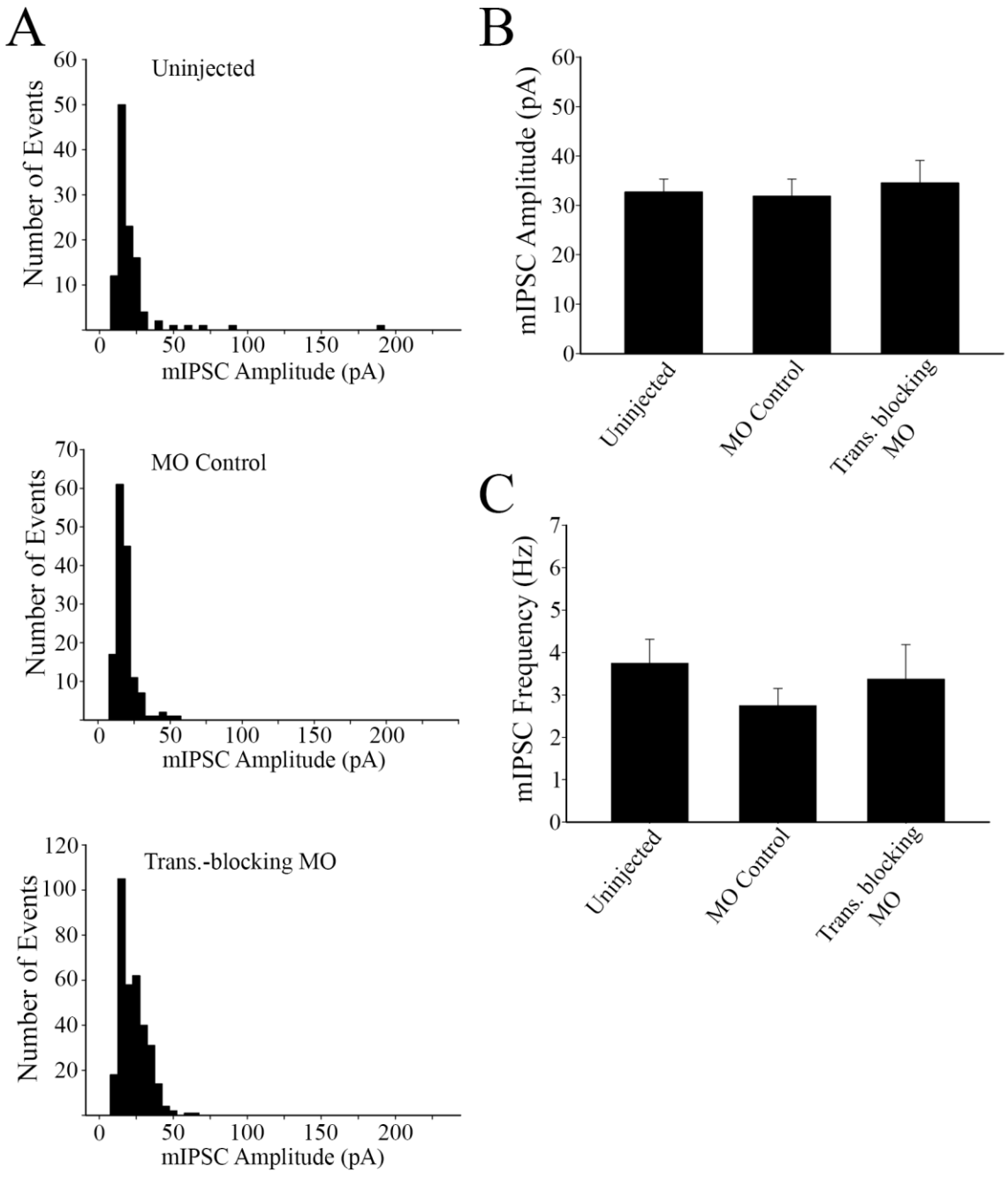
A
Uninjected
Number of Events
mIPSC Amplitude (pA)
MO Control
Trans.-blocking MO
B
mIPSC Amplitude (pA)
Uninjected
MO Control
Trans. blocking MO
C
mIPSC Frequency (Hz)

Figure 5.9 Distributions of Glycine mIPSCs. Example histograms of (A) amplitude (bin width = 10 pA) and (B) 20-80 % rise times (bin width = 100 μs) of mIPSCs obtained from uninjected (n = 112 events), control morpholino injected (n = 147 events) and translation-blocking morpholino injected (n = 336 events) embryos.

Figure 5.10

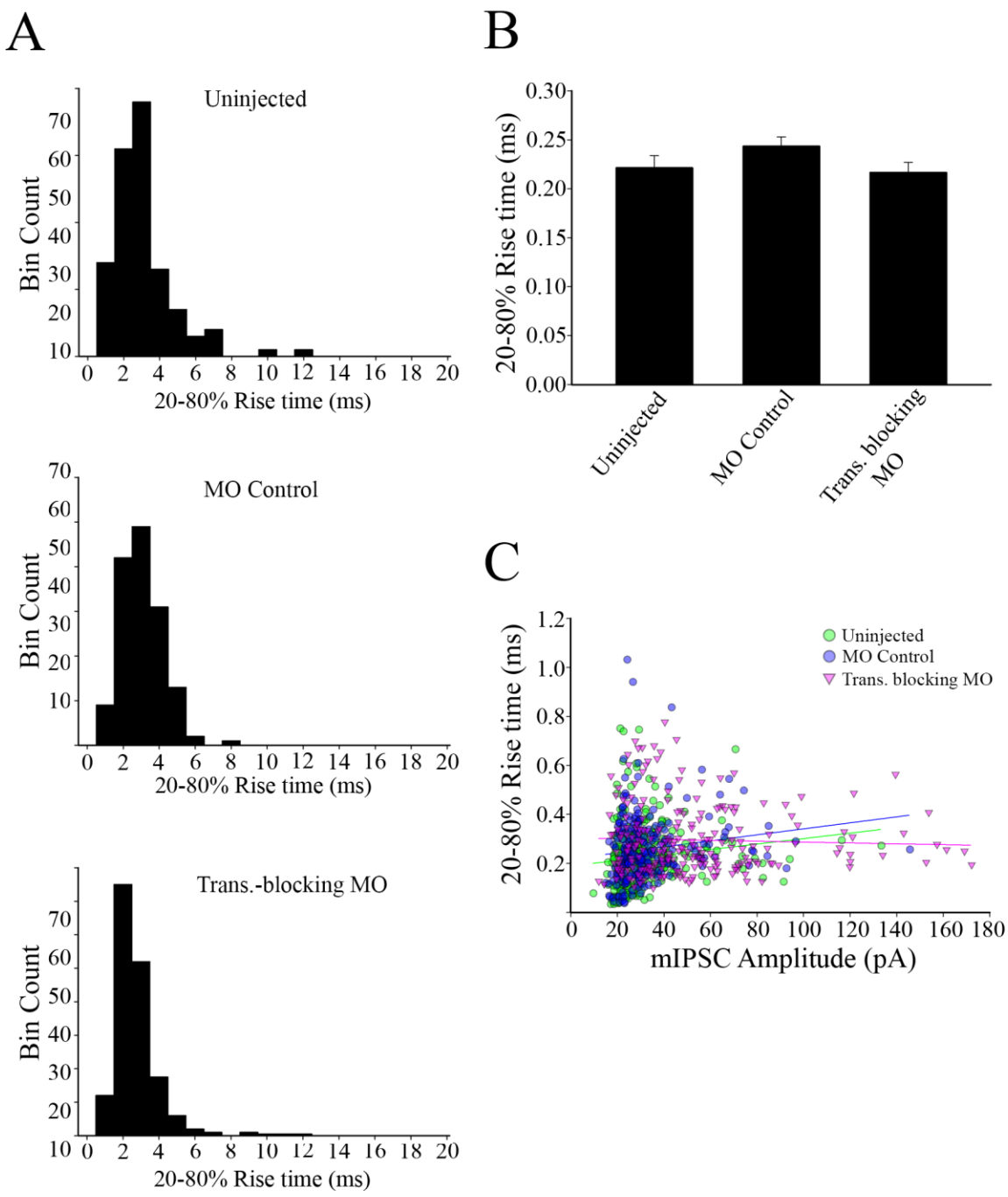
A
Uninjected
Bin Count
20-80% Rise time (ms)
MO Control
Trans.-blocking MO
B
20-80% Rise time (ms)
Uninjected
MO Control
Trans. blocking MO
C
Uninjected
MO Control
Trans. blocking MO
20-80% Rise time (ms)
mIPSC Amplitude (pA)

Figure 5.10 Properties of glycine mIPSCs. Bar graphs showing (A) frequency, (B) amplitude, and (C) rise time of glycine currents recorded from uninjected (n = 10), control morpholino injected (n = 7), and translation blocking morpholino injected (n = 6) 2 dpf embryos.

Figure 5.11

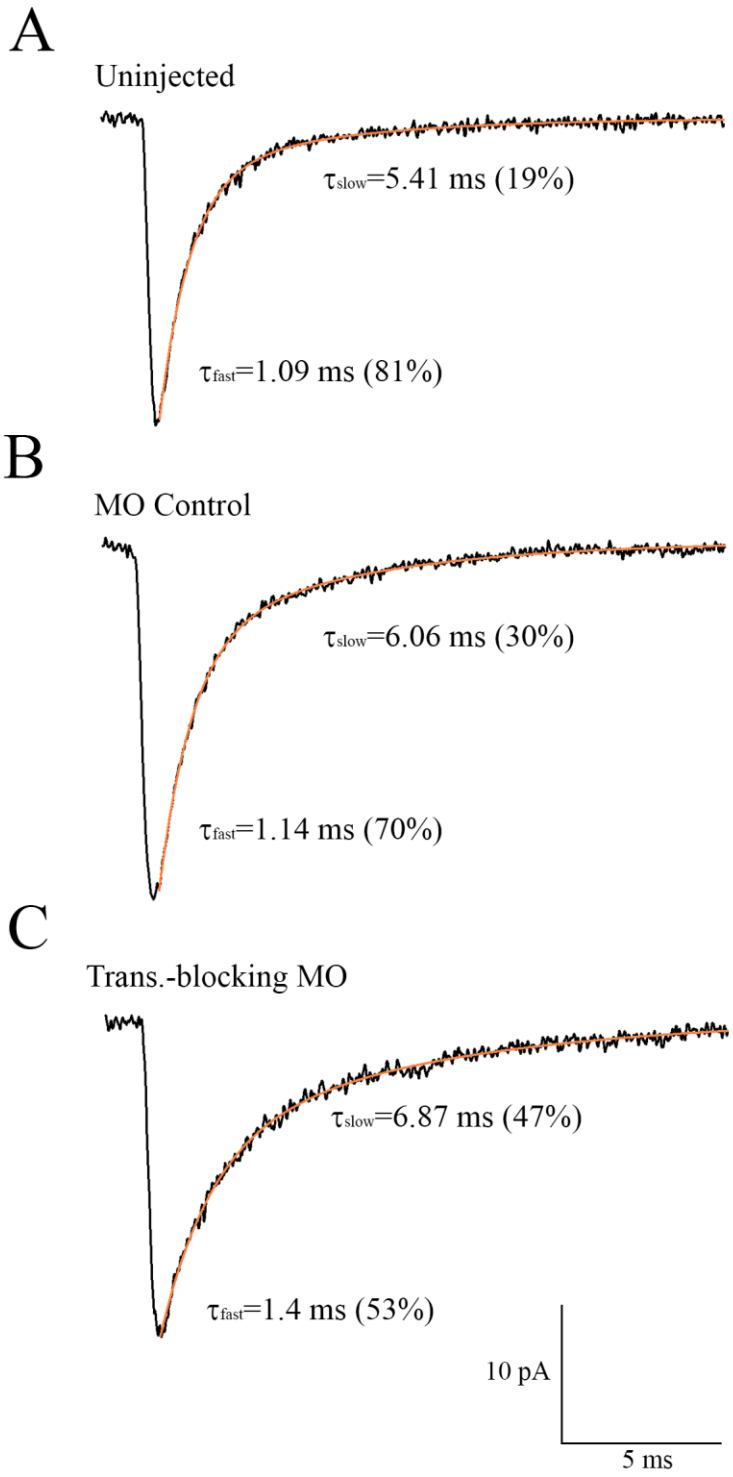
A
Uninjected
τslow=5.41 ms (19%)
τfast=1.09 ms (81%)
B
MO Control
τslow=6.06 ms (30%)
τfast=1.14 ms (70%)
C
Trans.-blocking MO
τslow=6.87 ms (47%)
τfast=1.4 ms (53%)
10 pA
5 ms

Figure 5.11 Averaged glycine mIPSCs. The decay phases of the average traces are best fitted with a double exponential function. Example average traces from (A) an uninjected embryo with τ_{fast} = 1.41 ms and τ_{slow} = 5.48 ms, (B) a control morpholino injected embryo with τ_{fast} = 1.14 ms and τ_{slow} = 6.06 ms and (C) a translation blocking morpholino injected embryo with τ_{fast} = 1.4 ms and τ_{slow} = 6.87 ms.

Figure 5.12

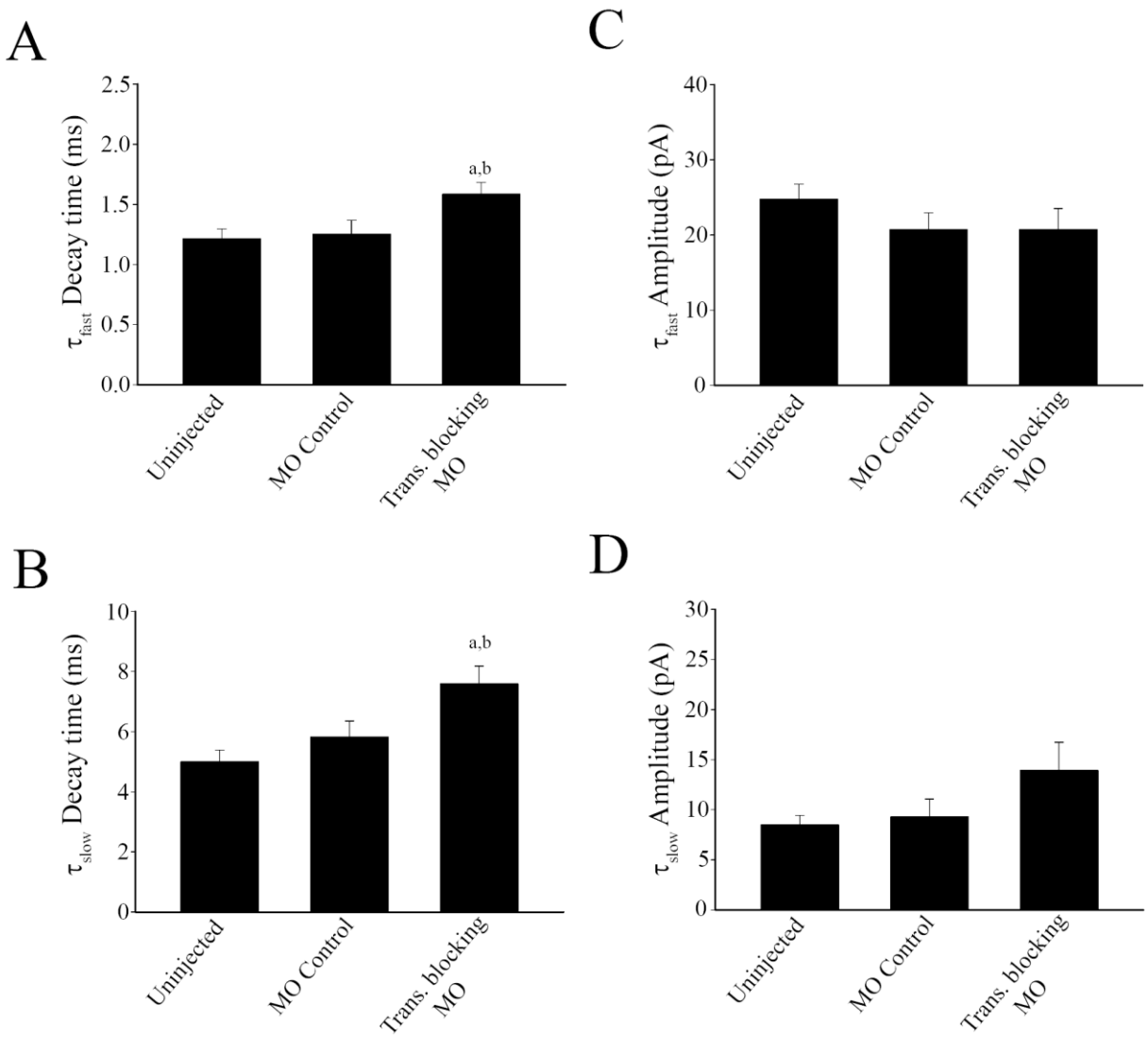
A
τ_{fast} Decay time (ms)
2.5
2.0
1.5
1.0
0.5
0.0
a,b
Uninjected
MO Control
Trans. blocking MO
C
τ_{fast} Amplitude (pA)
40
30
20
10
0
Uninjected
MO Control
Trans. blocking MO
B
τ_{slow} Decay time (ms)
10
8
6
4
2
0
a,b
Uninjected
MO Control
Trans. blocking MO
D
τ_{slow} Amplitude (pA)
30
25
20
15
10
5
0
Uninjected
MO Control
Trans. blocking MO

Figure 5.12 Glycine mIPSC decay kinetics. Bar graphs comparing (A) the decay time constant of the fast component, τ_{fast} (B), the amplitude of the fast component, (C) the decay time constant of the slow component, τ_{slow}, and (D) the amplitude of the slow component. a, significantly different from uninjected $p<0.05$, b, significantly different from MO Control $p<0.05$.

Chapter 6: Discussion

6.1 Overview of findings

In this thesis I present results from studies designed to determine the expression and function of CaMKII isoforms in the developing fish. Specifically, my goals were to determine exactly which isoforms of CaMKII are expressed in the M-cells of embryonic zebrafish and then determine their roles in synaptic physiology and locomotor responses. My first aim was to use single cell RT-qPCR to determine CaMKII expression in M-cells as shown in Chapter 3. To quantify CaMKII gene expression, I designed gene specific primer and probe sets for real-time amplification and detection of each of the seven genes. The primers were designed to anneal on two different exons separated by an intron, thus preventing false positive results due to genomic DNA amplification Single cells contain very minute amount of nucleic acid, typically in the low picogram range (Kawasaki, 2004). Therefore, I synthesized cDNA directly from the cells in the same tube where they were collected without an RNA extraction step to prevent sample loss. Additionally, TaqMan PreAmp mastermix was used to linearly amplify all target cDNA prior to qPCR. To ensure that the single cells were processed successfully, each sample was tested for the ubiquitously expressed transcription factor, *ef1a* alongside the CaMKII genes in the qPCR. Cells that did not express *ef1a* were deemed a processing failure and removed from further analysis, which prevented false negative results. My findings strongly suggest that *camk2a* is the predominantly expressed gene in 48 hpf M-cells, which encode the CaMKII-α □soform. To determine if CaMKII has a role in synaptic development and behavior, I knocked down its expression via morpholino technology. I

found that knockdown resulted in increased dendritic branching (of the M-cell), as has been shown in other organisms. Furthermore, knockdown of CaMKII-α affected the embryo's gross morphology and led to altered escape response. In Chapter 4, I examined the effect of knocking down CaMKII-α on the properties and activity of excitatory synapses that contain AMPA and NMDA receptors. I found that knockdown of CaMKII-α had no significant effect on the development of AMPA currents, but led to altered development of NMDAR currents. Specifically, the slow decay component of NMDA mEPSCs was reduced in amplitude in the knockdowns compared with controls. In Chapter 5, I examined the effect of CaMKII on $GABA_A$ and Glycine receptor mediated synaptic currents. I first characterized the $GABA_A$ receptor activity since this had not been done previously in zebrafish. My results suggest that there are 3 general groups of $GABA_A$R-containing synapses: the first (group I) expresses a homogeneous type of receptor with a broad distribution and a single exponential decay time peaking around 40-60 ms; the second (group II) expresses $GABA_A$Rs with a single decay time peaking around 120-160 ms, and the third (group III) appears to express a combination of the first two groups. I found that CaMKII-α has very little, if any effect on the development of GABA containing synapses. Lastly, I examined the properties of glycinergic synapses. Here, my results indicate that the time course of glycine mIPSCs was significantly slowed when CaMKII levels were reduced. Taken together, these findings support a role of CaMKII-α in the development of synaptic NMDARs and possibly GlyRs in embryonic zebrafish but suggest that it has little or no effect on the development of synapses that contain AMPARs and GABAARs. I discuss each of these areas in the following sections.

6.2 Zebrafish Mauthner cells express primarily *camk2a* at 2 dpf

My single-cell qRT-PCR results showed that the *camk2a* gene was preferentially expressed in M-cells of 2 dpf zebrafish embryos, while other isoforms (β1, β2, γ1, γ2, δ1, δ2) were mostly undetectable. In a previous whole mount in situ hybridization study on tissue specific expression of CaMKII genes, Rothschild et al (2007) demonstrated that γ1, γ2 and δ2 mRNA are the most prevalent in 2 dpf zebrafish hindbrain. It was intriguing to find that the expression pattern of CaMKII genes in M-cells was different from their tissue distribution. This apparent discrepancy between my findings and those of Rothschild et al (2007) may occur because we specifically targeted a single cell type rather than examining whole tissue. Thus, my results represent a significant difference in CaMKII gene expression in M-cells from the reported levels of *camk2a* in whole tissue.

CaMKII is the major protein in post-synaptic density (PSD), constituting 2-6% of total PSD protein (Chen et al., 2005). The enzyme is essential for the induction of long-term potentiation (LTP) (Malenka et al., 1989). Activity-dependent plasticity mechanisms such as LTP are believed to play important roles in learning and memory (Lisman et al., 2002; Martin et al., 2000; Mayford et al., 2012). Active CaMKII up-regulates AMPA receptor gating and trafficking, and alters dendritic spine volume via an interaction with cytoskeleton components (Hayashi et al., 2000; Kristensen et al., 2011; Lu et al., 2010; Rongo, 2002). In mammals an up-regulation of CaMKII-α's expression coincides with the restriction of dendritic neuronal arborizations in developing optic tectum (Wu and Cline, 1998; Zou and Cline, 1999), hippocampus (Ahmed et al., 2006) and dorsal horn neurons (Pattinson et al., 2006). Moreover, mice that are heterozygous for null mutation

in CaMKII-α gene show severe deficit in working memory, profound dysregulation of gene expression in the dentate gyrus, and aberrant cellular and synaptic physiology that is indicative of immature cells (Yamasaki et al., 2008). In the hippocampus, CaMKII-α is initially expressed at relatively low levels, and increases to adult levels within 2-3 weeks after birth, (Burgin et al., 1990; Kelly and Vernon, 1985). Thus, CaMKII-α plays a significant role during development and disruption of its function can lead to aberrant cellular behavior and physiology, as well as deficit in learning and memory in adult animals.

I used two independent morpholinos to knockdown the production of CaMKII-α. The first was a translation blocking morpholino that had been used in previous studies and that was independently verified via CaMKII peptide assay, to knockdown CaMKII-α (Francescatto et al., 2010). The second was a splice-blocking morpholino that was used to prevent the proper splicing of CaMKII-α pre-mRNA. My attempts to determine CaMKII-α protein expression in the embryonic zebrafish were not successful. Although the immunoblots using an anti-CaMKII antibody detected the protein from adult zebrafish CNS tissue, it failed to do so in embryonic tissue; possibly due to the difference in the isoforms expressed in embryonic and adult zebrafish. Both of these morpholinos gave almost identical results in all aspects of my study. Moreover, the splice-blocking morpholino resulted in a decrease in CaMKII-α mRNA ascertained by RT-PCR, and an increase in dendritic branching of the M-cell; a result that essentially mirrors findings in other systems (Pattinson et al., 2006; Wu and Cline, 1998; Zou and Cline, 1999). Thus, I am confident that CaMKII-α was knocked down in my studies, and that my findings

represent an effect resulting from a reduction in the expression of CaMKII-α during development.

6.3 Morphology and touch response

My immunohistochemical data show an increase in the number of dendritic branches associated with the ventral dendrite of splice-blocked morphants compared with control-injected fish. The increased branches were evident on the ventral dendrites and in some cases, directly from the M-cell body. These findings are similar to those in developing optic tectum, hippocampus and dorsal horn neurons, where reduced CaMKII activity or expression leads to an increase in dendritic arborization.

To determine if knockdown of CaMKII-α affected behavior, I examined the c-start escape response of the organism, which requires activation of the M-cell. My results indicate the morpholino knockdown of CaMKII-α prolonged the time course of the c-start in the translation-blocked morphants, although the splice-blocked embryos were not affected. Both morphants took longer time for the second bend of the trunk, which represents the onset of swimming away from the stimulus after the c-start. The c-start occurs via the strong activation of the Mauthner cell largely brought about through electrical transmission and fast glutamatergic chemical transmission. Although I found no change in synaptic AMPAR currents, NMDAR currents were significantly affected in morphants embryos. Moreover, knock down of *camk2a* altered dendritic morphology in the M-cell, and possibly in the other neurons on the escape network as well. Therefore, it is not surprising that the c-start escape response is disrupted in the morphants.

Additionally, about 50% of the splice-blocked fish showed some type of abnormal response by either not responding to the stimulus, or by responding with a sharp c-start followed by a relaxation of the tail, rather than swimming movements. Taken together, these data suggest that knockdown of CaMKII-α leads to abnormal escape response in embryonic zebrafish.

6.4 AMPA mEPSCs are not affected in CaMKII-α morphants

CaMKII is an important regulator of synaptic strength of AMPA receptors. It is well established that CaMKII is essential for induction of hippocampus-dependent long term potentiation (LTP), which depends on an increase in AMPA transmission following activation of NMDARs and subsequent rise in intracellular Ca^{2+} (Nicoll and Roche, 2013). Early evidence showed that application of CaMKII inhibitors prevented LTP induction. For example, injection of a synthetic peptide that mimics the autoinhibitory domain of CaMKII, blocked LTP (Malinow et al., 1989), while delivery of a constitutively active form of CaMKII increased the amplitude of spontaneous AMPA mEPSCs and occluded further synaptic enhancement by LTP protocol (Lledo et al., 1995). CaMKII-α increases synaptic AMPAR strength by increasing receptor number (Hayashi et al., 2000; Opazo et al., 2010) and channel conductance (Barria et al., 1997b; Benke and Isaac, 1998; Derkach et al., 1999; Kristensen et al., 2011). The GluA1 subunit of AMPARs contains two phosphorylation sites for CaMKII: S831, which is also phosphorylated by protein kinase c (PKC), and S567. Evidence suggests that phosphorylation of S831 by CaMKII during the early stages of LTP, increases AMPAR conductance (Barria et al., 1997a). For instance, pseudophosphorylation of this site

inhibits the increase in conductance when active CaMKII is expressed, and single channel recordings show that S831 phosphorylation enhances the probability of activation of the high conductance states of the AMPARs, rather than increasing the magnitude of any conductance states. Delivery of AMPARs to the synaptic site is a multistep process that includes trafficking of the receptors to the membrane from an intracellular pool, and capturing of the membrane receptors into synaptic sites during increased activity (Opazo and Choquet, 2011). Inhibition of CaMKII by KN 62 partially blocks exocytosis of AMPARs (Patterson et al., 2010). Finally, the capture of AMPARs is also blocked by inhibition of CAMKII (Opazo et al., 2010).

Since CaMKII plays a vital role in the upregulation of AMPARs in mammals, I conducted experiments to test if CaMKII-α also mediates activity dependent enhancement of AMPAR transmission in zebrafish. My results are in general in agreement with the published literature. I used an elevated K^+ solution to induce cellular depolarization for 5-10 minutes. Comparison of AMPAR mEPSCs recorded before and after depolarization revealed that the amplitude and frequency of the mEPSCs increased significantly following cellular depolarization. To assess whether CaMKII was involved in this process, I used two different pharmacological blockers to inhibit CaMKII activity. One of the blockers, KN 62 binds to the calmodulin binding site of CaMKII, thereby blocking the enzyme's interaction with calmodulin and its subsequent activation (Tokumitsu et al., 1990). However, KN 62 does not inhibit CaMKII that is already autophosphosphorylated and thus functions independently of Ca^{2+}/calmodulin binding. The second blocker, autocamtide-2-related inhibitory peptide (AIP), is a synthetic peptide

that is modeled after the autoinhibitory region of the enzyme and does not compete with calmodulin. Thus, KN-62 and AIP have different modes of action and yet were both able to block the depolarization induced increase in AMPA mEPSC amplitude. The inhibitors did not affect mEPSC frequency, as expected from their intracellular application into the postsynaptic cell.

Application of constitutively active CaMKII to CA1 hippocampal pyramidal cells increases AMPA receptor mediated synaptic transmission (Lledo et al., 1995). I used a truncated form of rat CaMKII-α monomer to further examine the effect of the enzyme on AMPAR mEPSCs directly but did not find any significant effect on the properties of the mEPSCs, possibly because I used a rat derived enzyme that may not be effective in zebrafish. Even though there are similarities between rat and zebrafish CaMKII-α, the amino acid sequences are not identical. Additionally, I only maintained the whole cell patch for 10 minutes, but longer incubation times may be required to see an effect of intracellularly applied CaMKII-α.

My primary objective was to examine the role of CaMKII-α in the development of AMPARs. AMPARs switch subunits during embryonic development (Patten and Ali, 2007, 2009). Given that CaMKII-α plays important roles in the activity-dependent trafficking of AMPARs, I hypothesized that CAMKII-α is also involved in the developmental regulation of the AMPAR s. To explore a developmental role of CaMKII-α, I reduced its expression in zebrafish embryos by injecting two different morpholinos and obtained AMPAR mediated mEPSC recordings from morphant and control embryos.

AMPAR mEPSCs in morphant fish were not different from controls. This was unexpected since CaMKII-α upregulates AMPA trafficking and acute block of its activity reduces current amplitude. However, my RT-PCR results indicate that there is about 60% knockdown of CaMKII-α mRNA in the splice-blocking morphants, suggesting that the ~40% production of CaMKII-α may be enough to ensure normal development of AMPARs. Alternatively, CaMKII may only be involved in activity-dependent trafficking and play insignificant role in the developmental regulation of AMPARs in zebrafish. Previous findings in the Ali lab indicate that the enzyme PKCγ is involved in both acute and developmental trafficking of GluA2-containing AMPA receptors into membranes (Patten and Ali, 2007, 2009; Patten et al., 2010). Thus, it is possible that while CaMKII-α is important for acute trafficking of AMPRS, it is primarily PKCγ that regulates developmental trafficking of AMPARs.

6.5 NMDA receptor development

CaMKII is capable of binding to the GluN2B subunit of NMDARs at two potential sites: the first is present within residues 1290-1309 while the second is found within residues 839-1120 (Bayer et al., 2001; Leonard et al., 1999; Strack and Colbran, 1998a; Strack et al., 2000). When CaMKII is activated, this interaction allows for its localization at synapses (Bayer et al., 2006). Since CaMKII physically interacts with NMDARs, I wondered whether knockdown of CaMKII-α might affect NMDAR activity at developing synapses. I found that this was indeed the case as NMDA receptor currents were reduced in the CaMKII-α morphants compared with morphant controls. Averaged NMDA miniature currents in both uninjected controls and morphant controls displayed a

clear bi-exponential decay in which τ_{fast} was around 35 ms, and τ_{slow} about 330 ms. These time courses correspond well with published values in which mammalian forms of GluN1/GluN2A receptors decay with a time course of ~30 ms and GluN1/2B or GluN1/2C receptors decay with a time course of ~300 ms (Paoletti et al., 2013). Therefore, it is tempting to speculate that zebrafish express GluN1/2A and either the GluN1/2B or 2C types NMDA receptors, but I was unable to make this determination based on the present study. Additional experiments using antibodies targeted against GluN subunits, using single cell qRT-PCR or using probes for in situ-hybridization might allow for the identification of the NMDAR subunits associated with the M-cells.

A reduction in the amplitude of the slow component without affecting τ_{fast} suggests that there might be fewer functional GluN2B or 2C containing receptors when CaMKII-α levels are reduced. The double exponential decay of my averaged NMDAR mEPSCs could occur through a number of scenarios. First, an individual synapse may contain a single subtype of receptor that experiences complex kinetics as the channels close; second, there may be more than one receptor subtype present at a single synapse, each with its own characteristic decay constant, and third, an individual synapse may contain a single type of NMDAR, but there are different NMDARs at different synapses. An examination of the electrophysiological recordings indicates that individual mEPSCs decayed with bi-exponential time courses on the order of 30 ms (τ_{fast}) and 300 ms (τ_{slow}) suggesting that individual synapses likely contain multiple NMDA receptor subtypes.

Why is the mEPSC amplitude reduced by knockdown of CaMKII-α, and specifically, why is the slow component preferentially affected in the morphants? The simplest explanation is that τ_{slow} occurs due to the presence of the GluN2B subunit (which binds CaMKII-α), and that an association between the two is required for proper targeting, trafficking or function of 2B containing NMDARs during development. CaMKII has been postulated to play a non-enzymatic role due to its extremely high abundance and density in the PSD (Erondu and Kennedy, 1985; Petersen et al., 2003). It acts as a scaffold to recruit proteasomes to dendritic spines, where proteasomal degradation regulates activity-induced spine outgrowth (Bingol et al., 2010; Hamilton et al., 2012). A second possibility underlying the effect of CaMKII-α on the slow decay component relates to the ability of calmodulin to directly bind to and regulate NMDA receptor activity (Ehlers et al., 1996; Wyszynski et al., 1997; Zhang et al., 1998). Calmodulin regulates NMDA receptors by binding to the C0 region of the GluN1 subunit (Ehlers et al., 1996). Therefore, a reduction in CaMKII level could potentially lead to an increased availability of calmodulin, which down-regulates NMDA receptor activity.

6.6 Role of CaMKII-α in synaptic $GABA_A$ receptor current development

The GABA system plays crucial roles in regulating and controlling neural networks and ionotropic $GABA_A$Rs are key targets for the treatment of disorders such as schizophrenia, autism, epilepsy and depression (Rudolph and Mohler, 2014). Here I provide electrophysiological evidence that $GABA_A$ responses from 48 hpf zebrafish Mauthner cells can be classified into 3 separate groups based on mIPSC decay kinetics. Group I decays with a single exponential time course around 40-60 ms, but appears to

range from a low of ~10 ms to a high of approximately 100 ms. The second group (group II) is markedly longer, with decay kinetics peaking at 120-160 ms, but ranges as high as 280 ms. The third group (group III) consists of events which decay with 2 separate time courses, τ_1 and τ_2, where τ_1 = 28.7±2.5 ms and τ_2 = 153±11 ms. I assigned events to the first two groups based on the distribution in Fig 5.3A; however, it is possible that all of the single decaying events belong to a single population with quite variable kinetics. Indeed, as much as 40% of the variability in the decay of $GABA_AR$-mediated currents may be due to quantal charge differences and variations in transmitter concentration (Nusser et al., 2001). However, the decay times of the group I and group II events that we have observed are about 3 fold different from each other (50 ms vs 150 ms), suggesting that their differences are due to more than just variations in transmitter concentration.

About 15% of the GABA mIPSCs from the M-cells display a double exponential decay. mIPSCs that exhibit slow rise times and bi-exponential decays may occur due to spillover of GABA onto extrasynaptic receptors (Ferando and Mody, 2013). However, many of the bi-exponential events had fast rise times implying that they were due to the activation of synaptic rather than extrasynaptic $GABA_ARs$.

The kinetic properties of the fast $GABA_A$-mediated events from M-cells are quantitatively similar to those recorded from hippocampus, neocortex, pyramidal and cerebellar granule (Banks and Pearce, 2000; Hajos and Mody, 1997; Houston et al., 2008; Hutcheon et al., 2000; Sceniak and Maciver, 2008) where the single decay time courses generally range from ~4 ms to ~60 ms. The slow $GABA_A$ events from zebrafish M-cells

decay with a time course (~150 ms) that is longer than those found in the literature and it will be necessary, although difficult, to determine the exact subunit identity of the $GABA_A$Rs in zebrafish. The majority of the inhibitory input onto M-cells of 48 hpf zebrafish occurs due to glycinergic activity, whereby the mIPSCs have a greater amplitude, a faster time course and occur at a frequency that is ~500-fold greater than the GABA events (Ali et al., 2000b), suggesting that the glycinergic inputs are developmentally more advanced compared to the GABA inputs.

The β and γ subunits of $GABA_A$ receptors are major substrates for CaMKII-α phosphorylation (McDonald and Moss, 1994). Depending on receptor subunit composition and localization at the synaptic or extrasynaptic sites, CaMKII-α shows differential regulation of GABA IPSCs. In hippocampus, CaMKII-α increases $GABA_A$ IPSC by recruiting receptors to the cell surface (Wei et al., 2004). In cultured rat cerebellar granule neurons, application of constitutively active CaMKII-α increases IPSC amplitude of β2 subunit-containing $GABA_A$ receptors. In contrast, active CaMKII-α increases only the duration of IPSCs but not amplitude in β3 subunit-containing receptor IPSCs (Houston and Smart, 2006). It was proposed that phosphorylation by CaMKII-α modulates IPSC decay kinetics at synaptic $GABA_A$ receptors that contain predominantly the β3 subunit (Herd et al., 2008). Increases in IPSC amplitude may result from CaMKII-α mediated synaptic recruitment of extrasynaptic $GABA_A$ receptors that are primarily composed of the β2 subunit. My findings from the morpholino knockdown experiments are in line with the existing literature. It is possible that the reduction I observed in the

time course of single decay fast events (Group I) is a consequence of decreased β3 subunit phosphorylation in CaMKII-α morphants.

6.7 Development of glycine receptor current

Fast inhibitory neurotransmission in embryonic zebrafish M-cells is mediated primarily through inotropic glycine receptors (GlyRs). GlyRs are expressed in a developmentally regulated pattern in the CNS, where they continuously move along the plasma membrane by lateral diffusion, and anchor at the postsynaptic sites by binding to the scaffolding protein gephyrin. Formation and maturation of functional GlyR synapses require clustering of these receptors at the postsynaptic membrane following neuronal activity and Ca^{2+} influx (Kirsch and Betz, 1998). Inhibition of CaMKII in cultured neurons impairs clustering of GlyR at postsynaptic sites (Charrier et al., 2010). Conversely, intracellular application of activated CaMKII-α enhances glycine currents in spinal neurons (Wang and Randic, 1996). Inhibition of CaMKII in zebrafish perturbs GlyR clustering (Yamanaka et al., 2013). Specifically, application of a CaMKII-specific inhibitor, KN-93, to the developing embryo, as well as transgenic expression of a CaMKII inhibitory peptide, autocamtider-2-related inhibitory peptide 2 (AIP2), in zebrafish M-cells impair GlyR clustering. The maturation of GlyRs in mammals leads to a progressive decrease in the duration of glycinergic inhibitory response, which has been proposed to result from switching of slower α2 subunits for faster α1 subnuits (Krupp et al., 1994; Singer et al., 1998; Takaishi et al., 1992). Embryonic zebrafish also show developmental upregulation of glycine receptor kinetics (Ali et al., 2000b). For example, between 30-40 hpf and >50 hpf of development, the frequency of GlyR mediated mIPSCs

increased greatly, concurrent with a significant decrease in the decay kinetics, where the off kinetics of τ_{Fast} component fell about 55% and the τ_{Slow} component reduced by 28%. The mean amplitude of the events, although varied, was similar for the different groups.

I recorded spontaneous GlyR mIPSCs from CaMKII-α morphant embryos and compared them to the mIPSCs obtained from control embryos. Knockdown of CaMKII-α had no effect on the amplitude, frequency or rise times of the mIPSCs (Figure 5.9B, C; 5.10B). Given that CaMKII regulates GlyR clustering, it was surprising that the amplitude or frequency of the mIPSCs was not affected in the morphants. However, immune-electron micsroscopic observation of zebrafish M-cells showed that glycinergic synapses on the cell body and dendrites are already mature in 2 dpf embryos, although dendritic endings contained synapses with immature appearances (Triller et al., 1997). Thus, the majority GlyR synapses in morphants are probably already established by 2 dpf, leading to mIPSC frequencies and amplitudes similar to those from the control embryos. Additionally, I reduced the expression of CaMKII-α but did not confirm the possible upregulation of any other isoforms of CaMKII that could account for the continued clustering of GlyRs. Moreover, only ~50% CaMKII knockdown may not have been enough to affect GlyR clustering. Certainly further experiments are needed to more closely examine the effects of either knocking down or knocking out the expression of CaMKII-α on synaptic inhibitory receptors.

The morphants in my study however exhibited significantly longer decay time constants for both the fast and slow components compared to the controls (Figure 5.12).

Specifically, the decay times of the fast and slow components of mIPSCs in the morphants were about 33% and 31% greater than the control groups respectively. This result is in line with previous finding that decay time of GlyRs change with the progression of development (Ali et al., 2000b). The longer decay time in the morphants suggest that maturation of GlyRs in these organisms may have been delayed.

6.8 Future research

To further explore the roles of CaMKII-α in the development of Mauthner cell excitability properties and general neurodevelopment of zebrafish brain, the following areas of research could be addressed in future:

1. Generation of CaMKII-α knockouts via CRISPR technology. In this study I used morpholinos to reduce the levels of CaMKII-α, but producing a knockout would have several advantages if the animals are viable and survive beyond the first week of development. In particular, a knockout would likely result in the total absence of CaMKII-α rather than a ~50% reduction in levels. Moreover, morpholinos may have non-specific, off-target effects and a knockout would hopefully alleviate errors due to any non-specific activity. Synaptic activity should be examined in the knockouts to confirm the morpholino results.

2. An examination of the excitability properties of the M-cells to determine if these have also been affected in the morphants, and in the knockouts (if they are available). Action potentials from M-cell could be recorded in whole-cell current clamp configuration. Zebrafish M-cells fire single action potential when depolarized to threshold but can fire multiple times at the onset of suprathreshold stimuli (Brewster and Ali, 2013). To assess the effect of CaMKII-α on neuronal excitability, action potential peak amplitude, afterhyperpolarization amplitude, half width, voltage threshold and input current threshold could be analyzed and compared between morphants and control embryos. Based on my previous findings, I hypothesize that CaMKII-α morphants will

demonstrate altered firing properties due to synaptic and morphological changes of M-cell.

3. Examining the role of CaMKII-α in neuronal development in CNS. CaMKII-α regulates structural development of neurons. Neuronal development could be monitored in zebrafish brain using Isl1-GFP transgenic zebrafish embryos and immunohistochemistry as described previously (Hanington et al., 2008). Briefly, the Isl1-GFP transgenic zebrafish line could be used to assess sensory and motor neuron development. These embryos express GFP in motor neurons (Higashijima et al., 2000). In addition, immunohistochemistry using anti-acetylated tubulin antibody, which stains mature neurites could be used for sensory neuron development (Chitnis and Kuwada, 1990). Based on my recent finding, I hypothesize that CaMKII-α morphants will show reduced stabilization of the dendritic structures and impairment in network integration of the neurons.

4. A determination of which NMDAR subunits comprise the NMDARs during development. My data suggest that the synaptic NMDARs in 48 hpf M-cells are composed of GluN1+GluN2A subunits and GluN1+GluN2B/C subunits, but the exact identities have not been confirmed. Use of immunohistochemical techniques, pharmacological studies, in-situ hybridization and RT-qPCR might help confirm the identity of NMDARs on the M-cell. To electrophysiologically characterize zebrafish NMDA receptors, various drugs such as CP-101 that blocks GluN2B containing receptors, TCN-201 that blocks GluN2A containing receptors and CIQ that potentiates

GluN2C/2D containing receptors could be used. Immunohistochemistry using antibodies targeting different subunits of the NMDARs could also be used to visualize localization of the receptors. Expression pattern of the NMDAR subunits could be examined by in situ hybridization and RT-qPCR. Finally, heterologous expression systems could be used to characterize subunit specific zebrafish NMDAR currents.

References

Ahmed, R., Zha, X.M., Green, S.H., and Dailey, M.E. (2006). Synaptic activity and F-actin coordinately regulate CaMKIIalpha localization to dendritic postsynaptic sites in developing hippocampal slices. Molecular and Cellular Neuroscience 31, 37-51.

Ali, D.W., Buss, R.R., and Drapeau, P. (2000a). Properties of miniature glutamatergic EPSCs in neurons of the locomotor regions of the developing zebrafish. Journal of Neurophysiology 83, 181-191.

Ali, D.W., Drapeau, P., and Legendre, P. (2000b). Development of spontaneous glycinergic currents in the Mauthner neuron of the zebrafish embryo. Journal of Neurophysiology 84, 1726-1736.

An, M., Luo, R., and Henion, P.D. (2002). Differentiation and maturation of zebrafish dorsal root and sympathetic ganglion neurons. Journal of Comparative Neurology 446, 267-275.

Anggono, V., and Huganir, R.L. (2012). Regulation of AMPA receptor trafficking and synaptic plasticity. Current Opinion in Neurobiology 22, 461-469.

Arruda-Carvalho, M., Restivo, L., Guskjolen, A., Epp, J.R., Elgersma, Y., Josselyn, S.A., and Frankland, P.W. (2014). Conditional deletion of alpha-CaMKII impairs integration of adult-generated granule cells into dentate gyrus circuits and hippocampus-dependent learning. Journal of neuroscience 34, 11919-11928.

Baer, K., Essrich, C., Benson, J.A., Benke, D., Bluethmann, H., Fritschy, J.M., and Luscher, B. (1999). Postsynaptic clustering of gamma-aminobutyric acid type A receptors by the gamma3 subunit in vivo. Proceedings of the National Academy of Sciences of the United States of America 96, 12860-12865.

Banks, M.I., and Pearce, R.A. (2000). Kinetic differences between synaptic and extrasynaptic GABA(A) receptors in CA1 pyramidal cells. Journal of Neuroscience 20, 937-948.

Barnes, J.M., Dev, K.K., and Henley, J.M. (1994). Cyclothiazide unmasks AMPA-evoked stimulation of [3H]-L-glutamate release from rat hippocampal synaptosomes. British Journal of Pharmacology 113, 339-341.

Barria, A., Derkach, V., and Soderling, T. (1997a). Identification of the Ca2+/calmodulin-dependent protein kinase II regulatory phosphorylation site in the alpha-amino-3-hydroxyl-5-methyl-4-isoxazole-propionate-type glutamate receptor. Journal of Biological Chemistry 272, 32727-32730.

Barria, A., and Malinow, R. (2005). NMDA receptor subunit composition controls synaptic plasticity by regulating binding to CaMKII. Neuron 48, 289-301.

Barria, A., Muller, D., Derkach, V., Griffith, L.C., and Soderling, T.R. (1997b). Regulatory phosphorylation of AMPA-type glutamate receptors by CaM-KII during long-term potentiation. Science 276, 2042-2045.

Bayer, K.U., De Koninck, P., Leonard, A.S., Hell, J.W., and Schulman, H. (2001). Interaction with the NMDA receptor locks CaMKII in an active conformation. Nature 411, 801-805.

Bayer, K.U., LeBel, E., McDonald, G.L., O'Leary, H., Schulman, H., and De Koninck, P. (2006). Transition from reversible to persistent binding of CaMKII to postsynaptic sites and NR2B. Journal of Neuroscience 26, 1164-1174.

Bayer, K.U., Lohler, J., Schulman, H., and Harbers, K. (1999). Developmental expression of the CaM kinase II isoforms: ubiquitous gamma- and delta-CaM kinase II are the early isoforms and most abundant in the developing nervous system. Molecular Brain research 70, 147-154.

Ben-Ari, Y. (2002). Excitatory actions of gaba during development: the nature of the nurture. Nature Reviews Neuroscience 3, 728-739.

Ben-Ari, Y., Khalilov, I., Kahle, K.T., and Cherubini, E. (2012). The GABA excitatory/inhibitory shift in brain maturation and neurological disorders. Neuroscientist 18, 467-486.

Bengtsson, M., Ståhlberg, A., Rorsman, P., and Kubista, M. (2005). Gene expression profiling in single cells from the pancreatic islets of Langerhans reveals lognormal distribution of mRNA levels. Genome Research 15, 1388-1392.

Benke, T.A., and Isaac, J.T.R. (1998). Modulation of AMPA receptor unitary conductance by synaptic activity. Nature 393, 793-797.

Bernhardt, R.R., Chitnis, A.B., Lindamer, L., and Kuwada, J.Y. (1990). Identification of spinal neurons in the embryonic and larval zebrafish. Journal of Comparative Neurology 302, 603-616.

Betz, H., and Laube, B. (2006). Glycine receptors: Recent insights into their structural organization and functional diversity. Journal of Neurochemistry 97, 1600-1610.

Bill, B.R., Petzold, A.M., Clark, K.J., Schimmenti, L.A., and Ekker, S.C. (2009). A primer for morpholino use in zebrafish. Zebrafish 6, 69-77.

Bingol, B., Wang, C.F., Arnott, D., Cheng, D., Peng, J., and Sheng, M. (2010). Autophosphorylated CaMKIIalpha acts as a scaffold to recruit proteasomes to dendritic spines. Cell 140, 567-578.

Blake, W.J., M, K.A., Cantor, C.R., and Collins, J.J. (2003). Noise in eukaryotic gene expression. Nature 422, 633-637.

Brewster, D.L., and Ali, D.W. (2013). Expression of the voltage-gated potassium channel subunit Kv1.1 in embryonic zebrafish Mauthner cells. Neuroscience Letters 539, 54-59.

Brocke, L., Chiang, L.W., Wagner, P.D., and Schulman, H. (1999). Functional implications of the subunit composition of neuronal CaM kinase II. Journal of Biological Chemistry 274, 22713-22722.

Burgess, H.A., and Granato, M. (2007). Sensorimotor gating in larval zebrafish. Journal of Neuroscience 27, 4984-4994.

Burgin, K.E., Waxham, M.N., Rickling, S., Westgate, S.A., Mobley, W.C., and Kelly, P.T. (1990). In situ hybridization histochemistry of Ca2+/calmodulin-dependent protein kinase in developing rat brain. Journal of Neuroscience 10, 1788-1798.

Cai, L., Friedman, N., and Xie, X.S. (2006). Stochastic protein expression in individual cells at the single molecule level. Nature 440, 358-362.

Capogna, M., and Pearce, R.A. (2011). GABA A,slow: causes and consequences. Trends in Neurosciences 34, 101-112.

Celio, M.R., Gray, E.G., and Yasargil, G.M. (1979). Ultrastructure of the Mauthner axon collateral and its synapses in the goldfish spinal cord. Journal of Neurocytology 8, 19-29.

Chang, S., and De Camilli, P. (2001). Glutamate regulates actin-based motility in axonal filopodia. Nature Neuroscience 4, 787-793.

Chang, Y.T., Lin, J.W., and Faber, D.S. (1987). Spinal inputs to the ventral dendrite of the teleost Mauthner cell. Brain Research 417, 205-213.

Charrier, C., Machado, P., Tweedie-Cullen, R.Y., Rutishauser, D., Mansuy, I.M., and Triller, A. (2010). A crosstalk between beta1 and beta3 integrins controls glycine receptor and gephyrin trafficking at synapses. Nature Neuroscience 13, 1388-1395.

Chen, X., Vinade, L., Leapman, R.D., Petersen, J.D., Nakagawa, T., Phillips, T.M., Sheng, M., and Reese, T.S. (2005). Mass of the postsynaptic density and enumeration of three key molecules. Proceedings of the National Academy of Sciences of the United States of America 102, 11551-11556.

Chitnis, A.B., and Kuwada, J.Y. (1990). Axonogenesis in the brain of zebrafish embryos. Journal of Neuroscience 10, 1892-1905.

Citri, A., and Malenka, R.C. (2008). Synaptic plasticity: multiple forms, functions, and mechanisms. Neuropsychopharmacology 33, 18-41.

Cline, H.T. (2001). Dendritic arbor development and synaptogenesis. Current Opinion in Neurobiology 11, 118-126.

Colbran, R.J. (2004a). Protein phosphatases and calcium/calmodulin-dependent protein kinase II-dependent synaptic plasticity. Journal of Neuroscience 24, 8404-8409.

Colbran, R.J. (2004b). Targeting of calcium/calmodulin-dependent protein kinase II. Biochemical Journal 378, 1-16.

Collingridge, G.L., Olsen, R.W., Peters, J., and Spedding, M. (2009). A nomenclature for ligand-gated ion channels. Neuropharmacology 56, 2-5.

Corringer, P.J., Le Novere, N., and Changeux, J.P. (2000). Nicotinic receptors at the amino acid level. Annual Review of Pharmacology and Toxicology 40, 431-458.

Coultrap, S.J., and Bayer, K.U. (2012). CaMKII regulation in information processing and storage. Trends in Neurosciences 35, 607-618.

Cox, J.A., Kucenas, S., and Voigt, M.M. (2005). Molecular characterization and embryonic expression of the family of N-methyl-D-aspartate receptor subunit genes in the zebrafish. Developmental Dynamics 234, 756-766.

Dahan, M., Levi, S., Luccardini, C., Rostaing, P., Riveau, B., and Triller, A. (2003). Diffusion dynamics of glycine receptors revealed by single-quantum dot tracking. Science 302, 442-445.

Deidda, G., Bozarth, I.F., and Cancedda, L. (2014). Modulation of GABAergic transmission in development and neurodevelopmental disorders: investigating physiology and pathology to gain therapeutic perspectives. Frontiers in Cellular Neuroscience 8, 119.

Derkach, V., Barria, A., and Soderling, T.R. (1999). Ca2+/calmodulin-kinase II enhances channel conductance of alpha-amino-3-hydroxy-5-methyl-4-isoxazolepropionate type glutamate receptors. Proceedings of the National Academy of Sciences of the United States of America 96, 3269-3274.

Dhanasekaran, S., Doherty, T.M., and Kenneth, J. (2010). Comparison of different standards for real-time PCR-based absolute quantification. Journal of Immunological Methods 354, 34-39.

Doldan, M.J., Prego, B., Holmqvist, B.I., and de Miguel, E. (1999). Distribution of GABA-immunolabeling in the early zebrafish (Danio rerio) brain. European Journal of Morphology 37, 126-129.

Drapeau, P., Ali, D.W., Buss, R.R., and Saint-Amant, L. (1999). In vivo recording from identifiable neurons of the locomotor network in the developing zebrafish. Journal of Neuroscience Methods 88, 1-13.

Dutertre, S., Becker, C.M., and Betz, H. (2012). Inhibitory glycine receptors: An update. Journal of Biological Chemistry.287, 40216-40223.

Eaton, R.C., Bombardieri, R.A., and Meyer, D.L. (1977). The Mauthner-initiated startle response in teleost fish. Journal of Experimental Biology 66, 65-81.

Eaton, R.C., DiDomenico, R., and Nissanov, J. (1988). Flexible body dynamics of the goldfish C-start: implications for reticulospinal command mechanisms. Journal of Neuroscience 8, 2758-2768.

Eaton, R.C., and Farley, R.D. (1973). Development of the Mauthner Neurons in Embryos and Larvae of the Zebrafish. Copeia 4, 673-682.

Eaton, R.C., Lee, R.K.K., and Foreman, M.B. (2001). The Mauthner cell and other identified neurons of the brainstem escape network of fish. Progress in Neurobiology 63, 467-485.

Ehlers, M.D., Zhang, S., Bernhadt, J.P., and Huganir, R.L. (1996). Inactivation of NMDA receptors by direct interaction of calmodulin with the NR1 subunit. Cell 84, 745-755.

Eisen, J.S., Myers, P.Z., and Westerfield, M. (1986). Pathway selection by growth cones of identified motoneurones in live zebra fish embryos. Nature 320, 269-271.

Ekker, S.C. (2000). Morphants: a new systematic vertebrate functional genomics approach. Yeast 17, 302-306.

Elowitz, M.B., Levine, A.J., Siggia, E.D., and Swain, P.S. (2002). Stochastic gene expression in a single cell. Science 297, 1183-1186.

Erondu, N.E., and Kennedy, M.B. (1985). Regional distribution of type II Ca2+/calmodulin-dependent protein kinase in rat brain. Journal of Neuroscience 5, 3270-3277.

Essrich, C., Lorez, M., Benson, J.A., Fritschy, J.M., and Luscher, B. (1998). Postsynaptic clustering of major GABAA receptor subtypes requires the gamma 2 subunit and gephyrin. Nature Neuroscience 1, 563-571.

Faber, D.S., and Korn, H. (1975). Inputs from the posterior lateral line nerves upon the goldfish Mauthner cells. II. Evidence that the inhibitory components are mediated by interneurons of the recurrent collateral network. Brain Research 96, 349-356.

Farrant, M., and Nusser, Z. (2005). Variations on an inhibitory theme: phasic and tonic activation of GABA(A) receptors. Nature Reviews Neuroscience 6, 215-229.

Feng, B., Raghavachari, S., and Lisman, J. (2011). Quantitative estimates of the cytoplasmic, PSD, and NMDAR-bound pools of CaMKII in dendritic spines. Brain Research 1419, 46-52.

Feng, G., Tintrup, H., Kirsch, J., Nichol, M.C., Kuhse, J., Betz, H., and Sanes, J.R. (1998). Dual requirement for gephyrin in glycine receptor clustering and molybdoenzyme activity. Science 282, 1321-1324.

Ferando, I., and Mody, I. (2013). Interneuronal GABA receptors inside and outside of synapses. Current Opinion in Neurobiology 26C, 57-63.

Fetcho, J.R. (1992). Excitation of motoneurons by the Mauthner axon in goldfish: complexities in a "simple" reticulospinal pathway. Journal of Neurophysiology 67, 1574-1586.

Fetcho, J.R., and O'Malley, D.M. (1995). Visualization of active neural circuitry in the spinal cord of intact zebrafish. Journal of Neurophysiology 73, 399-406.

Fink, C.C., Bayer, K.U., Myers, J.W., Ferrell, J.E., Jr., Schulman, H., and Meyer, T. (2003). Selective regulation of neurite extension and synapse formation by the beta but not the alpha isoform of CaMKII. Neuron 39, 283-297.

Foreman, M.B., and Eaton, R.C. (1993). The direction change concept for reticulospinal control of goldfish escape. Journal of Neuroscience 13, 4101-4113.

Francescatto, L., Rothschild, S.C., Myers, A.L., and Tombes, R.M. (2010). The activation of membrane targeted CaMK-II in the zebrafish Kupffer's vesicle is required for left-right asymmetry. Development 137, 2753-2762.

Furukawa, T., and Furshpan, E.J. (1963). Two inhibitory mechanisms in the Mauthner neurons of goldfish. Journal of Neurophysiology 26, 140-176.

Gaertner, T.R., Kolodziej, S.J., Wang, D., Kobayashi, R., Koomen, J.M., Stoops, J.K., and Waxham, M.N. (2004). Comparative analyses of the three-dimensional structures and enzymatic properties of alpha, beta, gamma and delta isoforms of Ca2+-calmodulin-dependent protein kinase II. Journal of Biological Chemistry 279, 12484-12494.

Gahtan, E., and O'Malley, D.M. (2003). Visually guided injection of identified reticulospinal neurons in zebrafish: a survey of spinal arborization patterns. The Journal of Comparative Neurology 459, 186-200.

Gahtan, E., Sankrithi, N., Campos, J.B., and O'Malley, D.M. (2002). Evidence for a widespread brain stem escape network in larval zebrafish. Journal of Neurophysiology 87, 608-614.

Gallo, V., and Russell, J.T. (1995). Excitatory amino acid receptors in glia: different subtypes for distinct functions? Journal of Neuroscience Research 42, 1-8.

Gallo, V., Upson, L.M., Hayes, W.P., Vyklicky, L., Jr., Winters, C.A., and Buonanno, A. (1992). Molecular cloning and development analysis of a new glutamate receptor subunit isoform in cerebellum. Journal of Neuroscience 12, 1010-1023.

Grenningloh, G., Pribilla, I., Prior, P., Multhaup, G., Beyreuther, K., Taleb, O., and Betz, H. (1990a). Cloning and expression of the 58 kd beta subunit of the inhibitory glycine receptor. Neuron 4, 963-970.

Grenningloh, G., Schmieden, V., Schofield, P.R., Seeburg, P.H., Siddique, T., Mohandas, T.K., Becker, C.M., and Betz, H. (1990b). Alpha subunit variants of the human glycine receptor: primary structures, functional expression and chromosomal localization of the corresponding genes. The EMBO Journal 9, 771-776.

Grunwald, D.J., Kimmel, C.B., Westerfield, M., Walker, C., and Streisinger, G. (1988). A neural degeneration mutation that spares primary neurons in the zebrafish. Developmental Biology 126, 115-128.

Guetg, N., Abdel Aziz, S., Holbro, N., Turecek, R., Rose, T., Seddik, R., Gassmann, M., Moes, S., Jenoe, P., Oertner, T.G.*, et al.* (2010). NMDA receptor-dependent GABAB receptor internalization via CaMKII phosphorylation of serine 867 in GABAB1. Proceedings of the National Academy of Sciences of the United States of America 107, 13924-13929.

Hagihara, H., Takao, K., Walton, N.M., Matsumoto, M., and Miyakawa, T. (2013). Immature dentate gyrus: an endophenotype of neuropsychiatric disorders. Neural Plasticity 2013, 318596.

Hajos, N., and Mody, I. (1997). Synaptic communication among hippocampal interneurons: properties of spontaneous IPSCs in morphologically identified cells. Journal of Neuroscience 17, 8427-8442.

Hamilton, A. M., Oh, W. C., Vega-Ramirez, H., Stein, I. S., Hell, J. W., Patrick, G. N., and Zito, K. (2012). Activity-Dependent Growth of New Dendritic Spines Is Regulated by the Proteasome. Neuron 74, 1023-1030.

Hanington, P.C., Patten, S.A., Reaume, L.M., Waskiewicz, A.J., Belosevic, M., and Ali, D.W. (2008). Analysis of leukemia inhibitory factor and leukemia inhibitory factor receptor in embryonic and adult zebrafish (Danio rerio). Developmental Biology 314, 250-260.

Hardingham, N., Glazewski, S., Pakhotin, P., Mizuno, K., Chapman, P.F., Giese, K.P., and Fox, K. (2003). Neocortical long-term potentiation and experience-dependent synaptic plasticity require alpha-calcium/calmodulin-dependent protein kinase II autophosphorylation. Journal of Neuroscience 23, 4428-4436.

Hayashi, Y., Shi, S.H., Esteban, J.A., Piccini, A., Poncer, J.C., and Malinow, R. (2000). Driving AMPA receptors into synapses by LTP and CaMKII: Requirement for GluR1 and PDZ domain interaction. Science 287, 2262-2267.

Hell, J.W. (2014). CaMKII: claiming center stage in postsynaptic function and organization. Neuron 81, 249-265.

Herd, M.B., Haythornthwaite, A.R., Rosahl, T.W., Wafford, K.A., Homanics, G.E., Lambert, J.J., and Belelli, D. (2008). The expression of GABAA beta subunit isoforms in synaptic and extrasynaptic receptor populations of mouse dentate gyrus granule cells. Journal of Physiology 586, 989-1004.

Higashijima, S., Hotta, Y., and Okamoto, H. (2000). Visualization of Cranial Motor Neurons in Live Transgenic Zebrafish Expressing Green Fluorescent Protein Under the Control of the Islet-1 Promoter/Enhancer. Journal of Neuroscience 20, 206-218.

Hojjati, M.R., van Woerden, G.M., Tyler, W.J., Giese, K.P., Silva, A.J., Pozzo-Miller, L., and Elgersma, Y. (2007). Kinase activity is not required for alphaCaMKII-dependent presynaptic plasticity at CA3-CA1 synapses. Nature Neuroscience 10, 1125-1127.

Hollmann, M., and Heinemann, S. (1994). Cloned glutamate receptors. Annual Review of Neuroscience 17, 31-108.

Hoppmann, V., Wu, J.J., Soviknes, A.M., Helvik, J.V., and Becker, T.S. (2008). Expression of the eight AMPA receptor subunit genes in the developing central nervous system and sensory organs of zebrafish. Developmental Dynamics 237, 788-799.

Hou, Y., Zhang, H., Miranda, L., and Lin, S. (2010). Serious overestimation in quantitative PCR by circular (supercoiled) plasmid standard: microalgal pcna as the model gene. PloS One 5, e9545.

Houston, C.M., Hosie, A.M., and Smart, T.G. (2008). Distinct regulation of beta2 and beta3 subunit-containing cerebellar synaptic GABAA receptors by calcium/calmodulin-dependent protein kinase II. Journal of Neuroscience 28, 7574-7584.

Houston, C.M., and Smart, T.G. (2006). CaMK-II modulation of GABA(A) receptors expressed in HEK293, NG108-15 and rat cerebellar granule neurons. European Journal of Neuroscience 24, 2504-2514.

Hudmon, A., and Schulman, H. (2002). Structure-function of the multifunctional Ca2+/calmodulin-dependent protein kinase II. Biochemical Journal 364, 593-611.

Hutcheon, B., Morley, P., and Poulter, M.O. (2000). Developmental change in GABAA receptor desensitization kinetics and its role in synapse function in rat cortical neurons. Journal of Physiology 522 Pt 1, 3-17.

Imboden, M., Devignot, V., Korn, H., and Goblet, C. (2001). Regional distribution of glycine receptor messenger RNA in the central nervous system of zebrafish. Neuroscience 103, 811-830.

Ito, I., Hidaka, H., and Sugiyama, H. (1991). Effects of KN-62, a specific inhibitor of calcium/calmodulin-dependent protein kinase II, on long-term potentiation in the rat hippocampus. Neuroscience Letters 121, 119-121.

Kawasaki, E.S. (2004). Microarrays and the gene expression profile of a single cell. Annals of the New York Academy of Sciences 1020, 92-100.

Kelly, P.T., and Vernon, P. (1985). Changes in the subcellular distribution of calmodulin-kinase II during brain development. Brain Research 350, 211-224.

Kennedy, M.B., Bennett, M.K., and Erondu, N.E. (1983). Biochemical and immunochemical evidence that the "major postsynaptic density protein" is a subunit of a calmodulin-dependent protein kinase. Proceedings of the National Academy of Sciences of the United States of America 80, 7357-7361.

Kimmel, C.B., Ballard, W.W., Kimmel, S.R., Ullmann, B., and Schilling, T.F. (1995). Stages of embryonic development of the zebrafish. Developmental Dynamics 203, 253-310.

Kimmel, C.B., Hatta, K., and Metcalfe, W.K. (1990). Early axonal contacts during development of an identified dendrite in the brain of the zebrafish. Neuron 4, 535-545.

Kimmel, C.B., Sessions, S.K., and Kimmel, R.J. (1981). Morphogenesis and synaptogenesis of the zebrafish Mauthner neuron. Journal of Comparative Neurology 198, 101-120.

Kirsch, J., and Betz, H. (1998). Glycine-receptor activation is required for receptor clustering in spinal neurons. Nature 392, 717-720.

Kohashi, T., and Oda, Y. (2008). Initiation of Mauthner- or non-Mauthner-mediated fast escape evoked by different modes of sensory input. Journal of Neuroscience 28, 10641-10653.

Kornau, H.C., Schenker, L.T., Kennedy, M.B., and Seeburg, P.H. (1995). Domain interaction between NMDA receptor subunits and the postsynaptic density protein PSD-95. Science 269, 1737-1740.

Kristensen, A.S., Jenkins, M.A., Banke, T.G., Schousboe, A., Makino, Y., Johnson, R.C., Huganir, R., and Traynelis, S.F. (2011). Mechanism of Ca2+/calmodulin-

dependent kinase II regulation of AMPA receptor gating. Nature Neuroscience 14, 727-735.

Krupp, J., Larmet, Y., and Feltz, P. (1994). Postnatal change of glycinergic IPSC decay in sympathetic preganglionic neurons. Neuroreport 5, 2437-2440.

Kumar, J., and Mayer, M.L. (2013). Functional insights from glutamate receptor ion channel structures. Annual Review of Physiology 75, 313-337.

Kuwada, J.Y., Bernhardt, R.R., and Nguyen, N. (1990). Development of spinal neurons and tracts in the zebrafish embryo. Journal of Comparative Neurology 302, 617-628.

Laurie, D.J., Seeburg, P.H., and Wisden, W. (1992a). The distribution of 13 GABAA receptor subunit mRNAs in the rat brain. II. Olfactory bulb and cerebellum. Journal of Neuroscience 12, 1063-1076.

Laurie, D.J., Wisden, W., and Seeburg, P.H. (1992b). The distribution of thirteen GABAA receptor subunit mRNAs in the rat brain. III. Embryonic and postnatal development. Journal of Neuroscience 12, 4151-4172.

Lee, H.-K. (2006). Syanptic plasticity and phosphorylation. Pharmacology & Therapeutics 112, 810-832.

Lee, R.K., Eaton, R.C., and Zottoli, S.J. (1993). Segmental arrangement of reticulospinal neurons in the goldfish hindbrain. Journal of Comparative Neurology 329, 539-556.

Legendre, P. (1998). A reluctant gating mode of glycine receptor channels determines the time course of inhibitory miniature synaptic events in zebrafish hindbrain neurons. Journal of Neuroscience 18, 2856-2870.

Legendre, P., and Korn, H. (1994). Glycinergic inhibitory synaptic currents and related receptor channels in the zebrafish brain. European Journal of Neuroscience 6, 1544-1557.

Leonard, A.S., Lim, I.A., Hemsworth, D.E., Horne, M.C., and Hell, J.W. (1999). Calcium/calmodulin-dependent protein kinase II is associated with the N-methyl-D-aspartate receptor. Proceedings of the National Academy of Sciences of the United States of America 96, 3239-3244.

Lewis, K.E., and Eisen, J.S. (2003). From cells to circuits: development of the zebrafish spinal cord. Progress in Neurobiology 69, 419-449.

Lisman, J., Schulman, H., and Cline, H. (2002). The molecular basis of CaMKII function in synaptic and behavioural memory. Nature Reviews Neuroscience 3, 175-190.

Lisman, J.E., and Zhabotinsky A.M. (2001). A model of synaptic memory: a CaMKII/PP1 switch that potentiates transmission by organizing an AMPA receptor anchoring assembly. Neuron 31, 191-201.

Liu, K.S., and Fetcho, J.R. (1999). Laser ablations reveal functional relationships of segmental hindbrain neurons in zebrafish. Neuron 23, 325-335.

Liu, Q., Chen, B., Ge, Q., and Wang, Z.W. (2007). Presynaptic Ca2+/calmodulin-dependent protein kinase II modulates neurotransmitter release by activating BK channels at Caenorhabditis elegans neuromuscular junction. Journal of Neuroscience 27, 10404-10413.

Lledo, P.M., Hjelmstad, G.O., Mukherji, S., Soderling, T.R., Malenka, R.C., and Nicoll, R.A. (1995). Calcium/calmodulin-dependent kinase II and long-term potentiation enhance synaptic transmission by the same mechanism. Proceedings of the National Academy of Sciences of the United States of America 92, 11175-11179.

Lo Iacono, L., and Gross, C. (2008). Alpha-Ca2+/calmodulin-dependent protein kinase II contributes to the developmental programming of anxiety in serotonin receptor 1A knock-out mice. Journal of Neuroscience 28, 6250-6257.

Lu, F.M., and Hawkins, R.D. (2006). Presynaptic and postsynaptic Ca(2+) and CamKII contribute to long-term potentiation at synapses between individual CA3 neurons. Proceedings of the National Academy of Sciences of the United States of America 103, 4264-4269.

Lu, W., Isozaki, K., Roche, K.W., and Nicoll, R.A. (2010). Synaptic targeting of AMPA receptors is regulated by a CaMKII site in the first intracellular loop of GluA1. Proceedings of the National Academy of Sciences of the United States of America 107, 22266-22271.

Lynch, J.W. (2004). Molecular structure and function of the glycine receptor chloride channel. Physiological Reviews 84, 1051-1095.

Malenka, R.C., Kauer, J.A., Perkel, D.J., Mauk, M.D., Kelly, P.T., Nicoll, R.A., Waxham, M.N. (1989). An essential role for postsynaptic calmodulin and protein kinase activity in long-term potentiation. Nature 340, 554–557

Malinow, R., Schulman, H., and Tsien, R.W. (1989). Inhibition of postsynaptic PKC or CaMKII blocks induction but not expression of LTP. Science (New York, NY) 245, 862-866.

Malosio, M.L., Marqueze-Pouey, B., Kuhse, J., and Betz, H. (1991). Widespread expression of glycine receptor subunit mRNAs in the adult and developing rat brain. EMBO Journal 10, 2401-2409.

Marsden, K.C., Shemesh, A., Bayer, K.U., and Carroll, R.C. (2010). Selective translocation of Ca2+/calmodulin protein kinase IIalpha (CaMKIIalpha) to inhibitory synapses. Proceedings of the National Academy of Sciences of the United States of America 107, 20559-20564.

Martin, S. J., Grimwood, P. D., and Morris, R.G.M. (2000). Synaptic plasticity and memory: an evaluation of the hypothesis. Annual Reviews Neuroscience 23:649–711.

Mayford, M., Siegelbaum, S.A., and Kandel, E.R. (2012). Synapses and Memory Storage. Cold Spring Harbor Perspectives in Biology 4, 1-18.

McDonald, B.J., and Moss, S.J. (1994). Differential phosphorylation of intracellular domains of gamma-aminobutyric acid type A receptor subunits by calcium/calmodulin type 2-dependent protein kinase and cGMP-dependent protein kinase. Journal of Biological Chemistry 269, 18111-18117.

Mendelson, B. (1986). Development of reticulospinal neurons of the zebrafish. II. Early axonal outgrowth and cell body position. Journal of Comparative Neurology 251, 172-184.

Metcalfe, W.K., Myers, P.Z., Trevarrow, B., Bass, M.B., and Kimmel, C.B. (1990). Primary neurons that express the L2/HNK-1 carbohydrate during early development in the zebrafish. Development 110, 491-504.

Metzger, F. (2010). Molecular and cellular control of dendrite maturation during brain development. Current Molecular Pharmacology 3, 1-11.

Mody, I., and Pearce, R.A. (2004). Diversity of inhibitory neurotransmission through GABA(A) receptors. Trends in Neuroscience 27, 569-575.

Mosbacher, J., Schoepfer, R., Monyer, H., Burnashev, N., Seeburg, P.H., and Ruppersberg, J.P. (1994). A molecular determinant for submillisecond desensitization in glutamate receptors. Science 266, 1059-1062.

Mueller, T., Vernier, P., and Wullimann, M.F. (2006). A phylotypic stage in vertebrate brain development: GABA cell patterns in zebrafish compared with mouse. Journal of Comperative Neurology 494, 620-634.

Myers, P.Z., Eisen, J.S., and Westerfield, M. (1986). Development and axonal outgrowth of identified motoneurons in the zebrafish. Journal of Neuroscience 6, 2278-2289.

Nakayama, H., and Oda, Y. (2004). Common sensory inputs and differential excitability of segmentally homologous reticulospinal neurons in the hindbrain. Journal of Neuroscience 24, 3199-3209.

Nasevicius, A., and Ekker, S.C. (2000). Effective targeted gene 'knockdown' in zebrafish. Nature Genetics 26, 216-220.

Nicoll, R.A., and Roche, K.W. (2013). Long-term potentiation: peeling the onion. Neuropharmacology 74, 18-22.

Niethammer, M., Kim, E., and Sheng, M. (1996). Interaction between the C terminus of NMDA receptor subunits and multiple members of the PSD-95 family of membrane-associated guanylate kinases. Journal of Neuroscience 16, 2157-2163.

Nusser, Z., Naylor, D., and Mody, I. (2001). Synapse-specific contribution of the variation of transmitter concentration to the decay of inhibitory postsynaptic currents. Biophysical Journal 80, 1251-1261.

O'Leary, H., Lasda, E., and Bayer, K.U. (2006). CaMKIIbeta association with the actin cytoskeleton is regulated by alternative splicing. Molecular Biology of the Cell 17, 4656-4665.

Okamoto, K., Narayanan, R., Lee, S.H., Murata, K., and Hayashi, Y. (2007). The role of CaMKII as an F-actin-bundling protein crucial for maintenance of dendritic spine structure. Proceedings of the National Academy of Sciences of the United States of America 104, 6418-6423.

Opazo, P., and Choquet, D. (2011). A three-step model for the synaptic recruitment of AMPA receptors. Molecular and Cellular Neurosciences 46, 1-8.

Opazo, P., Labrecque, S., Tigaret, C.M., Frouin, A., Wiseman, P.W., De Koninck, P., and Choquet, D. (2010). CaMKII triggers the diffusional trapping of surface AMPARs through phosphorylation of stargazin. Neuron 67, 239-252.

Pang, Z.P., Cao, P., Xu, W., and Sudhof, T.C. (2010). Calmodulin controls synaptic strength via presynaptic activation of calmodulin kinase II. Journal of Neuroscience 30, 4132-4142.

Paoletti, P., Bellone, C., and Zhou, Q. (2013). NMDA receptor subunit diversity: impact on receptor properties, synaptic plasticity and disease. Nature Reviews Neuroscience 14, 383-400.

Patten, S.A., and Ali, D.W. (2007). AMPA receptors associated with zebrafish Mauthner cells switch subunits during development. Journal of Physiology 581, 1043-1056.

Patten, S.A., and Ali, D.W. (2009). PKCgamma-induced trafficking of AMPA receptors in embryonic zebrafish depends on NSF and PICK1. Proceedings of the National Academy of Sciences of the United States of America 106, 6796-6801.

Patten, S.A., Roy, B., Cunningham, M.E., Stafford, J.L., and Ali, D.W. (2010). Protein kinase Cgamma is a signaling molecule required for the developmental speeding of alpha-amino-3-hydroxyl-5-methyl-4-isoxazole-propionate receptor kinetics. European Journal of Neuroscience 31, 1561-1573.

Patterson, M.A., Szatmari, E.M., and Yasuda, R. (2010). AMPA receptors are exocytosed in stimulated spines and adjacent dendrites in a Ras-ERK-dependent manner during long-term potentiation. Proceedings of the National Academy of Sciences of the United States of America 107, 15951-15956.

Pattinson, D., Baccei, M., Karadottir, R., Torsney, C., Moss, A., McCutcheon, J., Giese, K.P., and Fitzgerald, M. (2006). Aberrant dendritic branching and sensory inputs in the superficial dorsal horn of mice lacking CaMKIIalpha autophosphorylation. Molecular and Cellular Neuroscience 33, 88-95.

Petersen, J.D., Chen, X., Vinade, L., Dosemeci, A., Lisman, J.E., and Reese, T.S. (2003). Distribution of postsynaptic density (PSD)-95 and Ca2+/calmodulin-dependent protein kinase II at the PSD. Journal of Neuroscience 23, 11270-11278.

Pi, H.J., Otmakhov, N., El Gaamouch, F., Lemelin, D., De Koninck, P., and Lisman, J. (2010). CaMKII control of spine size and synaptic strength: role of phosphorylation states and nonenzymatic action. Proceedings of the National Academy of Sciences of the United States of America 107, 14437-14442.

Poncer, J.C., Esteban, J.A., and Malinow, R. (2002). Multiple mechanisms for the potentiation of AMPA receptor-mediated transmission by alpha-Ca2+/calmodulin-dependent protein kinase II. Journal of Neuroscience 22, 4406-4411.

Rachidi, M., Lopes, C., Takamatsu, Y., Ohsako, S., Benichou, J.C., and Delabar, J.M. (1999). Dynamic expression pattern of Ca(2+)/calmodulin-dependent protein kinase II gene in the central nervous system of Drosophila throughout development. Biochemical and Biophysical Research Communications 260, 707-711.

Rasband, W.S. (1997-2014). ImageJ. (Bethesda, Maryland, USA, U. S. National Institutes of Health).

Reyes, R., Haendel, M., Grant, D., Melancon, E., and Eisen, J.S. (2004). Slow degeneration of zebrafish Rohon-Beard neurons during programmed cell death. Developmental Dynamics 229, 30-41.

Reynolds, A., Brustein, E., Liao, M., Mercado, A., Babilonia, E., Mount, D. B., and Drapeau, P. (2008). Neurogenic role of the depolarizing chloride gradient revealed by global overexpression of KCC2 from the onset of development. Journal of Neuroscience 28, 1588-1597.

Roberts, E., and Frankel, S. (1950). γ-Aminobutyric acid in brain: its formation from glutamic acid. Journal of Biological Chemistry 187, 55-63.

Roberts, E., and Frankel, S. (1951). Glutamic acid decarboxylase in brain. Journal of Biological Chemistry 188, 789-795.

Rongo, C. (2002). A fresh look at the role of CaMKII in hippocampal synaptic plasticity and memory. Bioessays 24, 223-233.

Rothschild, S.C., Easley, C.A., Francescatto, L., Lister, J.A., Garrity, D.M., and Tombes, R.M. (2009). Tbx5-mediated expression of Ca(2+)/calmodulin-dependent protein kinase II is necessary for zebrafish cardiac and pectoral fin morphogenesis. Developmental Biology 330, 175-184.

Rothschild, S.C., Lister, J.A., and Tombes, R.M. (2007). Differential expression of CaMK-II genes during early zebrafish embryogenesis. Developmental Dynamics 236, 295-305.

Roy, B., and Ali, D.W. (2013). Patch clamp recordings from embryonic zebrafish Mauthner cells. Journal of Visualized Experiments, 79, e50551, doi:10.3791/50551.

Rudolph, U., and Mohler, H. (2014). GABAA receptor subtypes: Therapeutic potential in Down syndrome, affective disorders, schizophrenia, and autism. Annual Review of Pharmacology and Toxicology 54, 483-507.

Saint-Amant, L., and Drapeau, P. (2000). Motoneuron Activity Patterns Related to the Earliest Behavior of the Zebrafish Embryo. Journal of Neuroscience 20, 3964-3972.

Sceniak, M.P., and Maciver, M.B. (2008). Slow GABA(A) mediated synaptic transmission in rat visual cortex. BMC Neuroscience 9, 8.

Shakiryanova, D., Klose, M.K., Zhou, Y., Gu, T., Deitcher, D.L., Atwood, H.L., Hewes, R.S., and Levitan, E.S. (2007). Presynaptic ryanodine receptor-activated calmodulin kinase II increases vesicle mobility and potentiates neuropeptide release. Journal of Neuroscience 27, 7799-7806.

Shakiryanova, D., Morimoto, T., Zhou, C., Chouhan, A.K., Sigrist, S.J., Nose, A., Macleod, G.T., Deitcher, D.L., and Levitan, E.S. (2011). Differential control of presynaptic CaMKII activation and translocation to active zones. Journal of Neuroscience 31, 9093-9100.

Shen, K., and Meyer, T. (1999). Dynamic control of CaMKII translocation and localization in hippocampal neurons by NMDA receptor stimulation. Science 284, 162-166.

Singer, J.H., Talley, E.M., Bayliss, D.A., and Berger, A.J. (1998). Development of glycinergic synaptic transmission to rat brain stem motoneurons. Journal of Neurophysiology 80, 2608-2620.

Sommer, B., Keinanen, K., Verdoorn, T.A., Wisden, W., Burnashev, N., Herb, A., Kohler, M., Takagi, T., Sakmann, B., and Seeburg, P.H. (1990). Flip and flop: a

cell-specific functional switch in glutamate-operated channels of the CNS. Science 249, 1580-1585.

Sommer, B., Kohler, M., Sprengel, R., and Seeburg, P.H. (1991). RNA editing in brain controls a determinant of ion flow in glutamate-gated channels. Cell 67, 11-19.

Stahlberg, A., Andersson, D., Aurelius, J., Faiz, M., Pekna, M., Kubista, M., and Pekny, M. (2011). Defining cell populations with single-cell gene expression profiling: correlations and identification of astrocyte subpopulations. Nucleic Acids Research 39, 1-12.

Strack, S., and Colbran, R.J. (1998). Autophosphorylation-dependent targeting of calcium/ calmodulin-dependent protein kinase II by the NR2B subunit of the N-methyl- D-aspartate receptor. Journal of Biological Chemistry 273, 20689-20692.

Strack, S., McNeill, R.B., and Colbran, R.J. (2000). Mechanism and regulation of calcium/calmodulin-dependent protein kinase II targeting to the NR2B subunit of the N-methyl-D-aspartate receptor. Journal of Biological Chemistry 275, 23798-23806.

Svoboda, K.R., and Fetcho, J.R. (1996). Interactions between the neural networks for escape and swimming in goldfish. Journal of Neuroscience 16, 843-852.

Tabor, R., and Friedrich, R.W. (2008). Pharmacological analysis of ionotropic glutamate receptor function in neuronal circuits of the zebrafish olfactory bulb. PLoS One 3, e1416.

Takaishi, T., Saito, N., and Tanaka, C. (1992). Evidence for distinct neuronal localization of gamma and delta subunits of Ca2+/calmodulin-dependent protein kinase II in the rat brain. Journal of Neurochemistry 58, 1971-1974.

Tallafuss, A., Gibson, D., Morcos, P., Li, Y., Seredick, S., Eisen, J., and Washbourne, P. (2012). Turning gene function ON and OFF using sense and antisense photo-morpholinos in zebrafish. Development 139, 1691-1699.

Tobimatsu, T., and Fujisawa, H. (1989). Tissue-specific expression of four types of rat calmodulin-dependent protein kinase II mRNAs. Journal of Biological Chemistry 264, 17907-17912.

Tokumitsu, H., Chijiwa, T., Hagiwara, M., Mizutani, A., Terasawa, M., and Hidaka, H. (1990). KN-62 , a Specific Inhibitor of Ca2 ”/ Calmodulin-dependent Protein Kinase II * protein. Journal of Biological Chemistry 265, 4315-4320.

Traynelis, S.F., Wollmuth, L.P., McBain, C.J., Menniti, F.S., Vance, K.M., Ogden, K.K., Hansen, K.B., Yuan, H., Myers, S.J., and Dingledine, R. (2010). Glutamate receptor ion channels: structure, regulation, and function. Pharmacological Reviews 62, 405-496.

Triller, A., Rostaing, P., Korn, H., and Legendre, P. (1997). Morphofunctional evidence for mature synaptic contacts on the Mauthner cell of 52-hour-old zebrafish larvae. Neuroscience 80, 133-145.

Turecek, R., and Trussell, L.O. (2001). Presynaptic glycine receptors enhance transmitter release at a mammalian central synapse. Nature 411, 587-590.

Wang, R.A., and Randic, M. (1996). Alpha-subunit of CaM-KII increase glycine currents in acutely isolated rat spinal neurons. Journal of Neurophysiology 75, 2651-2653.

Wang, Z.W. (2008). Regulation of synaptic transmission by presynaptic CaMKII and BK channels. Molecular Neurobiology 38, 153-166.

Wayman, G.a., Lee, Y.-S., Tokumitsu, H., Silva, A.J., Silva, A., and Soderling, T.R. (2008). Calmodulin-kinases: modulators of neuronal development and plasticity. Neuron 59, 914-931.

Wei, J., Zhang, M., Zhu, Y., and Wang, J.H. (2004). Ca(2+)-calmodulin signalling pathway up-regulates GABA synaptic transmission through cytoskeleton-mediated mechanisms. Neuroscience 127, 637-647.

Westerfield, M. (2007). The zebrafish book. A guide for the laboratory use of zebrafish (Danio rerio), 5th edn (Eugene: University of Oregon Press).

Wisden, W., Laurie, D.J., Monyer, H., and Seeburg, P.H. (1992). The distribution of 13 GABAA receptor subunit mRNAs in the rat brain. I. Telencephalon, diencephalon, mesencephalon. Journal of Neuroscience 12, 1040-1062.

Wu, G.Y., and Cline, H.T. (1998). Stabilization of dendritic arbor structure in vivo by CaMKII. Science 279, 222-226.

Wyszynski, M., Lin, J., Rao, A., Nigh, E., Beggs, A.H., Craig, A.M., and Sheng, M. (1997). Competitive binding of alpha-actinin and calmodulin to the NMDA receptor. Nature 385, 439-442.

Yamanaka, I., Miki, M., Asakawa, K., Kawakami, K., Oda, Y., and Hirata, H. (2013a). Glycinergic transmission and postsynaptic activation of CaMKII are required for glycine receptor clustering in vivo. Genes to Cells 18, 211-224.

Yamasaki, N., Maekawa, M., Kobayashi, K., Kajii, Y., Maeda, J., Soma, M., Takao, K., Tanda, K., Ohira, K., Toyama, K.*, et al.* (2008a). Alpha-CaMKII deficiency causes immature dentate gyrus, a novel candidate endophenotype of psychiatric disorders. Molecular Brain 1, 6.

Yao, C., Vanderpool, K.G., Delfiner, M., Eddy, V., Lucaci, A.G., Soto-Riveros, C., Yasumura, T., Rash, J.E., and Pereda, A.E. (2014). Electrical synaptic transmission in developing zebrafish: properties and molecular composition of

gap junctions at a central auditory synapse. Journal of Neurophysiology 112, 2102-2113.

Ye, J., Coulouris, G., Zaretskaya, I., Cutcutache, I., Rozen, S., and Madden, T.L. (2012). Primer-BLAST: a tool to design target-specific primers for polymerase chain reaction. BMC Bioinformatics 13, 134.

Yoshioka, A., Bacskai, B., and Pleasure, D. (1996). Pathophysiology of oligodendroglial excitotoxicity. Journal of Neuroscience Research 46, 427-437.

Zebrafish Nomenclature Committee (ZNC) (1992). ZFIN Zebrafish Nomenclature Guidelines. A. Singer, ed. (University of Oregon, Eugene, OR 97403-5274).

Zhang, S., Ehlers, M.D., Bernhardt, J.P., Su, C.T., and Huganir, R.L. (1998). Calmodulin mediates calcium-dependent inactivation of N-methyl-D-aspartate receptors. Neuron 21, 443-453.

Zottoli, S.J. (1977). Correlation of the startle reflex and Mauthner cell auditory responses in unrestrained goldfish. The Journal of Experimental Biology 66, 243-254.

Zottoli, S.J. (1978). Comparison of Mauthner cell size in teleosts. Journal of Comparative Neurology 178, 741-757.

Zou, D.J., and Cline, H.T. (1999). Postsynaptic calcium/calmodulin-dependent protein kinase II is required to limit elaboration of presynaptic and postsynaptic neuronal arbors. Journal of Neuroscience 19, 8909-8918.